GENERATION OF EXTREMELY HIGH PEAK POWER OPTICAL PULSATIONS FROM RUBY UTILIZING THE PULSED-REFLECTOR MODE

JAMES P. O'DONOVAN

GENERATION OF EXTREMELY HIGH PEAK POWER OPTICAL PULSATIONS FROM RUBY UTILIZING THE PULSED-REFLECTOR MODE

*****

James P. O'Donovan

GENERATION OF EXTREMELY HIGH PEAK POWER OPTICAL PULSATIONS FROM RUBY UTILIZING THE PULSED-REFLECTOR MODE

by

James P. O'Donovan
Lieutenant, United States Navy

Submitted in partial fulfillment of
the requirements for the degree of

MASTER OF SCIENCE
IN
ENGINEERING ELECTRONICS

United States Naval Postgraduate School

1962

GENERATION OF EXTREMELY HIGH PEAK POWER OPTICAL PULSATIONS FROM RUBY UTILIZING THE PULSED-REFLECTOR MODE

by

James P. O'Donovan

This work is accepted as fulfilling
The thesis requirements for the degree of
MASTER OF SCIENCE
IN
ENGINEERING ELECTRONICS
from the
United States Naval Postgraduate School

ABSTRACT

The "Pulsed-Reflector Mode" of operation of a solid state optical maser is demonstrated experimentally. This laser configuration utilizes a Kerr cell shutter with the normal Fabry-Perot laser system, to switch the cavity Q and hence the regenerative environment, from a condition of high value to one of low value. This mode produces giant output pulses, with peak-power increases of at least 100 to 1 over the same optical maser output pulsations while operating in the normal mode. Optical alignment of the system, operating in both the normal and "Pulsed-Reflector Mode", plus a method for determining the polarization of the emergent optical maser beam are covered in detail.

The writer wishes to express his thanks to Professors Carl E. Menneken and Eugene C. Crittenden Jr., of the United States Naval Postgraduate School, for their encouragement, guidance and helpful criticism in the preparation of this paper and to the members of the Laser Research and Development Group of the Hughes Aircraft Company, for their excellent advice on the performance of the experimental work. In particular, the writer is indebted to Dr. Eric J. Woodbury for his guidance and assistance throughout the ten weeks at Hughes. The obtainment by the author of the experimental data presented in this paper, was in many respects made possible by his supervision.

TABLE OF CONTENTS

LIST OF ILLUSTRATIONS

LIST OF SYMBOLS

A	surface area in cm^2
A^o	angstrom unit
A_{ij}	Einstein A coefficients for spontaneous emission
α	linear absorption coefficient or attenuation constant
c	velocity of light
cm^{-1}	reciprocal centimeter or number of waves per centimeter 1cm-1 = Boltzmann energy at 1.44°K
D	thickness (diameter)
f	initial fractional population excess above laser threshold level after Kerr cell switching
γ'	system loss factor defined as -lnR for normal Laser action
g_i	statistical weight of the level i
h	Planck's constant = 6.625×10^{-27} erg-sec
I	intensity of an electromagnetic wave after traversing a distance
I_o	intensity of an incident electromagnetic wave
^oK	degrees Kelvin
k	Boltzmann's constant = 1.38×10^{-23} joules/°K
λ	wavelength
ℓ	length of the ruby rod
L	separation in distance between the detached reflectors
L_r	reflection losses from the ruby end surfaces
L_k	reflection losses from the Kerr cell surfaces
L_w	reflection losses from the Wollaston prism surfaces
r	number of photons per second in spectral region of the absorption band
n_i	Laplace domain representation of ion population of level i per unit volume of ruby medium.
N_i	ion population density of level i per unit volume of

ruby material

N_o total active ion density per unit volume of ruby material

$p(\nu)$ density of modes as a function of frequency ν

ρ photodiode sensitivity in $\mu A/\mu w$

p energy flow per unit time (power)

σ_{ij} absorption cross section for the active laser transition between level i and j

R mean reflectivity of the detached reflectors

S_k percentage of incident light that is transmitted through the Kerr cell and directed into the end surface of the ruby rod

S_w percentage of incident light that is transmitted through the Wollaston Prism and directed into the end surface of the ruby rod

S_{ij} transition probability per unit time for a nonradiative process

τ rise time of giant output pulse

τ_i radiative lifetime of the level i with reference to spontaneous emission, thermal relaxation etc.

t_d time delay after Kerr cell switching until giant output pulse appears

t_Δ time that it takes for a readjustment in α from some initial value, α_i, to a value $\Delta\alpha$ lower after Kerr cell switching

t_o length of pump pulse

T transmittance

T_k temperature in degrees Kelvin

μ micron unit; 1 micron = 10^4 Angstroms

ν_{ij} frequency of emitted radiation as a result of transitions between level i and j

$\Delta\nu$ half width of the spectral line at half maximum of the molecular resonance

V volume of ruby material in cm^3

W_{ij} induced pumping transition probability per unit time between level i and j

SECTION I

INTRODUCTION

1. Background

The advent of the optical maser[1] has extended the range of controlled electromagnetic radiation to the infrared and visible light spectrum.

The first operating laser was a solid-state design produced by T. H. Maiman. It employed a synthetic ruby crystal doped with chromium. The crystal was machined to optical tolerance, with both ends of the resulting ruby rod silvered to enhance reflection. Bathed in white light from an electronic flash lamp, the green content of the incident pumping light provided energy to the crystal. The principles involved in generating the resulting stimulated emission of coherent and monochromatic light, at 6943A°, are discussed in Section II of this paper.

Actually laser history begins with the maser. J. Weber suggested the possibility of maser action in 1952. (2), (3) A maser was constructed by C. H. Townes in 1955. (4) A solid state version of the device was proposed in 1956 by N. Bloembergen. (5)

1. The name "MASER" is an acronym for Microwave amplification by Stimulated Emission of Radiation. The use of the name "LASER" as a short form for optical maser or Light Amplification by Stimulated Emission of Radiation, is currently in vogue. Because this device is simply a variant of the basic maser principle, the more accurate description of optical maser is preferrable. However, the term "LASER", because of its advantage of compactness, will be used throughout the major portions of this paper.

An extension of the basic maser principle to permit operation in the light spectrum was suggested by A. L. Schawlow and C. H. Townes in 1958. (1)

The ruby laser built by T. H. Maiman in 1960 was recognized by industry as the first to function. (6), (10) Next in the line of progress was a continuously operating gas laser announced in 1961 by A. Javan, W. R. Bennet, and D. R. Herriott. (7)

During 1961, amplification with gain on the order of two was reported by P. Kisliuk and W. S. Boyle. (9)

Early in 1961, R. W. Hellwarth reported on the theory of obtaining giant pulsations from ruby. (13) Several months later, this theory was successfully demonstrated at the Hughes Research Laboratory utilizing ruby in a configuration which has come to be known as the "Pulsed-Reflector Mode" of laser operation.

A compilation of data on currently operating lasers is presented in Table 1 below. (32) Doping material is shown in parenthesis following the primary laser material.

TABLE 1 Operating Lasers

Laser Material	Where Developed	Output Spectral Lines[2] (A^o)
He-Ne	Bell	11,180; 11,530; 11,600 11,990; 12,070
Ruby (0.05% Cr ion)	Hughes	6,943
Ruby (0.5% Cr ion)	Varian and Bell	7,009; 6,943; 7,041
CaF_2 (0.05% U ion)	IBM	25,000
CaF_2 (0.1% Sm)	IBM	7,082

2. Output wavelength varies with temperature.

BaF_2 (U ion)	MIT	27,000
$CaWO_4$ (Neodymuim ion)	Bell	10,600

2. Laser Applications[3]

The following are but a few of the many possible future applications where laser systems may play an important role:

(1) Short range optical ranging and tracking. In this application, angular resolution can be increased by many orders of magnitude over that possible at radar frequencies. In fact, beam spread can be kept to such low values that in many cases it may be possible to have the target completely intercept the beam. Then the $1/R^4$ dependence in the radar range equation is replaced by a $1/R^2$ dependence due to the return path alone.[4]

(2) Space, earth and undersea communications; medical applications such as suturing, cauterization and cell surgery appear to be promising.

Of these two primary areas of laser system applications the "Pulsed-Reflector Mode" will find more immediate application to the first of the two areas. Utilization of laser systems in the second area of consideration may be feasible, but it is felt that scientific investigation into the behaviour of molecular construction and chemical bonds within homogeneous substances, under high intensity radiation, may prove to be more fruitful for the immediate future.

3. For a more detailed and easily read coverage of this topic, refer to (32) and (27)

4. Discussion with Dr. M. L. Stitch, Hughes Aircraft Company.

3. Scope

The objective of this paper is to present the results of a systematic experimental investigation of the "Pulsed-Reflector Mode" operation of a ruby laser. The theory associated with the "Pulsed-Reflector Mode" of laser operation appears in Section III of this paper.

In order to perform a comprehensive investigation of the improvement in laser power output due to the "Pulsed-Reflector Mode" operating configuration, it is essential that one not only consider the "before" and "after" experimental results as contrasted to the normal mode of operation, but also the individual effects caused by each component part of the overall system.

For this reason attention is focused on the following topics:

(1) Effects of physical alignment of the interferometer system upon energy output during laser operation in the normal mode.

(2) A method for determining the direction of polarization of the laser output beam.

(3) Individual effect of the Kerr cell and Wollaston prism upon laser threshold energy and energy output.

(4) Optical alignment of the "Pulsed-Reflector Mode" laser system.

(5) Peak power and energy output while operating in the pulsed-reflector mode as contrasted to the normal mode of laser operation.

(6) Output pulse shape as compared to theoretical pulse.

SECTION II

GENERAL THEORY OF STIMULATED OPTICAL EMISSION FROM RUBY[1]

1. Introduction

In order to extend electronic techniques to submillimeter or shorter wavelengths and yet avoid the almost impossible task of fabricating cavity resonators with dimensions comparable to these short wavelengths, one turns reasonably to the idea of using natural atomic, ionic or molecular resonators.

One of the problems involved in obtaining radiation by the stimulated emission process is that competing relaxation mechanisms such as spontaneous emission have a good chance of removing the excitation energy from an excited ion before stimulated optical emission can occur. In the near infrared or shorter wavelength region, one is faced with fast rates of spontaneous emission. This implies that a high induced transition probability, W_{13}, is required to bring about stimulated emission. (See equation (16), Appendix E)

Consider the following table of radiative lifetimes of excited states. Thermal relaxation time has been neglected in the table below, with the rates of decay shown being primarily those due to spontaneous emission.

λ (cm)	τ_1 (sec)	τ_2 (sec)
1	3×10^6	3×10^{10}

1. The theory presented in this section is a compilation of the more detailed accounts contained in references (15), (20), (22), (27), (28), (36) and a private communication originated by Dr. M. L. Stitch entitled, "Laser-What It Is; What It Does", for interdepartmental distribution in Hughes Aircraft Company.

10^{-2}	3	3×10^{4}
10^{-4}	3×10^{-6}	3×10^{-2}

Where,

$$\tau\,(\text{SEC}) = \frac{3h\lambda^3}{64\pi^4\mu^2} \qquad (1)$$

and, μ , the matrix element involved in the transition is 1×10^{-18} esu for τ_1 and $.01 \times 10^{-18}$ esu for τ_2.

The column of values of τ_1 corresponds to an electric dipole transition and would be appropriate for electronic transitions of free atoms or vibrational or rotational transitions of polar molecules. The column of values of τ_2 corresponds to a magnetic dipole transition such as the paramagnetic resonances used for microwave and optical masers.

From the table, one sees that spontaneous emission occurs quite rapidly at optical wavelengths and slowly at centimeter wavelengths, thus imposing a limiting criteria upon sources of pump radiation for maser purposes. This limitation is characterized by equations (16) and (40) of Appendix E. From these two relationships it may be deduced that the faster τ_2 becomes as one goes to shorter wavelengths, the shorter the requisite pumping pulse length must be if one intends to produce stimulated emission.

2. Coherence and Stimulated Emission

To obtain a light source where the individual radiators may be made to work together and to radiate with the proper phase, that is, coherent radiation versus the incoherent radiation of present light sources, one must make use of the

stimulated emission process.

Spontaneous emission in a laser is incoherent, that is, the over all phase fluctuates randomly and there is almost no correlation between instantaneous phases at different points in a medium of excited ions. In the presence of a resonant cavity however, some of this spontaneous emission will excite one of the resonant modes of the cavity, and the field associated with the resonance will induce emission in the laser medium. This induced emission is phase coherent with the field which induces it, and, as a result, if the interaction is strong enough a coherent electromagnetic wave will build up corresponding to one of the modes of the resonant cavity.

There are two aspects of wave coherence; spatial and temporal. At this point definitions of both are in order.

A wave is spatially coherent, if there exist surfaces over which the wave amplitude as a function of time is highly correlated. If there is complete spatial coherence, the correlation will be unity and the voltage at one point will be proportional to the voltage at other points on the surface. As an example of spatial coherence, consider the voltage at any two points on an equiphase front in the light from a distant star. The voltage at the two points is the same function of time, and, similarly at a given time, the voltage along different rays is the same function of distance from the star.

A wave exhibits time coherence to the degree that there is correlation between the amplitude of the wave at a given

point at one time and at some later time. A single frequency represents the extreme case of time coherence; if the line components of a spectrum are broadened, the time coherence is lessened and in the extreme opposite case, coherence virtually disappears, as for example in the case of black body radiation, where the spectrum of the wave consists of a smooth distribution of frequencies.

Spectral purity or the degree to which the spectrum approaches a line spectrum can thus be taken as a measure of time coherence.

Although the spectral line width is clearly narrowed by laser action, the time coherence is relatively poor in the solid state ruby laser. Spectral line widths on the order of 1000 megacycles are typical. Spatial coherence is also far from perfect and is thought to be limited by optical imperfections in the ruby crystals themselves. CW gaseous lasers represent an excellent improvement in the coherence characteristics of laser emission, with spectral line widths on the order of 1 kilocycle having been obtained to date.

Although the complete physical and mathematical description of stimulated optical emission is complicated, it is possible to get a simplified picture of laser action with the aid of Figure II-1. For a more detailed mathematical analysis, references (1), (4), (17) and (22) are recommended.

Ruby, which is an aluminum oxide (Al_2O_3) crystal with a doping chromium (Cr^{+++}) ions thinly distributed through the lattice sites, possesses extremely strong internal fields, which permit the paramagnetic Cr^{+++} ions to exist

in many energy levels.

The distribution of paramagnetic ions among the many energy levels, normally conforms with the Boltzmann distribution, where the ratio of particles in an excited state of energy E_2, to particles in the ground state of energy E_1, is given by

$$\frac{N_2}{N_1} = \frac{e^{-E_2/kT}}{e^{-E_1/kT}} \qquad (2)$$

Thus there are normally fewer particles in a higher level state than in a lower state.

In order to form an atomic oscillator, the prime requisite is to prepare an active medium, such as ruby, with an excess of atoms in the upper state. If one then encloses the medium in a suitable resonator which has been modified so that all but a few propagation modes have high losses, then it can be used to make an oscillator.

Consider an idealized three level quantum system with state population densities of N_1, N_2, N_3 per unit volume of active medium and corresponding energies E_1, E_2 and E_3, such that $E_3 > E_2 > E_1$. Laser operation in ruby will involve these three levels for the purpose of this discussion, where the lowest or ground level, E_1, is actually a doublet, and E_2, E_3 are the two excited energy states. Figure II-1 shows this quantum system where the energy levels are spaced so that $(E_3 - E_1)/hc = 18 \times 10^3$ cm $^{-1}$, and $(E_2 - E_1)/hc = 14.4 \times 10^3$ cm^{-1}, to correspond to the appropriate energy differentials of a ruby system. These energies correspond to radiation at 5600A$^{\circ}$ (green) and 6943A$^{\circ}$ (red), respectively.

Excited energy level E_3, is not a narrow "line" but rather a broad band of energy levels. Hence the pumping radiation may occupy a bandwidth of the order of 20% of the center frequency instead of being a sharply defined frequency.

To set up the conditions for amplification, pumping radiation is applied to the ruby which causes some Cr^{+++} ions to go from the ground state E_1 to energy state E_3. From here they decay by a non-radiative thermal relaxation to the intermediate excited state E_2. State E_2 is actually composed of two neighboring levels, $\bar{E}(^2E)$ and $2\bar{A}(^2E)$, 870kMc apart, rather than a single number two state. Dr. T. H. Maiman has published some evidence[3] which indicates that the population shifts to the $\bar{E}$ level from the $2\bar{A}$ level under laser operating conditions by a thermal relaxation process. This process is so rapid at room temperature that for all practical purposes the population ratio between the two states is kept constant. But $\bar{E}$ decays much faster to the ground state than $2\bar{A}$, so almost the entire initial population of the two states decays through R_1 emission as shown in Figure II-1.

If the decay to energy state E_2 occurs rapidly enough, more ions join the E_2 state than decay from it to the ground state E_1, and N_2 will become greater than N_1. For this situation to exist, the temperature, T, in equation (2) must be negative, and hence the term negative temperature

3. T. H. Maiman, Brit. Commum. and Electronics 7, pp 674 (1960).

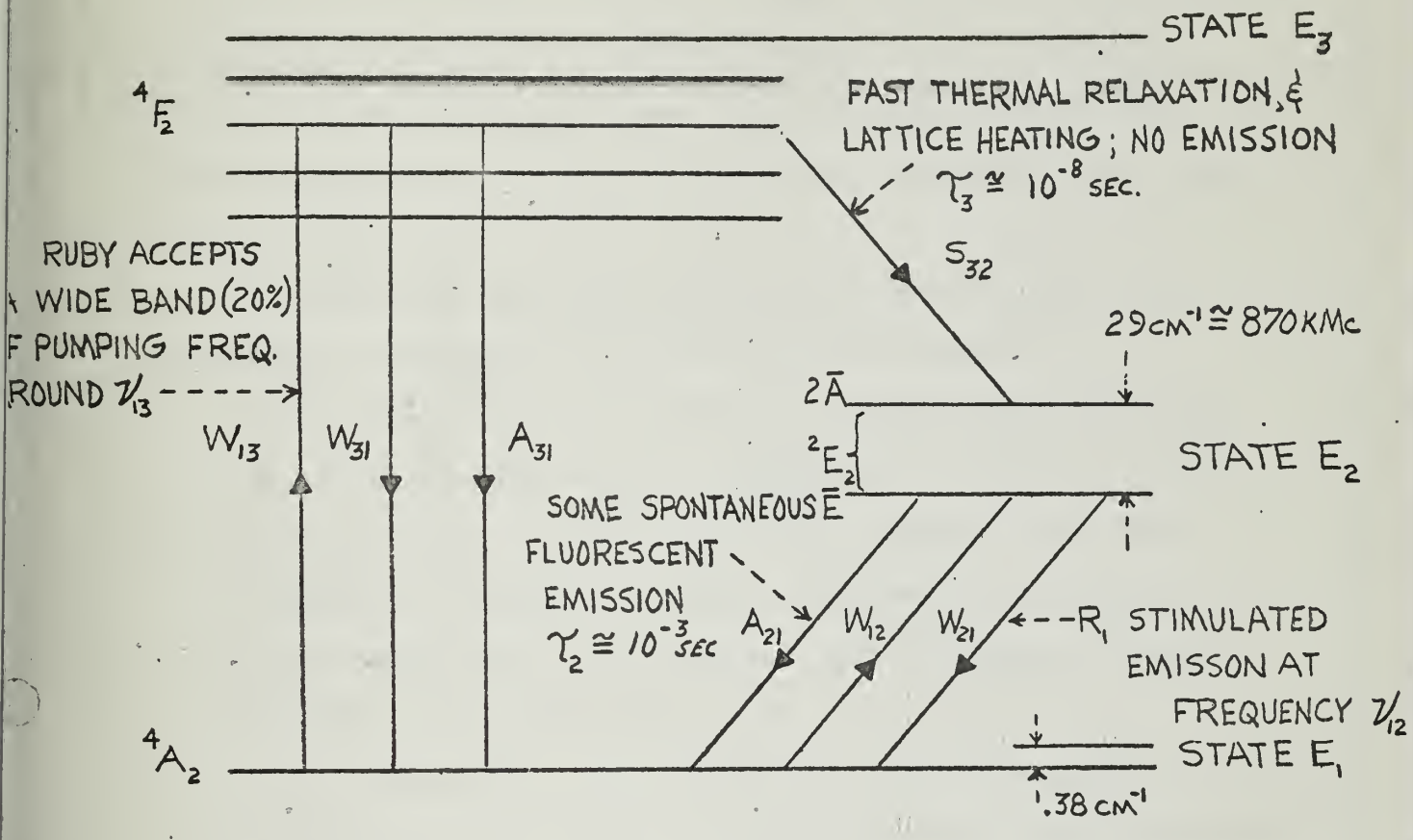

FIGURE II-1 PERTINENT ENERGY LEVELS FOR LASER ACTION IN RUBY.

NOTE:

$$\nu_{12} = \frac{E_2 - E_1}{h} = 4.3 \times 10^{14} \text{ CPS}, \text{ OR } \frac{\nu_{12}}{C} \cong 14.4 \times 10^3 \text{ cm}^{-1} \ (\sim 6943 \text{Å})$$

$$\nu_{13} = \frac{E_3 - E_1}{h} = 5.4 \times 10^{14} \text{ cps}, \text{ OR } \frac{\nu_{13}}{C} \cong 18 \times 10^3 \text{ cm}^{-1} \ (\sim 5600 \text{Å})$$

distribution as applied to maser action. As the pumping power is increased to the laser threshold, the population in level E_2 increases and most of this decays by spontaneous emission of radiation (fluorescence) to energy state E_1. Above the threshold for laser action, induced radiative transitions down to state E_1 begin to predominate over spontaneous emission.

To summarize the relaxation processes of ruby, the following conditions hold true for laser action:

(1) Relaxation from state E_3 occurs most rapidly by a non-radiative thermal relaxation to state E_2. This process takes place so much more rapidly than other competitive processes that it determines the characteristic lifetime of this state. This lifetime is given by[4] $\tau_3 = 5 \times 10^{-8}$ sec.

(2) Relaxation from state E_2 occurs predominantly by spontaneous emission to state E_1, with a characteristic lifetime given by[5] $\tau_2 = 3 \times 10^{-3}$ sec. This situation corresponds to fluorescent radiation in ruby.

If some of the energy released by the radiative transition from state E_2 to state E_1, which is at a frequency

$$\nu_{12} = (E_2 - E_1)/h \qquad (3)$$

is fed back into the system, more ions will be stimulated or tickled into emission. The result is a regenerative ampli-

4. See reference (10)

5. See reference (6) or refer to the information contained in footnote number 3.

fier which operates by the stimulated emission of radiation.

In order to obtain feedback or mode selection, the laser uses Fabry-Perot plates bounding the active medium on both ends. One of the plates is semi-transparent, the other totally reflecting. The ruby Fabry-Perot system is shown in Figure II-2(a). For the system shown, and operating in the normal configuration, a wave starting out anywhere in the active medium and traveling parallel to the axis of the system will be amplified until it strikes one of the reflecting plates. The amplification is derived from the fact that as the wave passes through the medium it stimulates the excited ions of the ruby crystal into emitting radiation. This radiation being of the same frequency and in phase with the stimulating wave, adds to its strength, causing it to stimulate more radiation. The wave thus grows until the loss due to multiple transmission through the partially transparent end plate plus other end plate losses[6], just equal the rate at which ions are being raised to energy state E_3 by the pumping radiation. The requisite condition for a steady oscillation of this kind to build up, is that the amplification during passage of the wave must be enough to make up for the losses in reflection at the end plates.

The result of the regenerative feedback is that one theoretically obtains the equivalent of high Q, single mode selection without being restricted to impossible small dimensions due to the short wavelength used. More will be

6. See reference (19) for an excellent analysis of effects of reflector losses on system characteristics.

said about mode behaviour in the following sub-heading.

An important factor in the success of this method of mode selection is that in building up oscillations in the axial mode all other off axis modes are competitively robbed of excited population to sustain the oscillation.

The axial mode in a uniformly excited homogeneous, strain free, carefully aligned and lapped ruby, whose ends serve as Fabry-Perot plates, (with reflectors attached) is as close to a plane wave as the diffraction limited end aperture will allow. For a cylinder with an aperture of diameter D (or diameter of the rod in the pulsed-reflector configuration), the angular width of the emitted beam is

$$\theta = \frac{1.22\lambda}{D} \qquad (4)$$

Refer to Figure II-2(b) for state of the art values for θ.

3. Oscillation Build up[7]

The degree of population inversion (or the rate of oscillation build up) needed to achieve laser action can be represented as follows.

The energy in a wave propagating through a material with an absorption coefficient α is attenuated by the factor $e^{-\alpha l}$, if l is the length of the material. If the initial intensity was I_o, then the intensity after passing a distance l through the medium under consideration, is given by

7. See Appendix E for a detailed presentation of the steady state rate equations and their simplified solution.

$$I = I_0 e^{-\alpha \ell} \tag{5}$$

where α is given by

$$\alpha = \frac{2}{\Delta\nu}\sqrt{\frac{\ln 2}{\pi}}\ \frac{\lambda^2}{8\pi}\left(\frac{g_2}{g_1}\right)\frac{(N_1 - N_2)}{\tau_2} \tag{6}$$

or in terms of the absorption cross section one can write,

$$\alpha = (N_1 - N_2)\sigma_{12} \tag{7}$$

If there are more ions in the upper state than in the lower state, $N_1 - N_2$ is negative, so that α is negative and there is amplification. Conversely, absorption occurs for $N_1 - N_2$ positive, i.e., more ions in the lower state than in the upper state, and α is positive.

Let the fraction of light reflected by the parallel Fabry-Perot end plates be proportional to R, where $R = \sqrt{R_1 R_2}$ is the mean reflectivity of the plates. Then if one follows the course of the growing wave corresponding to the axial mode which grows at a fractional rate of $\alpha = (N_1 - N_2)\sigma_{12}$ per unit length, one may write for the condition of oscillation build up,

$$Re^{2\alpha\ell} \geq 1 \tag{8}$$

where two passes through the medium have been assumed. As the amplitude of the oscillation builds up and depletes N_2, α decreases until at steady state the inequality in (8) is replaced by an equality.

Expanding (8), one sees that the condition of oscilla-

tion build up is

$$(N_1 - N_2)\sigma_{12}\ell \geq \frac{1}{2}(1-R) \tag{9}$$

The mean reflectivity R is related to the time t, during which light is stored in the resonator by the relationship

$$t \cong \frac{\ell\sqrt{\epsilon}}{c(1-R)} \tag{10}$$

where ϵ is the index of refraction for ruby.

Since one is normally concerned with the number of excited atoms which must be supplied per second, i.e., $(N_2 - N_1)/\tau_2$, equation (9) can be rewritten using equation (6) as follows

$$\left(\frac{N_2 - N_1}{\tau_2}\right)V \geq \frac{8\pi^2}{\sqrt{\pi \ln 2}}\left(\frac{g_1}{g_2}\right)\frac{V}{\lambda^3}\,\frac{\Delta\nu\,\phi}{2t\nu_{1/2}} \tag{11}$$

where both sides of the equation have been multiplied by V, the volume of the ruby material. The factor ϕ is defined as the fraction of excited ions which decay by emitting the desired radiation. It has been inserted to account for the fact that ions are lost from the excited state by emission at wavelengths other than the desired one, or by non-radiative processes.

4. Mode Behaviour

Schawlow and Townes in reference (1), considered the ideal limiting case of oscillations in a Fabry-Perot type system in which only a single mode was excited by the oscillations. This situation is possible with extremely precise fabrication in a gaseous or vapor system and under

low temperature conditions, in a solid state device.[8] In general though, this idealized case of single mode generation has not been realized in a solid state laser at room temperature.

Crystal imperfections in the ruby material, end plate misalignment, temperature effects and internal reflections all contribute to introduce ambiguity in the mode selection process. That is, there may be a very large number of modes which are of equal status in contrast to the perfect situation where a single axial or nearly axial cavity mode closest to the atomic resonance peak is clearly the preferred one. The distortion of mode patterns because of strains, inhomogeneities, and deviations from single crystallinity in the material must be lived with until such time as ruby fabrication becomes more nearly an exact science. Temperature shifts which give rise to frequency sweeping and mode hopping can be combated. The sum total of the effects mentioned above, has given rise to the term multimoding, as applied to light propagation in fluorescent solids.

Consider the ruby laser system as shown in Figure II-2 (a). The condition for resonance in the system depicted is

$$\frac{n\lambda}{2} = l\sqrt{\epsilon} \qquad (12)$$

where n in this case is the number of half wavelengths in a cavity of optical length $l\sqrt{\epsilon}$. This is the equation for axial modes ($\theta = 0$) in the system.

8. See references (35) and (36).

For off axis resonant modes, the resonance condition is given by

$$m\lambda = 2\ell\sqrt{\epsilon}\cos\theta \tag{13}$$

A graphical representation of this formulation is shown in Figure II-4.

By focusing attention on the axial modes for the moment, one can draw the following conclusions: the separation in wave numbers between the axial modes is given by

$$\Delta\nu_{SEP}\,(cm^{-1}) = \frac{1}{2\ell\sqrt{\epsilon}} \tag{14}$$

The number of axial modes per unit λ per unit length is given by

$$\frac{1}{\ell}\frac{dm}{d\lambda} = \frac{-2\sqrt{\epsilon}}{\lambda^2} \tag{15}$$

For ruby where the fluorescent line width is $4A^{\circ}$ at room temperature, one is interested in the number of axial modes per centimeter of cavity length, i.e.,

$$\frac{\Delta m}{\ell} = \frac{1}{\ell}\frac{dm}{d\lambda}\Delta\lambda \cong 28 \text{ modes per cm of cavity length} \tag{16}$$

for a $\Delta\lambda = 4A^{\circ}$ and $\epsilon = 1.75$ for the ordinary ray from Appendix B.

The situation then in ruby is that there are many axial cavity modes within the line width of the transition in which one wishes to induce emission. (See Figure II-3 for a representation of the results of equation (16).) The Q of the individual modes is the same to a few parts in 10^4; hence there is no a priori preference by the ruby system to

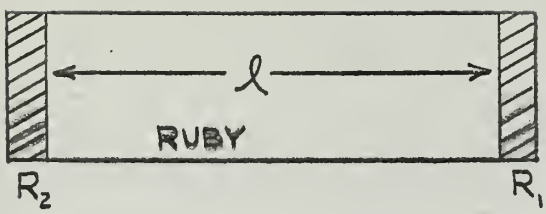

FIGURE II-2(A) RUBY FABRY-PEROT SYSTEM

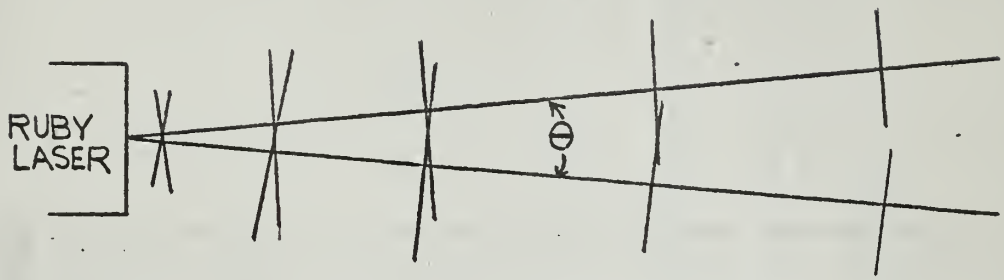

FIGURE II-2(B) LASER BEAM DIVERGENCE; STATE OF ART VALUE FOR $\theta = 0.5°$ TO $1.0°$ FOR D = 1cm LIMITING VALUE OF θ IS ~ 22 SEC. OF ARC

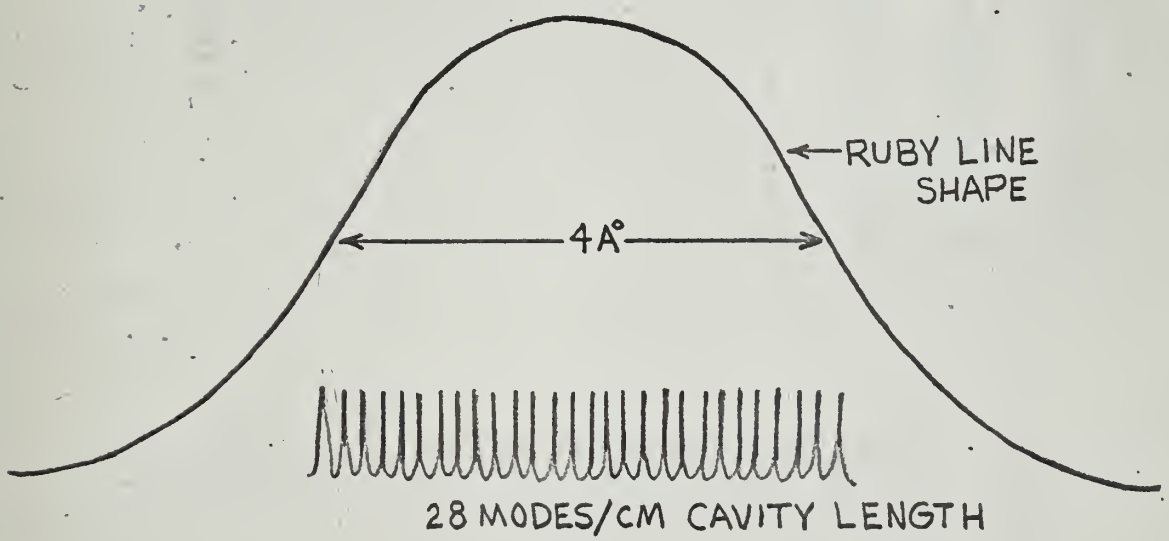

FIGURE II-3 RUBY LINE SHAPE AT 300° K AND CAVITY MODE STRUCTURE

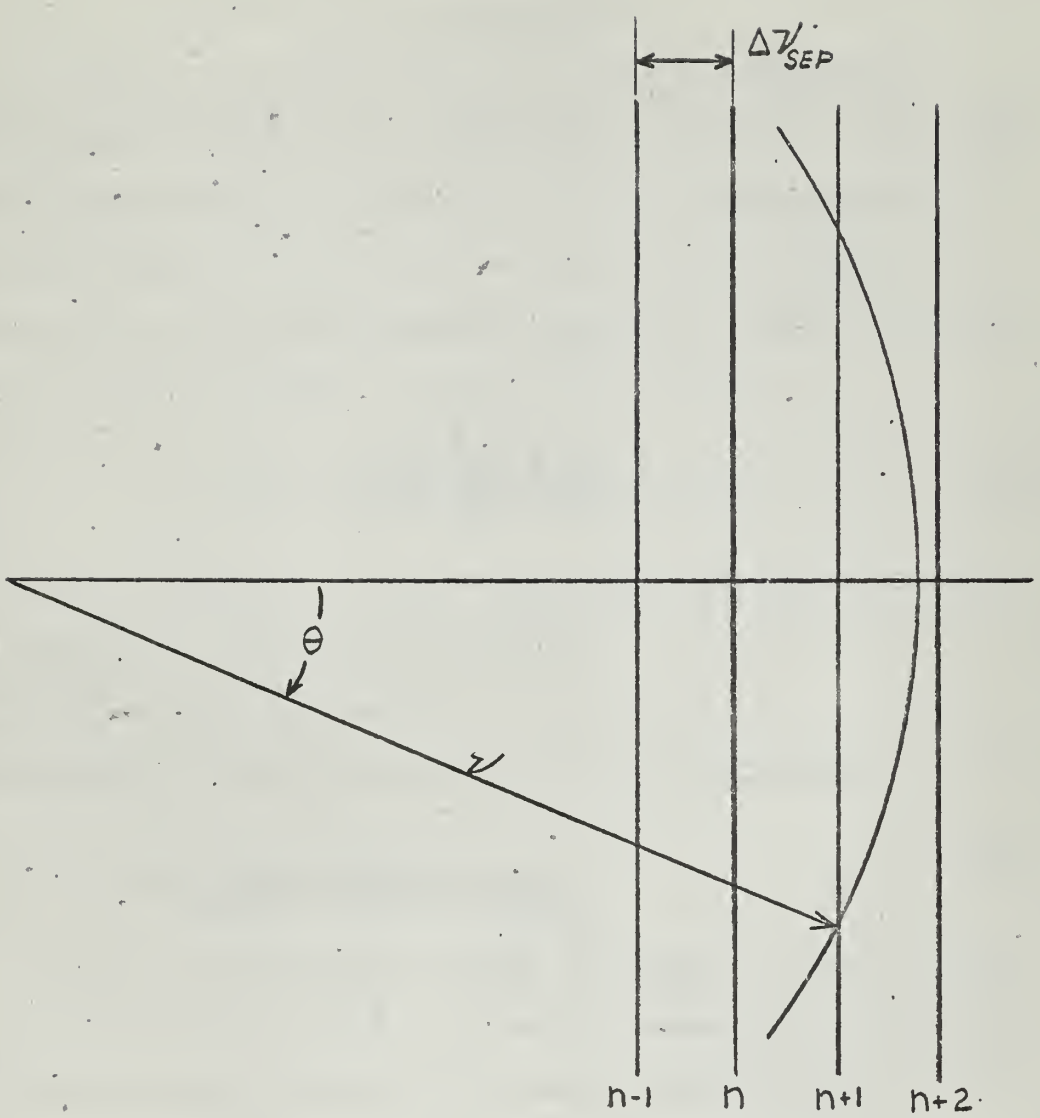

FIGURE II-4 FABRY-PEROT REPRESENTATION IN FREQUENCY K SPACE

oscillate in a particular axial mode. It therefore seems reasonable to expect the ruby laser to act as a multimode oscillator at least at room temperature.

It should be noted though, that when regeneration occurs, only the highest Q (axial or near axial) modes are excited appreciably. In practice, only a small number of the total number of modes may be excited, with crystal imperfections being the principal limitation, while theoretically the absolute number of modes is given by

$$P = \frac{8\pi^2 \nu^2 V \Delta\nu}{c^3} \qquad (17)$$

in a ruby of volume V. (In a ruby of 1 cm dimensions, the total number of modes is $\sim 2 \times 10^{11}$)

5. Resonator Quality Factor

Resonator quality factor, or Q, is defined as

$$Q = \omega \frac{\text{energy stored}}{\text{energy lost per cycle}} \qquad (18)$$

For the interferometer shown in Figure II-2(a), where the length of the ruby, ℓ, is large compared to the wavelength of the laser emission, an approximate cavity Q for mean reflectivities of $\sim$ .90 to .98 is given by

$$Q_c = \omega t = \frac{2\pi \ell \sqrt{\epsilon}}{\lambda(1-R)} \qquad (19)$$

where t, as defined by equation (10), may also be taken to be the mean decay time of photons moving perpendicular to the end plates. This "Q" is essentially for the axial modes of the cavity and neglects the effects of diffraction losses.

To account for the absorption (or emission) of energy

within the material itself, one can define a material Q by the following

$$Q_M = \frac{2\pi\sqrt{\epsilon}}{\alpha_{12}\lambda} \tag{20}$$

In terms of equations (19) and (20), one can write the marginal condition of laser oscillation as $Q_c \cong -Q_m$ where the frequency of the laser oscillator can be determined from

$$\nu_{12} = \frac{\nu_m Q_m + \nu_c Q_c}{Q_m + Q_c} \tag{21}$$

In this last equation, ν_c is the resonant frequency of the Fabry-Perot cavity and ν_m is the resonant frequency of the molecular system. ν_{12} is primarily determined by ν_m for $Q_m \gg Q_c$ and primarily determined by ν_c for $Q_m \ll Q_c$. In the later case, the frequency of oscillation is nearly directly proportional to the separation of the Fabry-Perot plates, L, for small changes in L.

SECTION III

THEORY OF THE "PULSED-REFLECTOR MODE" OF LASER OPERATION[1]

1. Laser Gain Equations for Normal Mode Operation

In the previous section it was seen that in order to obtain a light source wherein the individual radiators are made to work together and to radiate coherently, one must use the stimulated emission process. An incoming electromagnetic wave will force the excited ions in a material to radiate, if its direction of polarization is identical to that which is characteristic of the laser output it produces. Stimulated emission is always coherent with the driving radiation, that is, the phase of the stimulated emission does not fluctuate randomly but is controlled by the stimulating wave. At resonance the stimulated emission is exactly in phase with the driving radiation; off resonance it will lead or lag in phase compared to the stimulating wave, but by a fixed amount for each frequency. There is however always a component of stimulated emission in phase with, and of the same direction of polarization as the original wave.

For the purposes of this section, normal laser action can be described by the following equations, which are slightly different expressions of the theory of Section II.

The total gain over a two way path through the ruby must be ≥ 1 for laser action to occur. That is

1. The material in this section relies primarily on references (13), (35) and (36). It is also the result of many illuminating discussions with Dr. E. J. Woodbury of Hughes Aircraft Company.

$$G = T_1 T_2 R_1 R_2 e^{2\alpha \ell} \geq 1 \qquad (1)$$

Where T_1 and T_2 are the transmittance of the ruby end surfaces, R_1 and R_2 are the reflectivity of the end plates, ℓ is the length of the ruby rod and α is the absorption coefficient as defined in Section II.

Assume $T_1 = T_2$ and let $R = \sqrt{R_1 R_2}$, the mean reflectivity. Let the loss factor for the system be defined as

$$\gamma = -\ln RT^2 = -\frac{1}{2} \ln R_1 R_2 T^2 \qquad (2)$$

Where T, the transmittance, is equal to one minus the reflectivity and shall refer to all optical boundaries in the path of the laser beam. For the present we are concerned with the ruby end surfaces, therefore $T^2 = (1-L_r)^2$.

Taking the log of both sides of equation (1) we have,

$$-\frac{1}{2} \ln R_1 R_2 T^2 + 2\alpha \ell \geq 0 \qquad (3)$$

or upon substitution,

$$-\frac{1}{2} \ln R_1 R_2 (1-L_r)^2 + 2\alpha \ell \geq 0 \qquad (4)$$

It follows that

$$\alpha \geq \frac{\gamma}{\ell} \qquad (5)$$

This is the necessary condition for laser action to occur, that is, for sustained oscillations to be built up within the system.

2. Effect of a Kerr Cell on System Operation

A material which can be made to exhibit laser action at some particular wavelength can also be made to emit giant induced fluorescent pulsations, i.e., controlled pulsations, many orders of magnitude more intense than what one would obtain with the same laser under normal mode operating conditions. These giant pulses of stimulated emission result when the level of laser regeneration is switched from a low to a high level. The reason for this is that energy stored in the form of excess Cr^{+++} ions above threshold is different before and after switching and this differential in population excess must be liberated in the form of light energy in a laser beam. This light possesses the monochromaticity, coherence, and directionality characteristic of strong laser emission.

The method used to switch the laser system from an environment of high regeneration to one of low regeneration, is to insert an optical switch in the propagation path between one end of the ruby rod and a detached reflector.

Consider Figure III-1 which depicts a Kerr cell shutter as the optical switch. Theoretically, the effect of the Kerr cell is to alter the polarization of reflected laser light in a controllable manner. A brief description follows. (See Appendix A for a detailed discussion of Kerr cell effects.)

The c-axis of the ruby rod is perpendicular to the direction of propagation of the laser beam. The laser beam is essentially plane polarized with the direction of the

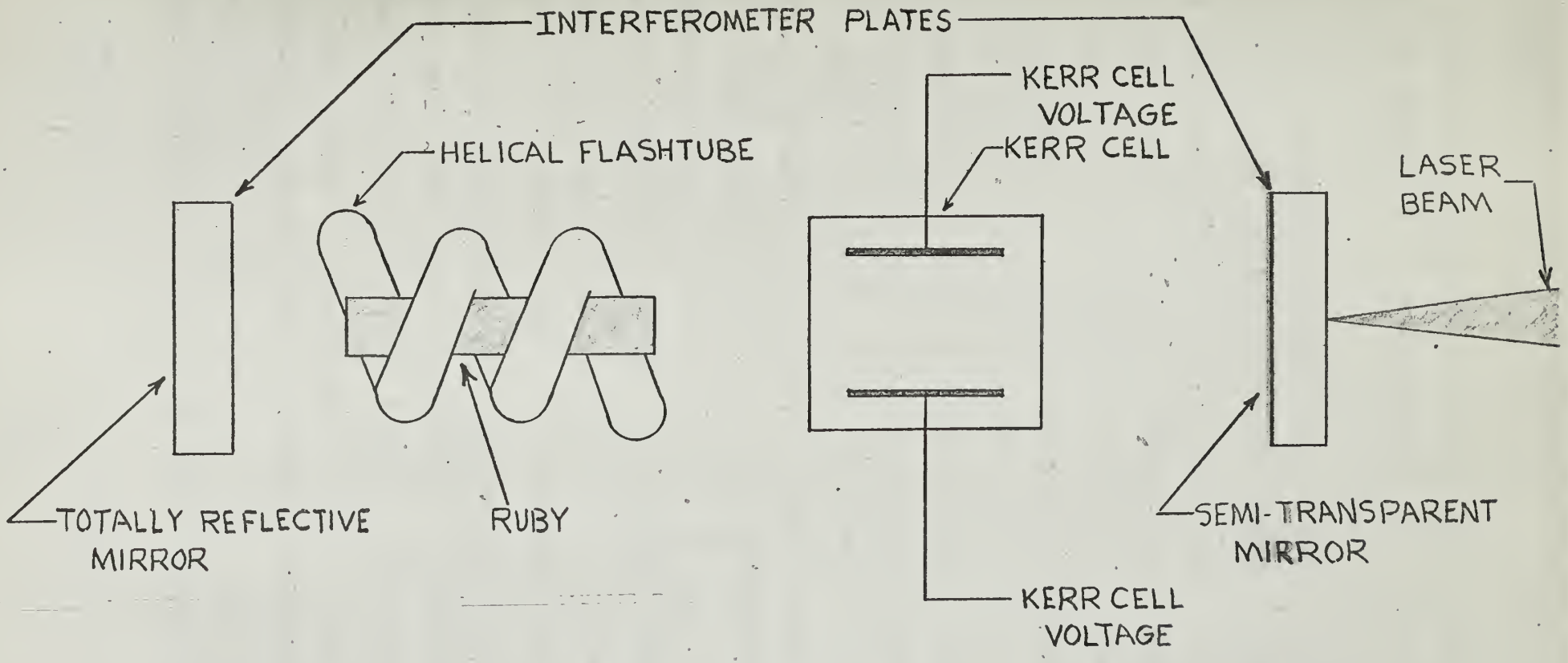

FIGURE III-1 SCHEMATIC DRAWING OF PULSED REFLECTOR MODE LASER SYSTEM WITH A KERR CELL AS THE OPTICAL SWITCH

$\mathcal{E}$-vector being perpendicular to a plane formed by the c-axis and the direction of propagation.[2] When the Kerr cell is activated so that light passing through and reflected back has its polarization changed (i.e., a 90° retardation), so that now it is orthogonal to the original polarization of the laser beam, then on every other pass of light through the ruby, there is little interaction with the excited chromium ions in the material. The losses upon reflection at the detached end plates remain essentially unaltered so that, when the Kerr cell is active we have the condition of low regeneration. That is to say the gain through the system no longer equals the losses in the system when the Kerr cell is activated. This discrepancy corresponding to the low regeneration condition, causes a significant effect in the peak power output, due to the higher build up in population excess one can obtain before the onset of laser action. (When the Kerr cell is inactive, there is high regeneration just as in a conventional or normal mode laser.) If the total phase retardation of the Kerr cell is δ for light passing back and forth through the cell, and if there is no appreciable time phase memory for light passing back and forth through the ruby, then the cell may be though of as transferring a fraction $\sin^2(\delta/2)$ of light from the laser polarization to the orthogonal polarization and also transferring the same fraction of entering light of orthogonal polarization back to the laser polarization.

2. See experimental results of Section V for further detail.

The following equations are presented to help clarify the action of the Kerr cell shutter in holding off laser action.

The two pass gain through the ruby is given by equation (1). With the Kerr cell in the optical path, we have the following gain equation.

$$G_2 = T_k^2 R_1 R_2 e^{2\alpha' l} \tag{6}$$

In the above equation,

$$\alpha' = \alpha \cos\theta \tag{7}$$

where θ is the angle between the c-axis and the cylindrical axis of the ruby, and T_K designates the transmission through the Kerr cell surface.

The total gain of the system is now given by the product of equations (1) and (6) as follows.

$$G = G_1 G_2 = T_k^2 T_r^2 (R_1 R_2)^2 e^{2(\alpha+\alpha')l} \tag{8}$$

One can term this equation as the marginal gain equation since, for $G > 1$ the system is oscillatory and laser action occurs, and for $G < 1$ the system is non-oscillatory.

Following the same procedure applied in equations (1) through (5) and substituting equation (7) into our marginal gain equation we have

$$l_n R^4 (1-L_r)^2 (1-L_k)^2 + 2\alpha(1+\cos\theta) l = 0$$

or,

$$4 \ln R (1-L_r)^2 (1-L_k)^2 + 2\alpha (1+\cos\theta) \ell = 0 \qquad (9)$$

and finally,

$$\alpha \geq \frac{2\gamma}{(1+\cos\theta)\ell} \qquad (10)$$

for laser action to occur. We may conclude from this equation that, (a) a higher value of α is now required before stimulated emission is obtained as compared to equation (5), and (b) the use of a ruby with a 90° c-axis is the optimum selection one can make to obtain the highest value of peak power output.

Equation (9) is for the case of no voltage on the Kerr cell. For each value of applied voltage one can determine the theoretical transmission through the nitrobenzene in the cell from Appendix A. The loss factor in equation (10) above becomes

$$\gamma = -\ln R (1-L_r)^2 (1-L_k)^2 S_k \qquad (11)$$

where S_k is actually the percentage of incident light that is transmitted through the Kerr cell and directed into the end surface of the ruby rod expressed as a decimal fraction.

3. Effect of a Wollaston Prism on System Operation

Before discussing the characteristics of the "Pulsed-Reflector Mode" laser system upon addition of a Wollaston prism, consider first the physical orientation of the component parts with respect to each other.

It is imperative that the ruby and Kerr cell be at a 45° angle with respect to each other.[3] In this manner one obtains a component of the ruby $\mathcal{E}$ -vector parallel and perpendicular to the optic axis of the Kerr cell which is coincident with the applied electric field vector in the cell. The ruby $\mathcal{E}$ -vector and the angle at which the Wollaston prism is positioned must be identical. If either of the above orientations are inaccurate, then maximum power output will not be achieved for the following reasons. In the first case, the Kerr cell will not be operating on the maximum component of the ruby $\mathcal{E}$ -vector in both the ordinary and extraordinary ray directions; in the second case light emerging from the Wollaston prism will be divided into both an ordinary and extraordinary ray. If the system is optically aligned to give maximum reflection to the extraordinary ray, then the energy contained in the ordinary ray will be lost, since this is directed entirely out of the path of propagation, by virtue of the alignment.

Finally, the positioning of the optical switch between the ruby and one of the detached reflectors has no bearing on successful operation of the system. In Figure III-2(a) and Figure III-2(b) the optical switch is shown positioned between the semi-transparent reflector and the ruby. Positioning it between the non-transparent reflector and the ruby is just as acceptable.

With regard to the pulsed reflector scheme depicted

3. See Appendix A for the analytical reasoning to support this statement.

in Figure III-2(a) and assuming that optical alignment has been achieved, the system will exhibit action when the voltage applied to the Kerr cell is suddenly turned off. With $\lambda/4$ retarding voltage on the cell, the system operation is as described in this section. The laser light passes through the first half of the prism undeviated, and becomes the extraordinary ray upon entering the second half of the prism. Presumably we have aligned the system to reflect the extraordinary ray.[4] Passing through the Kerr cell and reflected back, the polarization is now orthogonal to its original direction. As such it becomes the ordinary ray upon entering the second prism half of the Wollaston on its return toward the ruby. Emerging from the first half of the prism, the returning optical fluorescence is diverted completely out of the system due to the fact that it is the extraordinary ray in this portion of the Wollaston.

To describe the foregoing sequence of events in equation form, we can expand on equation (11) as follows,

$$\gamma = -\ell_m R_1 R_2 (1-L_r)^2 (1-L_R)^2 (1-L_W)^2 S_R S_W \qquad (12)$$

where, L_W represents the reflected losses at the surface of the Wollaston prism and S_W is the percentage of light transmitted through the prism and directed into the end of the ruby rod. In Figure III-2(a), S_W is theoretically zero as long as the Kerr cell is on. Therefore in equation (10),

4. See Section V for a more detailed coverage of system alignment.

the absorption coefficient, α , must be greater than an extremely high value before the on set of laser action. The immediate conclusion is that one is able to hold off laser action regardless of the amount of pumping energy input to the ruby, as long as the Kerr cell is activated, thus allowing a much higher build up of excess population of chromium ions. When the Kerr cell is switched off, this high excess population is forced to radiate as a giant pulse of stimulated optical emission by the returning light, which is now back to its original direction of polarization, i.e., coincident with the direction of the ruby $\mathcal{E}$ -vector.

The sequence of events for operation of the pulsed reflector scheme as shown in Figure III-2(b) is analagous to the preceding explanation. For the system as shown, the optical fluorescence from the ruby traverses the propagation path undeviated only when the Kerr cell is on. It is important to note that the only primary distinction between the two schemes shown, is that the second system is optically aligned for the ordinary ray from the Wollaston, whereas in the first system the stimulating wave was the extraordinary ray from the prism. Obviously the Kerr cell voltage is different in each case, as well as the condition under which laser output is obtained. The point to be made here is that in both schemes it is the alignment of the system which is the most critical variable.

Clarification of the optical role played by the Wollaston prism, and features about the output pulse shape and optical alignment will be covered in latter sections.

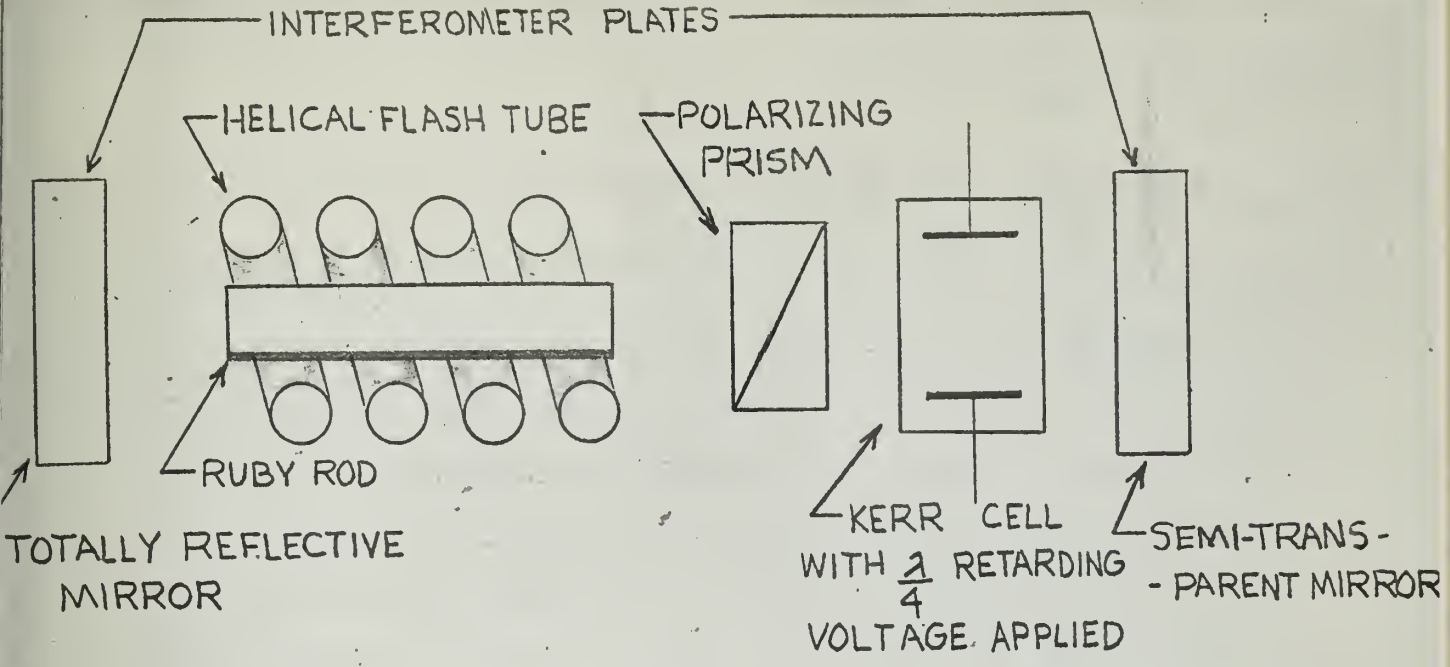

FIGURE III-2(A) PULSED REFLECTOR MODE SCHEME WHEREBY LASER OUTPUT PULSE OCCURS WHEN KERR CELL IS SWITCHED OFF

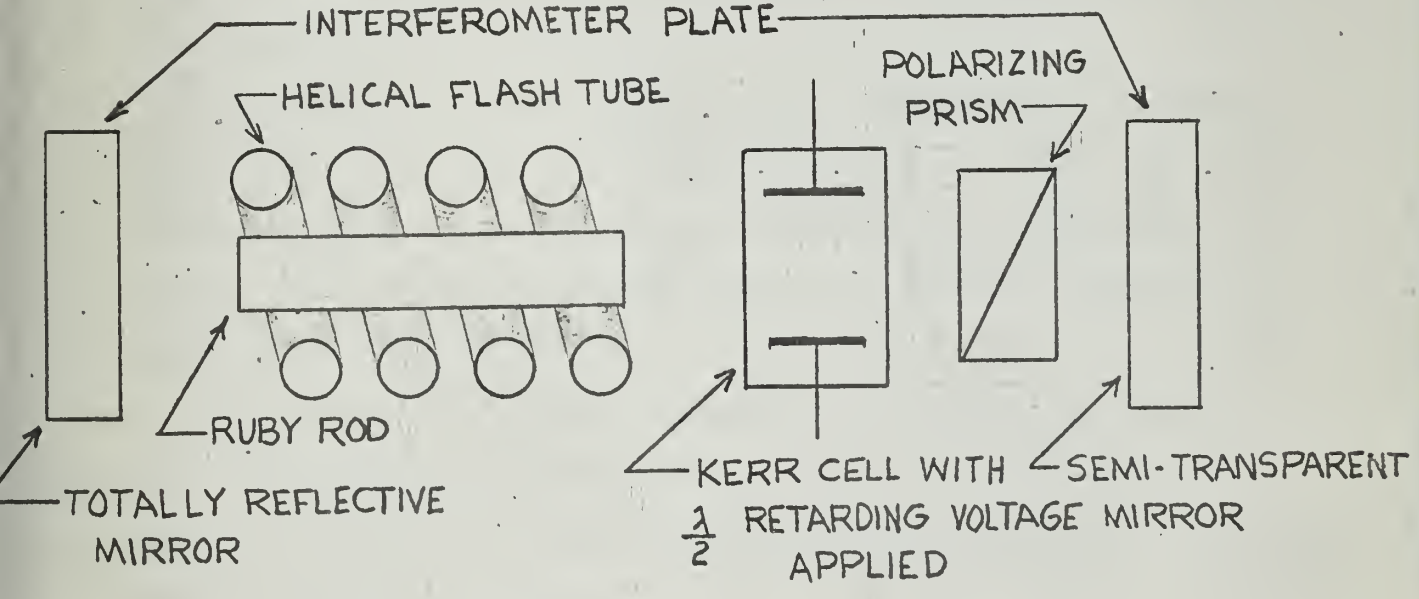

FIGURE III-2(B) PULSED REFLECTOR MODE SCHEME WHEREBY LASER OUTPUT PULSE OCCURS WHEN KERR CELL IS SWITCHED ON

SECTION IV

DESCRIPTION OF EQUIPMENT AND EXPERIMENTAL UTILIZATION

1. Spectral Transmission Characteristics of the Detached Reflectors

The two detached reflectors utilized in the "Pulsed-Reflector Mode" laser system, were made of fused quartz with multi-layer dielectric coatings on one surface.[1] The surfaces of each flat were held parallel to within two seconds of arc during the production process, in accordance with specifications stipulated by the Laser Research and Development group at Hughes Aircraft Company.

The multi-layer optical films applied to each flat were, by specification, supposed to render one reflector semi-transparent with a reflectivity, R, on the order of 60 percent, and the other flat totally reflective with R being equal to 100 percent.

In order to determine the exact reflectivities of the two flats at the ruby wavelength of 6943A°, the spectral transmission characteristics were measured by the author, using a Cary Recording Spectrophotometer Model 14 shown in Figure IV-1(a).

The Model 14 spectrophotometer is designed for automatic recording of absorption spectra in the wavelength region of 1860A° to 26,000A° with good resolving power and high photometric accuracy.

Utilizing a logarithmic slidewire, the instrument records in absorption units. Also available is a linear

1. See Appendix C

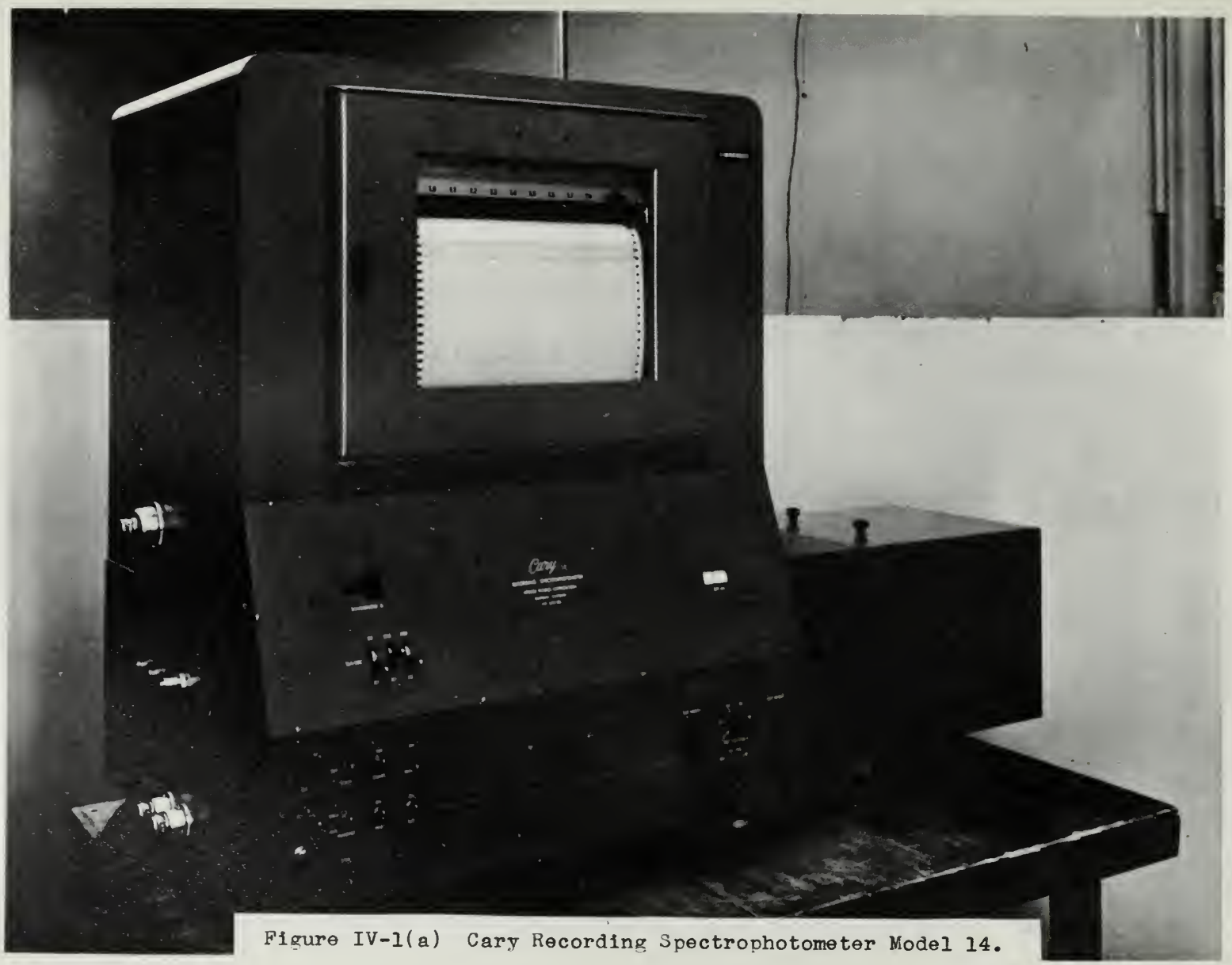

Figure IV-1(a) Cary Recording Spectrophotometer Model 14.

wavelength scale slidewire which permits recording percent transmission versus wavelength directly.

Three light sources are available with the instrument,

(1) A tungsten lamp for the visible region, .2μ -.35μ.

(2) A hydrogen lamp for the ultraviolet region, .30μ -.65μ .

(3) A tungsten lamp for the infrared region, .6μ -2.6μ.

The light sources are interchangeable through proper selection, but water cooling is required before lamps (2) and (3) above can be utilized. Two receivers were also available with the instrument, one a 1P28 multiplier phototube for the ultraviolet and visible regions, and the other, a lead sulfide cell for the IR region.

The spectrophotometer employs a double monochromator consisting of a 30° fused silica prism in series with a 600 line per millimeter echelette grating, each with its own collimating system of mirrors and slit system. Both halves of the monochromator operate with an aperature ratio of f/8; focal length for the prism collimator is 30 cm, and for the grating collimator the focal length is 40 cm. The monochromatic radiation from the exit slit when in the visible or ultraviolet region, is alternately sent at 30 cps, through the reference cell and sample cell by means of the photometric optical system provided.

The scanning range of the monochromator is 1860A° to 3μ, with scanning speed being variable from .5A°/sec to 500A°/sec.

The wavelength scale is accurate to better than 4A° and reproduces to better than .5A°. The resolving power of the

monochromator is approximately 1A° in the ultraviolet and visible range, and approximately 3A° in the near IR. The exit slit width was adjustable from 0 to 3 millimeters and slit height could be varied from 20 millimeters in the visible range to 7 millimeters in the IR range.

Using the spectrophotometer in the visible range with the reference cell blank and the flat whose characteristics are to be measured in the sample cell, the range from 4000A° to 8000A° was scanned at 25A°/sec. The recorded data is plotted in Figure IV-1(b) for the semi-transparent flat and in Figure IV-1(c) for the totally reflecting flat. The corresponding reflectivities at 693A° were noted as being 99.8 percent and 48.5 percent respectively.[2]

2. Optical Alignment of the Normal Mode Laser System

In order to prevent the laser beam from gradually "walking-off" the edge of the detached reflectors and causing an unnecessary decrease in energy output, it is essential that the two detached reflectors which make up the external Fabry-Perot Interferometer be aligned to a high degree of parallelism.

To achieve this high degree of parallelism, the Davidson Optronics Autocollimator as shown in Figure IV-3(a), was utilized.

With reference to Figure IV-2, the following pertinent facts about the optical autocollimator are noted:

(1) Source of illumination is a mercury lamp. Light

2. For further notes on spectrophotometry see Appendix D

SPECTROGRAPH FOR FUSED QUARTZ SEMI-TRANSPARENT OPTICAL FLAT

PERCENT TRANSMISSION vs WAVELENGTH

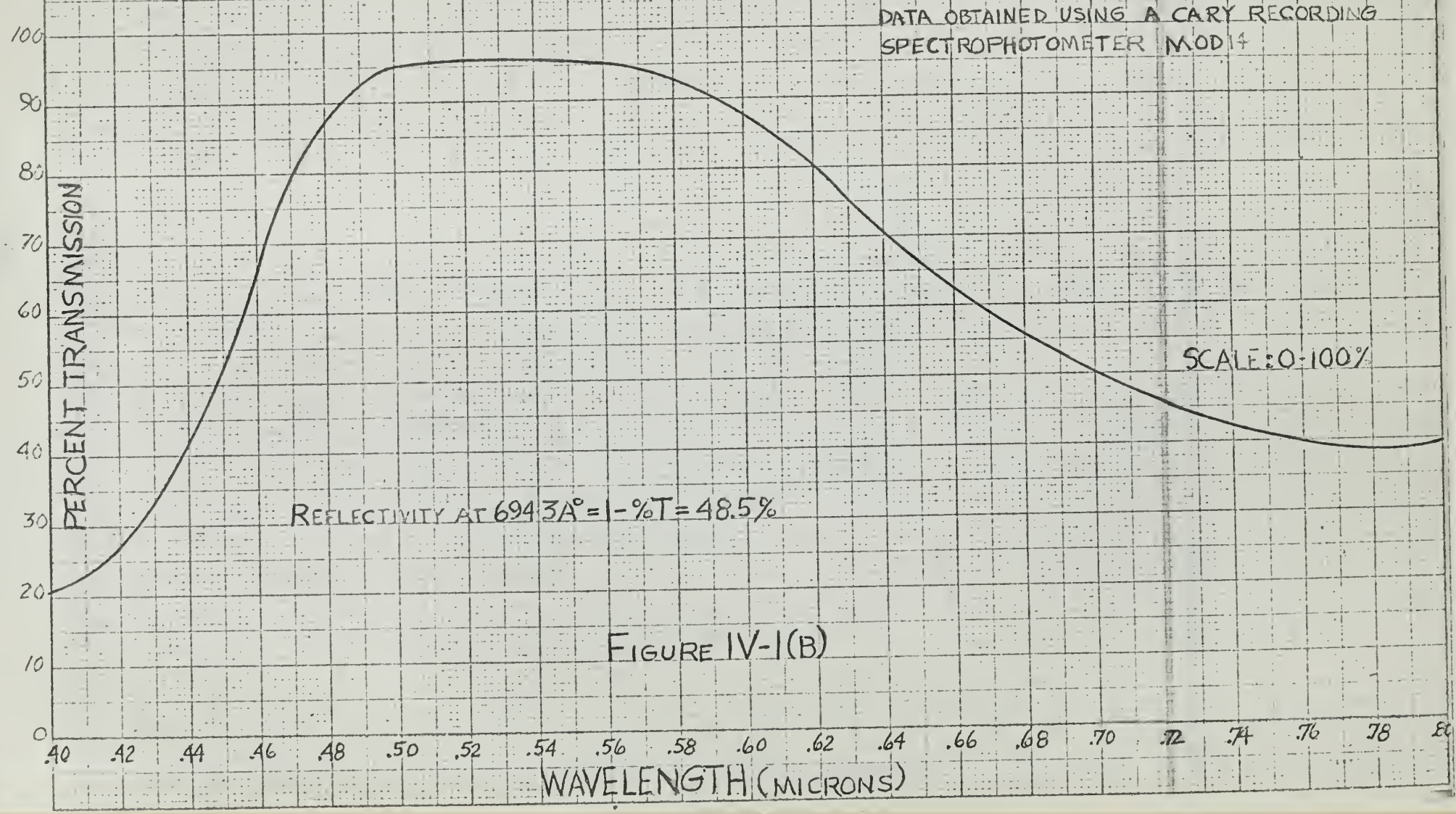

FIGURE IV-1(B)

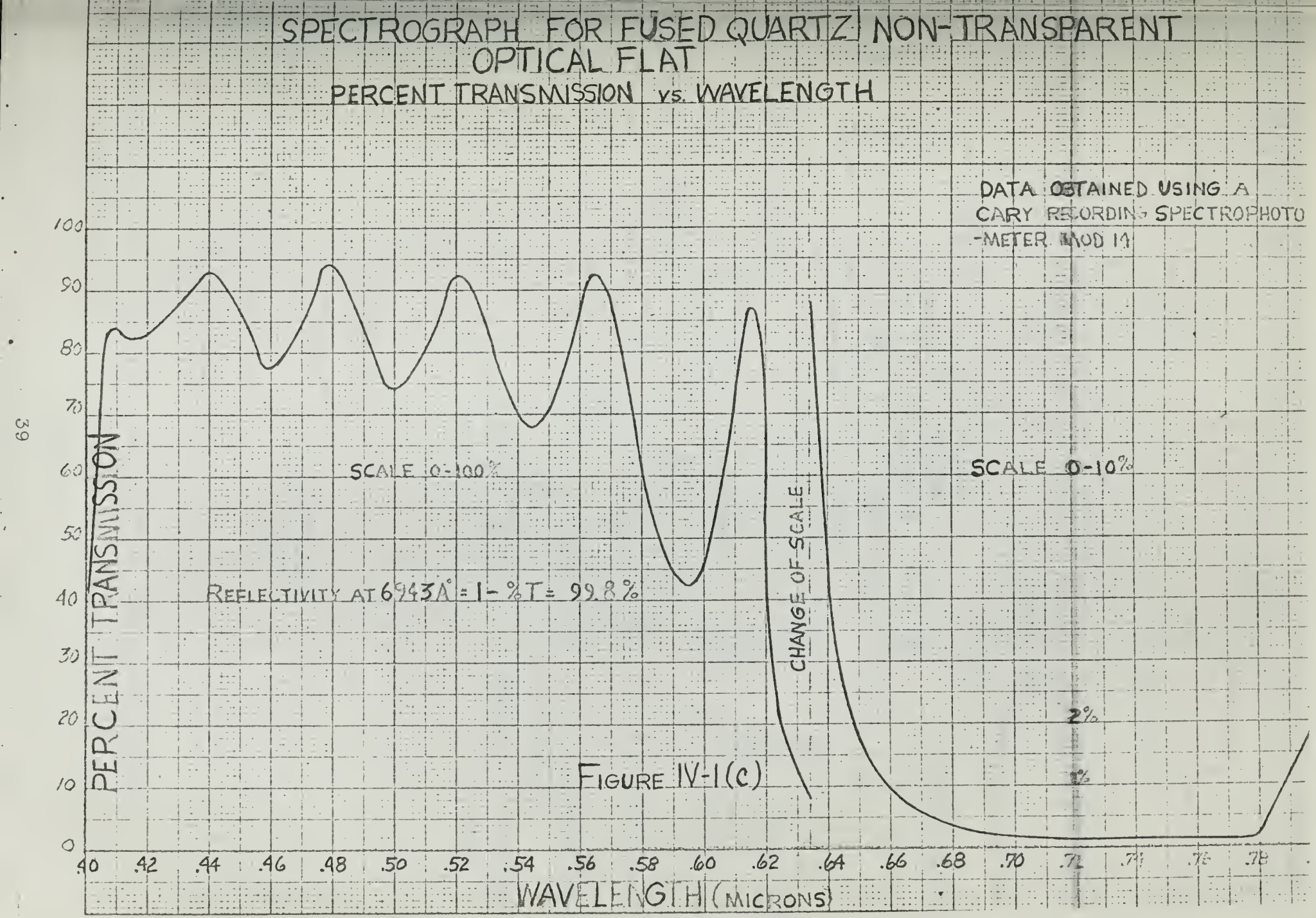
SPECTROGRAPH FOR FUSED QUARTZ NON-TRANSPARENT OPTICAL FLAT
PERCENT TRANSMISSION vs. WAVELENGTH
DATA OBTAINED USING A CARY RECORDING SPECTROPHOTO-METER MOD 14
PERCENT TRANSMISSION
100
90
80
70
60
50
40
30
20
10
0
SCALE 0-100%
SCALE 0-10%
REFLECTIVITY AT 6943Å = 1 - %T = 99.8%
CHANGE OF SCALE
2%
1%
.40
.42
.44
.46
.48
.50
.52
.54
.56
.58
.60
.62
.64
.66
.68
.70
.72
.74
.76
.78
WAVELENGTH (MICRONS)

FIGURE IV-1(c)

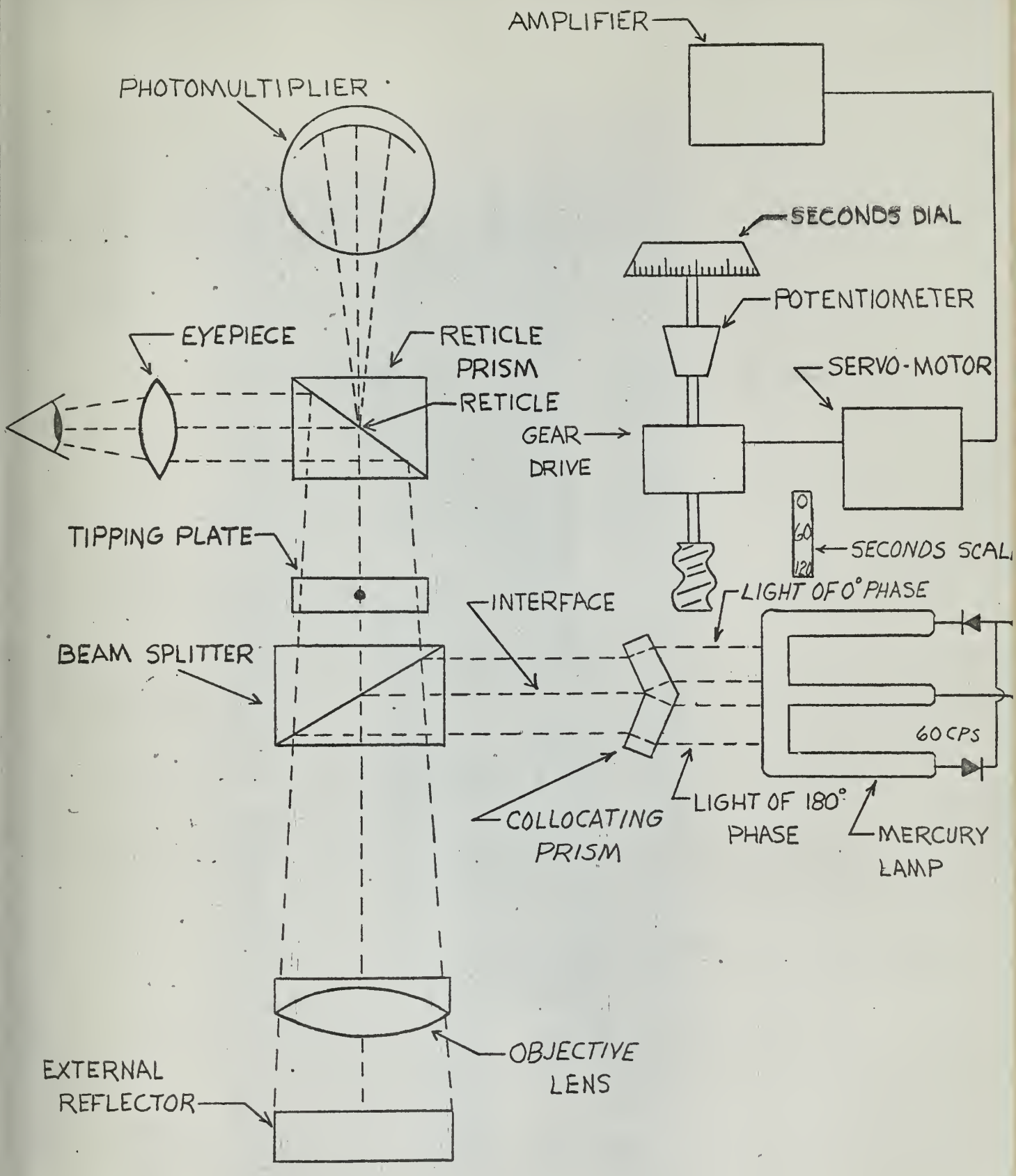

FIGURE IV-2 BLOCK DIAGRAM OF OPTICAL AUTOCOLLIMATOR

Figure IV-3(a) Davidson Optronics Autocollimator and Power Supply.

from one half of the lamp is 180° out of phase with light from the other half.

(2) The two halves of light pulsate out of phase with each other and the resulting light from the objective lens is thrown out in a parallel beam.

(3) The collocating prism consists of two prisms mated together, the intersection of which forms the interface between the two phases of light, as viewed in the eyepiece.

(4) Light reflected back into the objective lens from the detached reflectors is brought to both the eyepiece and a photomultiplier tube. Division of the light to each of these locations is accomplished by a reticle prism.

(5) In the eyepiece, the two out of phase light fields in the returning light beam appear to be contiguous, with a dividing interface which is sharply discernable. The position of the interface with respect to the phototube slit on the reticle prism can be observed in the eyepiece.

(6) The phototube slit admits light to the tube for generation of a control signal.

(7) Depending on whether the light received by the phototube is of one phase or the other, the associated electronics drives a servomotor in one direction or the other.

(8) The servo drives a tipping plate which offsets the return image of the interface, so that, in the eyepiece

the interface appears to move over until it is superimposed on the phototube slit. The phototube then receives an equal amount of light of both phases and the servomotor control signal goes to zero.

(9) The phototube slit is on the optical axis of the instrument, so that the angle through which the tipping plate has had to turn is a measure of the angle that exists between the optical axis and the beam returning from the external reflectors. The rotation of the tipping plate is coupled to a pointer and scale reading tens of seconds (zero to 120 seconds), and to a dial reading units and tenths of seconds.

(10) When the tipping plate is normal to the optical axis, the pointer indicates a mid-scale reading, i.e., 60 seconds.

The experimental setup for alignment of the detached reflectors is depicted in Figure IV-3(b). Under operating conditions, the ruby and flashtube would not be interposed between the reflectors. It would have been extremely helpful if the flats and ruby end surfaces could have been aligned parallel to each other with the aid of the autocollimator. Unfortunately, the end surfaces of the ruby are too small of an area to give a satisfactory reflection for the autocollimator.[3]

As shown in Figure IV-3(b), the autocollimator was mounted on the optical bench so as to sight through the

3. See Section V for calculation of percent reflection from the end surfaces of the ruby rod.

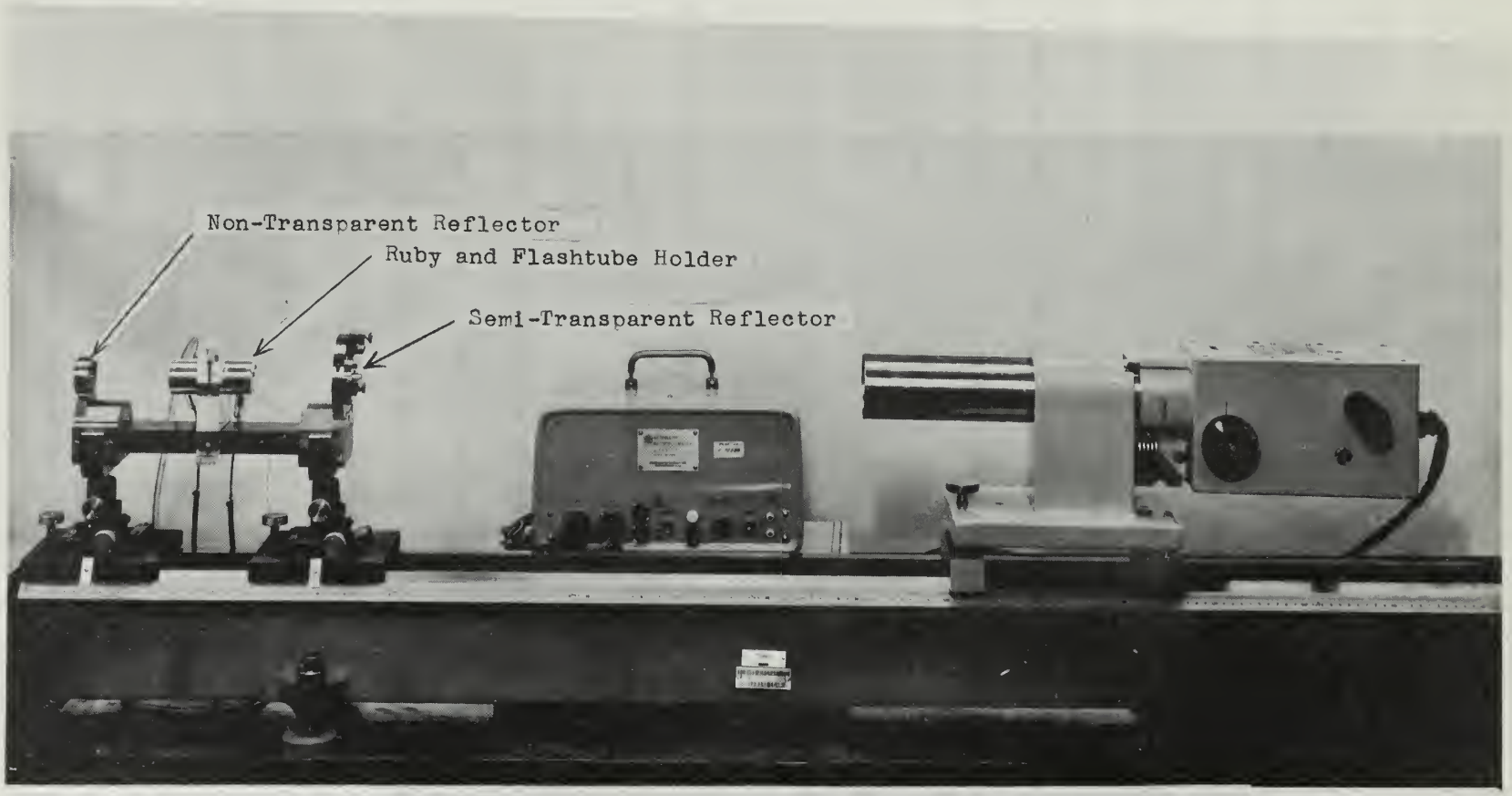

Figure IV-3(b) Optical Alignment Setup for Normal Mode Laser Showing Ruby and Flashtube Cavity Interposed between Reflectors.

adjustable flat to the fixed optical flat. The semi-transparent reflector was made adjustable by varying two differential screws, one for horizontal adjustment, the other for vertical adjustment. One full turn of either differential screw equaled .002 inches of travel. A blue field reflection from the variable reflector and a green field reflection from the fixed reflector were observed in the eyepiece of the autocollimator. In each of these two fields an interface was distinguishable. Alignment of the two reflectors was accomplished by bringing the interfaces into coincidence as observed through the eyepiece. It was concluded that the degree of parallelism of the two reflectors was accurate to less than one second of arc. After alignment in the horizontal plane, the autocollimator was rotated 90° on its mount and vertical alignment was achieved.

3. Exciter for Laser Pumping Source

The typical Laser output consists of a series of pulsations.[4] In order to concentrate this output into a few high energy pulses, the pulse forming network as shown in Figure IV-4(a), was used to store and deliver electrical energy to the helical, xenon filled flashtube, used to generate the noncoherent optical excitation required for laser pumping.

The variable length pulse forming network, is essentially a lumped constant transmission line. Consequently, when the line is discharged into its characteristic impedance, the stored energy appears as a rectangular pulse with an amplitude

4. See experimental results recorded in Section V.

of one-half the charging voltage.[5]

The line was initially conceived to handle gas discharge tubes with impedances between 1 and 2 ohms and maximum ratings of 4000 volts and 3200 joules input. The line was designed with eight equal sections with the maximum storage capacity required for each section being 400 joules at 8000 volts. From the equation,

$$E = 1/2\ CV^2 \qquad (1)$$

the capacity of each section is 12.5 microfarads. The inductance for each section is determined from the relationship,

$$Z = \sqrt{L/C} \qquad (2)$$

where Z, the line impedance was chosen equal to 1.4 ohms, a compromise between the impedance of the various discharge tubes. L is thus 25 microhenries.

The characteristic time per section is given by,

$$T = 2\sqrt{LC} \qquad (3)$$

which gives 35 microseconds per section or 280 microseconds for all eight sections. Control of pulse length and pulse shape are thus obtained by adding or removing capacitors; fine control is permitted by adding half sections of line through utilization of the intermediate taps on the coil.

With reference to the block diagram of the exciter shown in Figure IV-4(b), the ignitron switch prevents self

5. See reference (29) for more detailed information on this topic.

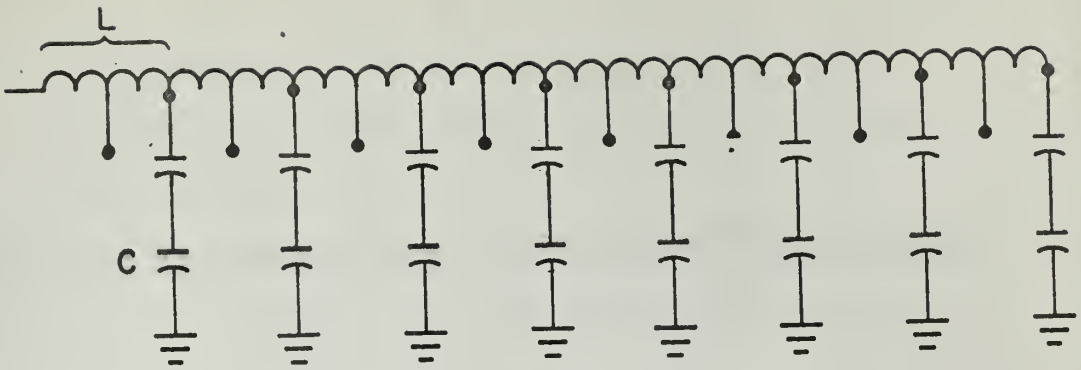

C = 25 μfd 4000 VOLT
L = 25 μh

Figure IV-4 (a) Variable Length Pulse Forming Network

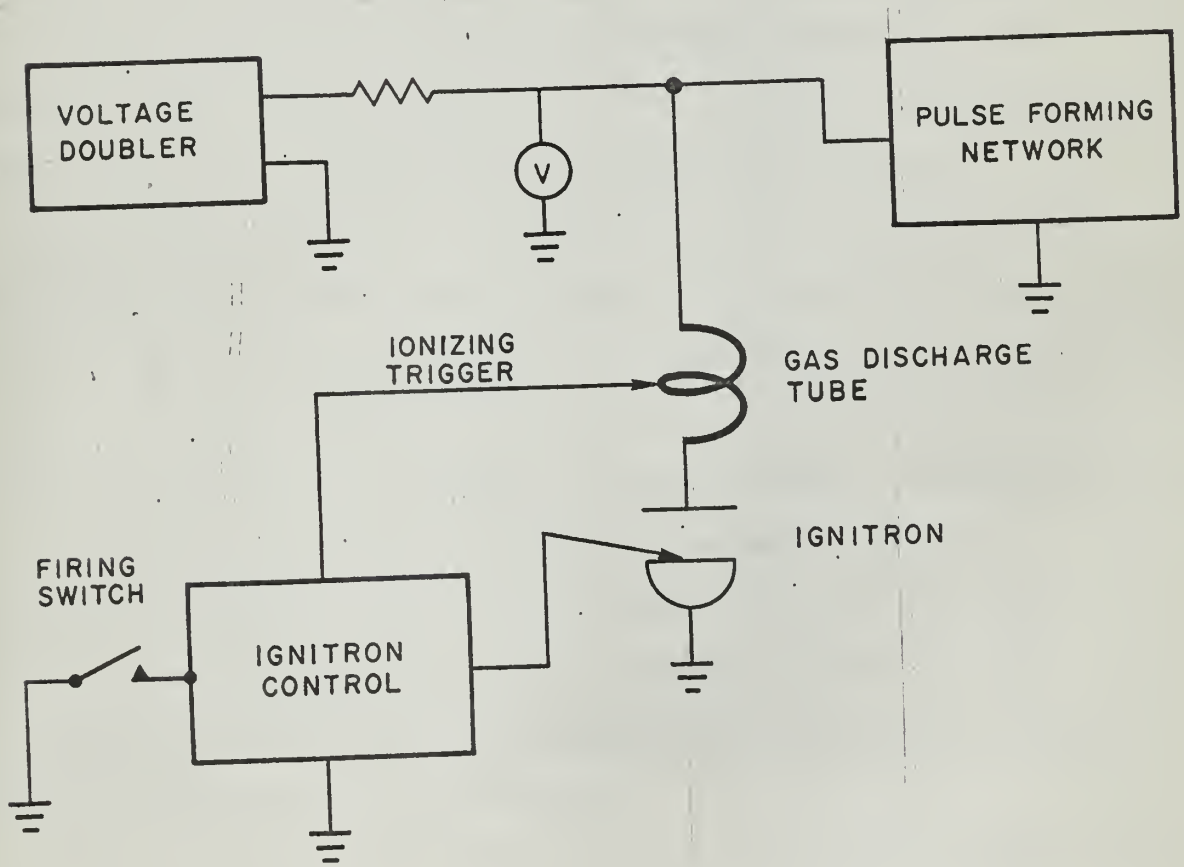

Figure IV-4 (b) Block Diagram of Exciter for Laser Pumping Source

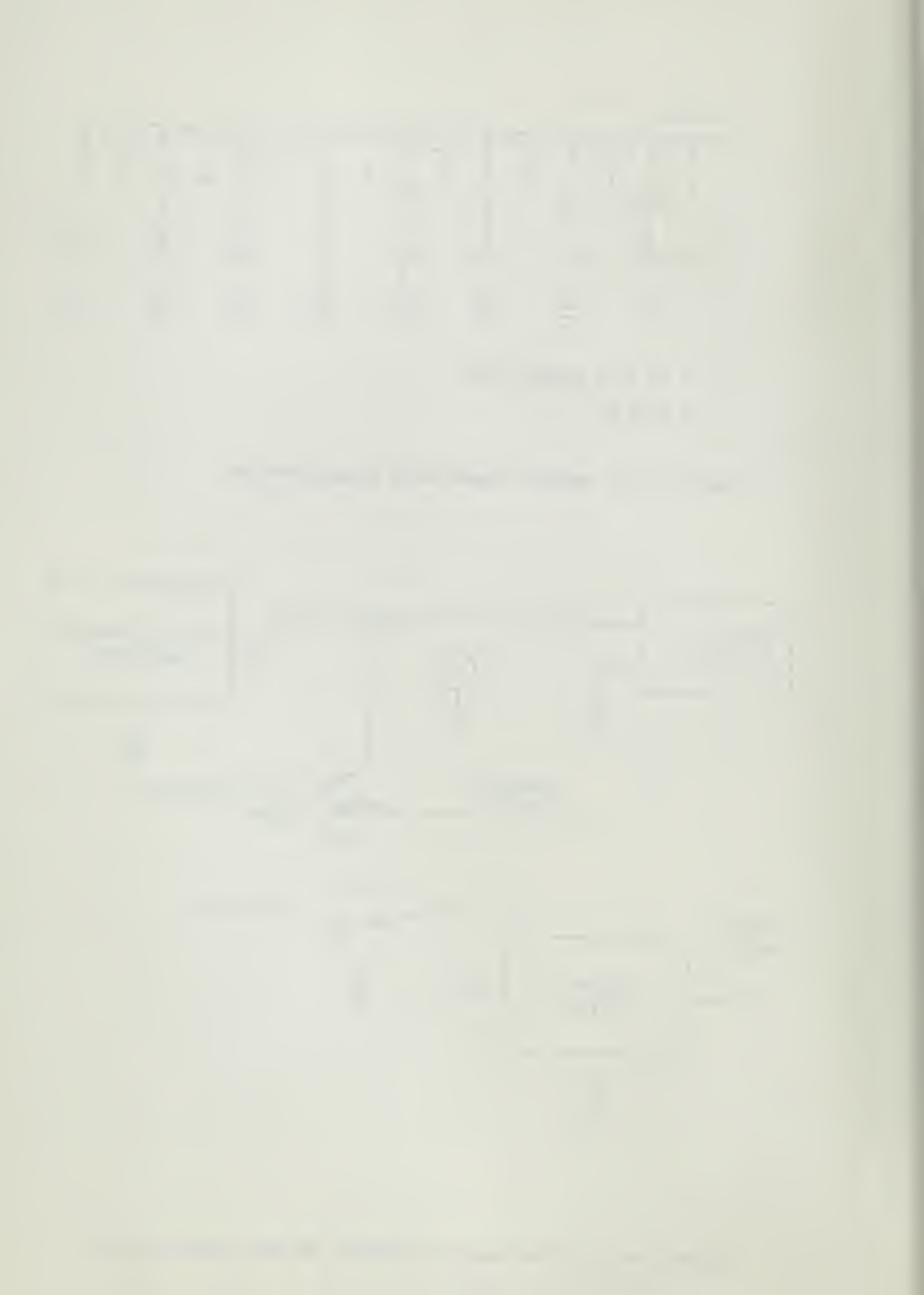

flashing of the tube before the delay line is fully charged to twice the voltage desired at discharge. The ignitron switch also serves as a diode clamp to prevent line oscillation.

The fully assembled exciter and pulse forming network currently in use at Hughes Aircraft Company is shown in Figure IV-4(c) and Figure IV-4(d).

4. Physical Characteristics of the Optical Switch

The optical switch, essential to the "Pulsed-Reflector Mode" of laser operation, is composed of the Kerr cell shutter as shown in Figure IV-5(a) and the Wollaston prism as depicted in Figure IV-6.

One should first of all direct their attention to the Kerr cell, the more critical (from the standpoint of operation) of the two components which make up the switch.

Isotropic transparent substances become doubly refracting when placed in an electric field, the behaviour being like that of a uniaxial crystal with the optic axis in the direction of the applied electric field. This property was discovered in 1875 by Kerr and is known as the "Kerr effect".

The molecular interpretation of the Kerr effect is based on recognition that the individual molecules of the medium are anisotropic. Without an applied electric field the molecules are oriented at random, and so the anisotropic properties are lost on the average.

The applied electric field acts to produce a partial statistical orientation so that now the anisotropic properties of individual molecules no longer average out complete-

Figure IV-4(c) Front Exterior View of Exciter.

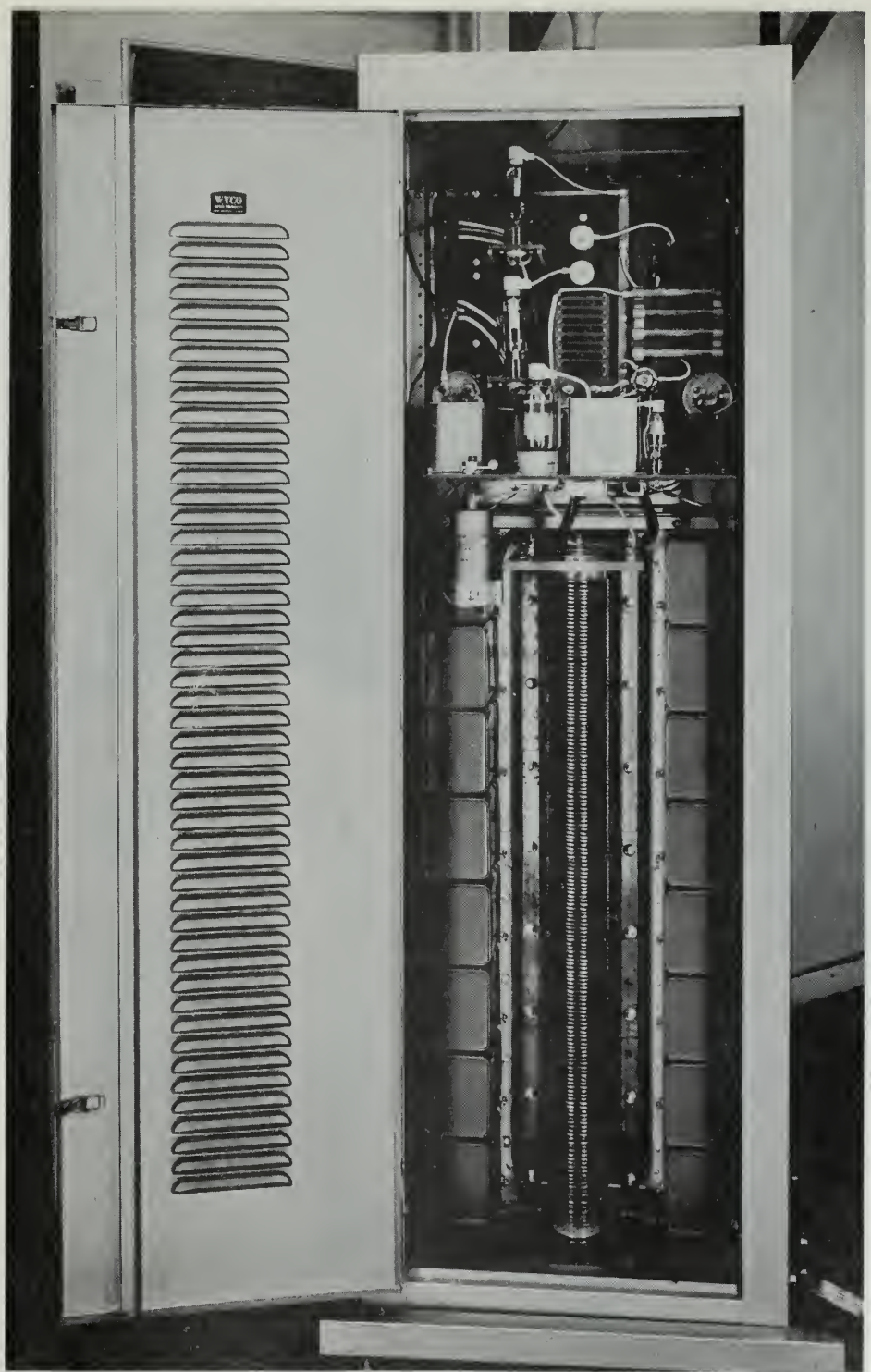

Figure IV-4(d) Internal Circuitry of Exciter Showing Variable Length Pulse Forming Network.

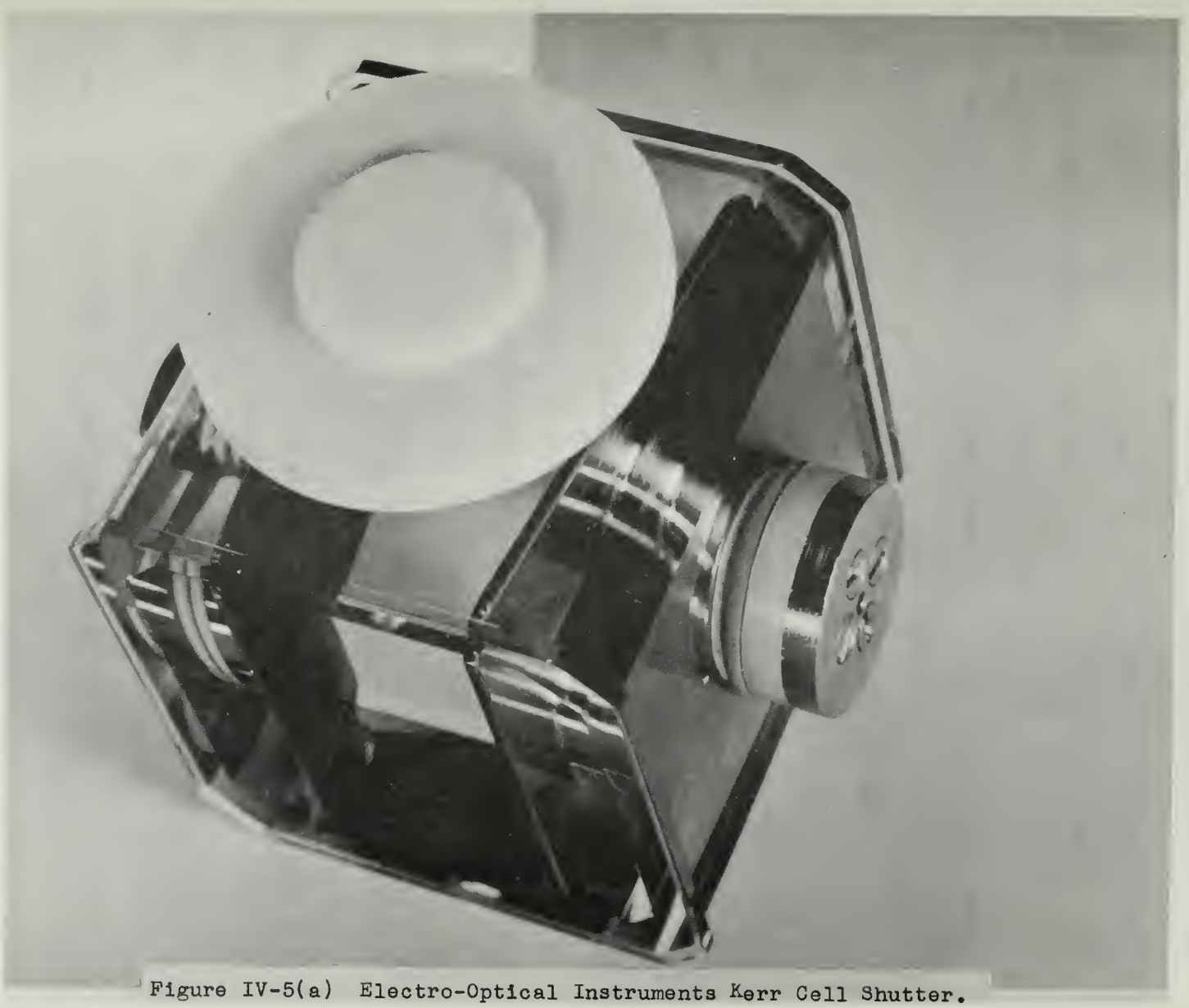

Figure IV-5(a) Electro-Optical Instruments Kerr Cell Shutter.

ly, giving rise to the observed stress birefringence. The effect is observed in gases and liquids as well as in solids, indicating that it is due also to a direct action of the electric field on the optical properties of the medium, rather than being entirely due to the indirect action of the $\bar{E}$ field in producting electrostriction.

The Kerr effect is characterized by the following equation

$$\eta_p - \eta_s = \lambda B E^2 \qquad (4)$$

where η_p and η_s are the refractive indicies for waves with the dielectric displacement, D, of the light wave parallel and perpendicular, respectively, to the applied $\bar{E}$ field. η_p refers to the extraordinary ray and η_s to the ordinary ray in the terminology of crystal optics.

By straightforward mathematical substitution, from equation (4), one obtains the relationship,[6]

$$\delta = 2\pi l B E^2 \qquad (5)$$

where l is the length of the light path under influence of the electric field, in centimeters, B is the Kerr constant, and δ is the angular retardation through the cell.

From equation (4) or equation (5) one can derive the relationship for "full open" voltage on the cell, i.e., $\delta = \pi$, as

6. See Appendix A for a detailed analysis of the Kerr cell shutter.

$$V = \frac{300d}{\sqrt{2Bl}} \text{ volts} \qquad (6)$$

This is the voltage required to give one half wavelength retardation through the cell. (The substitution 1 statvolt = 300 volts has been made in equation (6).)

Since the retardation through the cell is inversely proportional to the length of the cell, then by doubling the length, one has the equation for 1/4 λ retardation.

$$V = \frac{150d}{\sqrt{Bl}} \text{ volts} \qquad (7)$$

The physical constants of the Kerr cell available for use in these experiments were, a length of 4 centimeters, a front edge plate separation of 3 centimeters and rear edge separation of 2 centimeters. The dielectric constant for nitrobenzene is $\epsilon \sim 1.55$ and from Figure IV-5(b), which is a plot of Kerr constant versus wavelength, one obtains $B = 226 \times 10^{-7}$ for $\lambda = 6943A^{\circ}$.

Consequently, the optical path length through the Kerr cell is $l' = l\sqrt{\epsilon}$, which upon substitution becomes,

$$l' = 4\sqrt{1.55} \cong 5 \text{ cm}$$

Substituting into equations (6) and (7), and using the geometric mean value for d, of 2.45 centimeters, one obtains the corresponding voltages of 69 kilovolts and 34.6 kilovolts for $\lambda/2$ and $\lambda/4$ retardation respectively.

The power supply associated with the Kerr cell was limited to 38 kilovolts maximum; this proved to be the

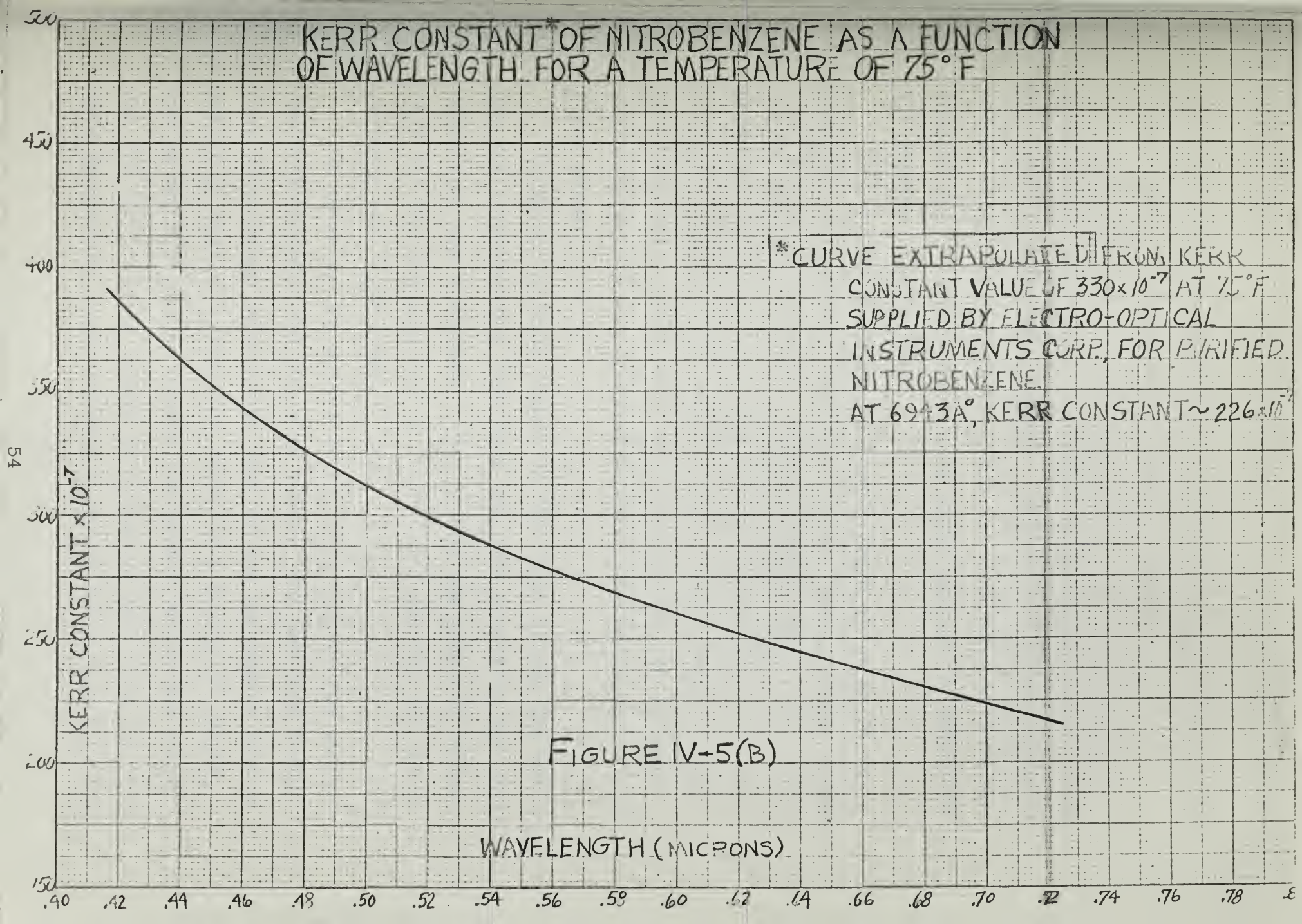
KERR CONSTANT* OF NITROBENZENE AS A FUNCTION OF WAVELENGTH FOR A TEMPERATURE OF 75° F
*CURVE EXTRAPOLATED FROM KERR CONSTANT VALUE OF 330×10⁻⁷ AT 75°F SUPPLIED BY ELECTRO-OPTICAL INSTRUMENTS CORP. FOR PURIFIED NITROBENZENE.
AT 6943A°, KERR CONSTANT ~ 226×10⁻⁷
KERR CONSTANT ×10⁻⁷
500
450
400
350
300
250
200
150
WAVELENGTH (MICRONS)
.40
.42
.44
.46
.48
.50
.52
.54
.56
.58
.60
.62
.64
.66
.68
.70
.72
.74
.76
.78

FIGURE IV-5(B)

deciding factor in restricting "Pulsed-Reflector Mode" operations to the scheme shown in Figure III-2(a).

As pointed out in the previous section, a high peak power output pulse can be obtained with the Kerr cell as the sole optical switching element. However it is the Wollaston prism, acting in conjunction with the Kerr cell to form the optical switch, which makes peak power outputs in excess of one megawatt attainable.

The Wollaston prism, or double image prism as it is sometimes classified, consists like the Nicol, of two crystal prisms cemented together. Consider Figure IV-6. The first prism has its optic axis parallel to the surface and perpendicular to an incident ray of light. In the second prism, the optic axis, while still perpendicular to the incident light ray is now also perpendicular to the optic axis of the first prism.

Normally incident light, in the first prism, the ordinary and extraordinary rays have the same direction but their velocities are different. (For quartz the index of refraction for the ordinary ray is $\eta_s \cong 1.544$ and for the extraordinary ray $\eta_p \cong 1.553$.) (39)

On entering the second prism, the ordinary ray becomes the extraordinary ray and vice versa. The two rays therefore interchange velocities; that is one ray passes from a medium of smaller refractive index to a medium of larger, and is hence refracted toward the normal, while the other ray for the contrary reason is refracted away from the normal. This phenomenon, combined with a second refraction upon emer-

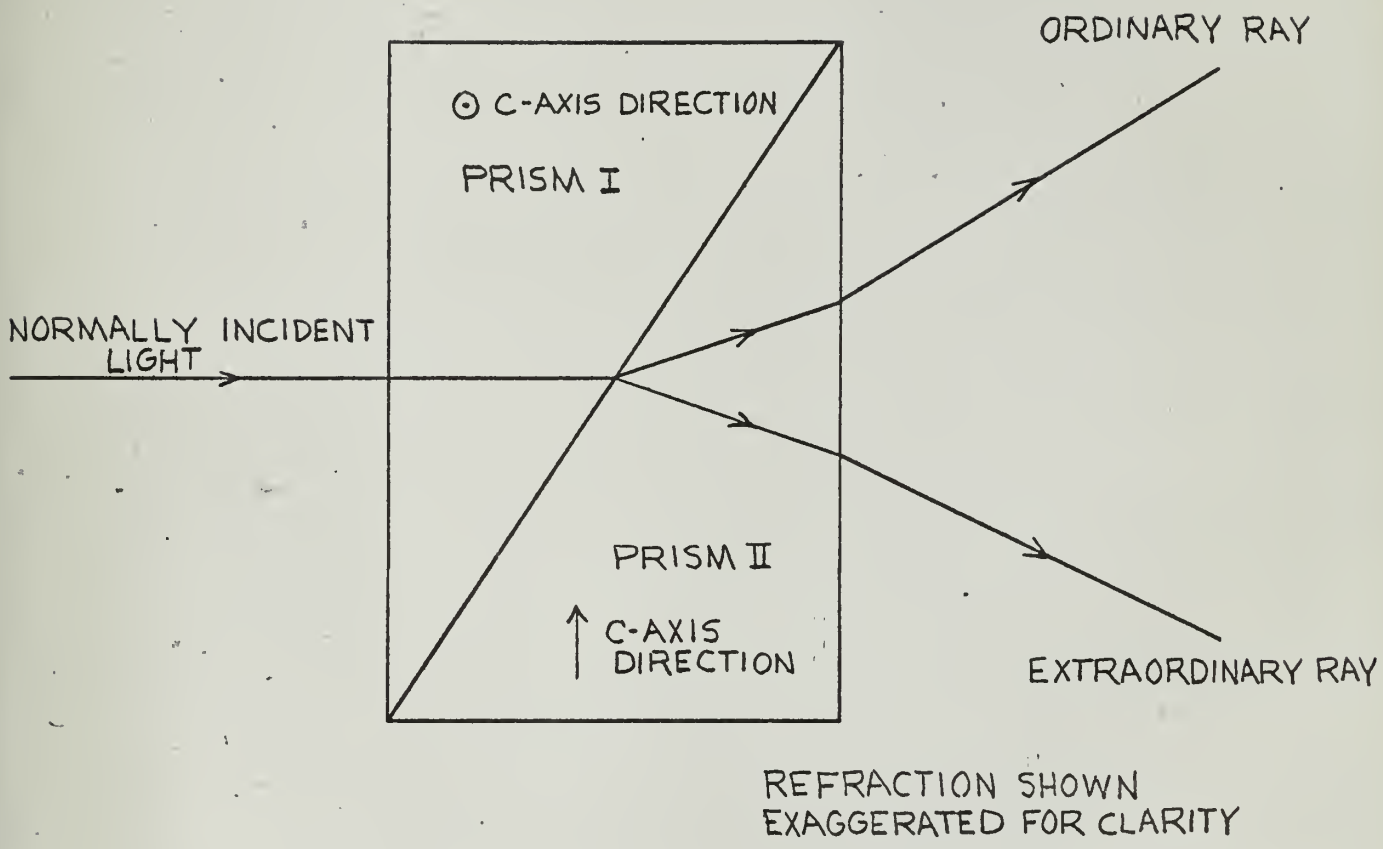

FIGURE IV-6 WOLLASTON PRISM

gence from the second prism, causes the two rays to diverge, not only upon entering the second prism but still more so upon leaving it.[7]

7. For a more detailed presentation on the Theory of Double Refraction see references (37) and (39), chapters 11 and 47 respectively.

SECTION V

EXPERIMENTAL CONSIDERATIONS AND RESULTS

1. Effects of Reflector Deviation on Efficiency and Output Energy

In order to measure the effect caused by an increasing degree of non-parallelism between the two detached reflectors, an RCA 6217 photomultiplier tube was substituted in place of the autocollimator as shown in Figure IV-3(b) of the previous section.

The tube was connected in the photodiode configuration, i.e., all of the dynodes were connected together and a -90 volt dc supply was connected in series with the cathode. For the purpose of energy measurement, the integrated output of the photodiode was desired. Consequently, a .01 microfarad capacitor shunted by a 10 megohm resistor was placed across the input to a Tektronix dual beam type 555 oscilloscope.

The tube utilized had a known calibration constant of $\rho = 1.85 \times 10^{-3}$ micro-amps per micro-watt at a ruby wavelength of $\lambda = 6943A^{\circ}$. Several wratin gelatin neutral density filters were inserted in line with the laser output beam to decrease its intensity and prevent the phototube from saturating. The total attenuation thus achieved was $10^{-7.4}$. The filtering combination was made up of numbers 0.1, 0.3, 1, 2 and 4 neutral density filters, inserted in that order with respect to the laser output beam. The optimum attenuation factor and filter ordering was determined by experimental trial and error.

The data calculated and presented in Figures V-1(a) and (b) is for a 3 inch by 1/4 inch Meller 90° c-axis ruby, doped with Cr_2O_3, .04% by weight.

The experimental procedure consisted of aligning the laser system for a known angle of deviation using the autocollimator, flashing the ruby, recording threshold energy at the exciter, and photographing the resulting oscilloscope trace of the voltage across the .01 microfarad capacitor.

The energy in the laser output beam is calculated from

$$E = \frac{CV}{\rho} \times \frac{1}{\text{filter attenuation factor}} \quad \text{joules} \qquad (1)$$

and the efficiency of the system from

$$\text{Efficiency} = \frac{\text{Energy output}}{\text{Exciter Energy above threshold}} \qquad (2)$$

The ruby rod and xenon filled Kemlite flashtube used in this portion of the experiment are shown in Figure V-1(c).

The peaking up of both energy output and efficiency in the region of 0 to 10 seconds of reflector deviation, indicates that optical alignment of the system is extremely critical if one intends to achieve the optimum operating environment for the ruby.[1] The decrease in energy output for increasing angle of deviation between the detached reflectors is shown by the oscilloscope traces of Figure V-1 (d) through Figure V-1(g).

2. Polarization of Laser Output Beam

1. This experimental conclusion is unverified, and contrary to current opinion. Several runs were made in this region and a 50% consistency of results was obtained which is far from conclusive.

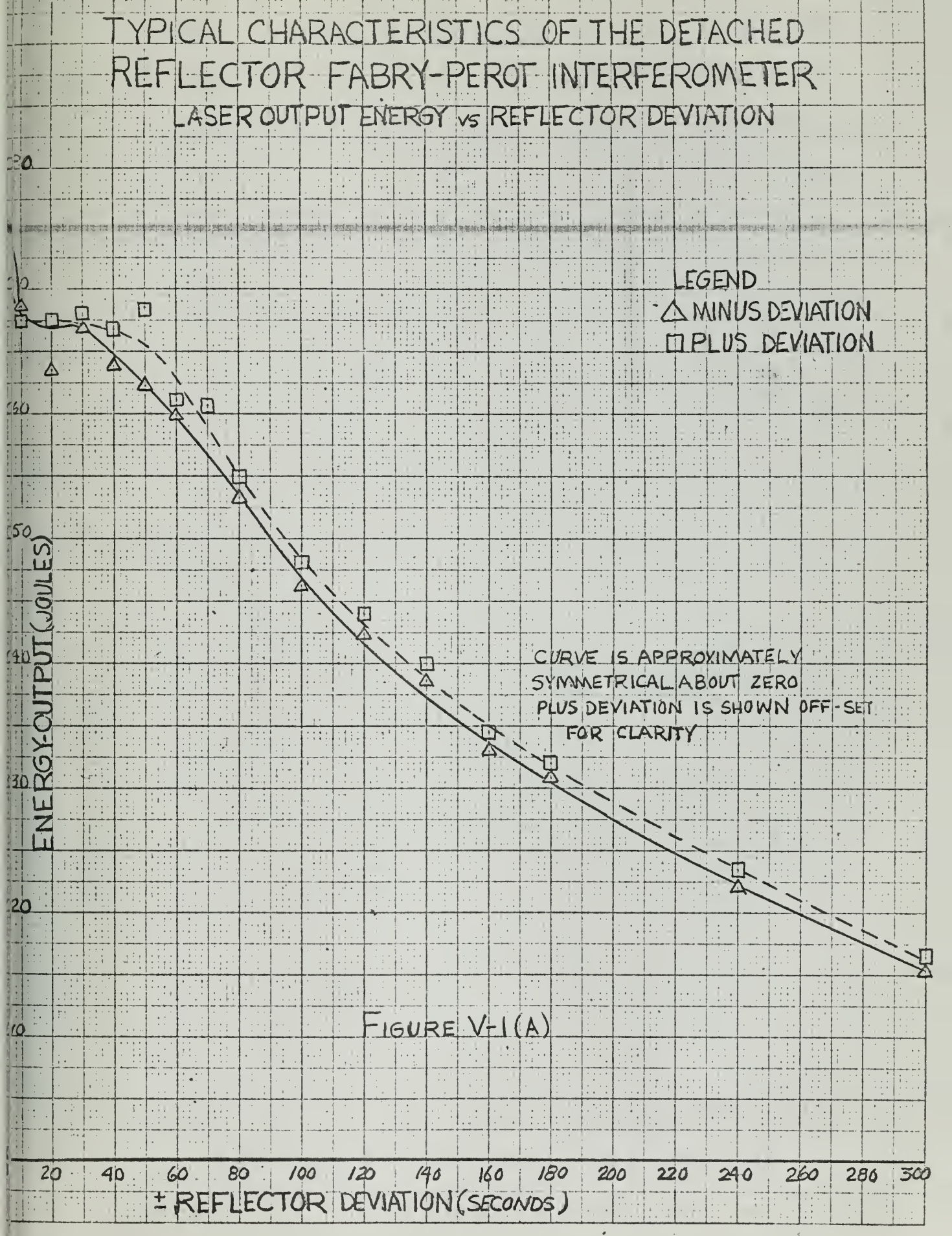
TYPICAL CHARACTERISTICS OF THE DETACHED
REFLECTOR FABRY-PEROT INTERFEROMETER
LASER OUTPUT ENERGY vs REFLECTOR DEVIATION
LEGEND
△ MINUS DEVIATION
□ PLUS DEVIATION
CURVE IS APPROXIMATELY
SYMMETRICAL ABOUT ZERO
PLUS DEVIATION IS SHOWN OFF-SET
FOR CLARITY
ENERGY-OUTPUT (JOULES)
60
50
40
30
20
10
20 40 60 80 100 120 140 160 180 200 220 240 260 280 300
± REFLECTOR DEVIATION (SECONDS)

FIGURE V-1(A)

TYPICAL CHARACTERISTICS OF THE DETACHED REFLECTOR FABRY-PEROT INTERFEROMETER

LASER PERCENT EFFICIENCY vs REFLECTOR DEVIATION

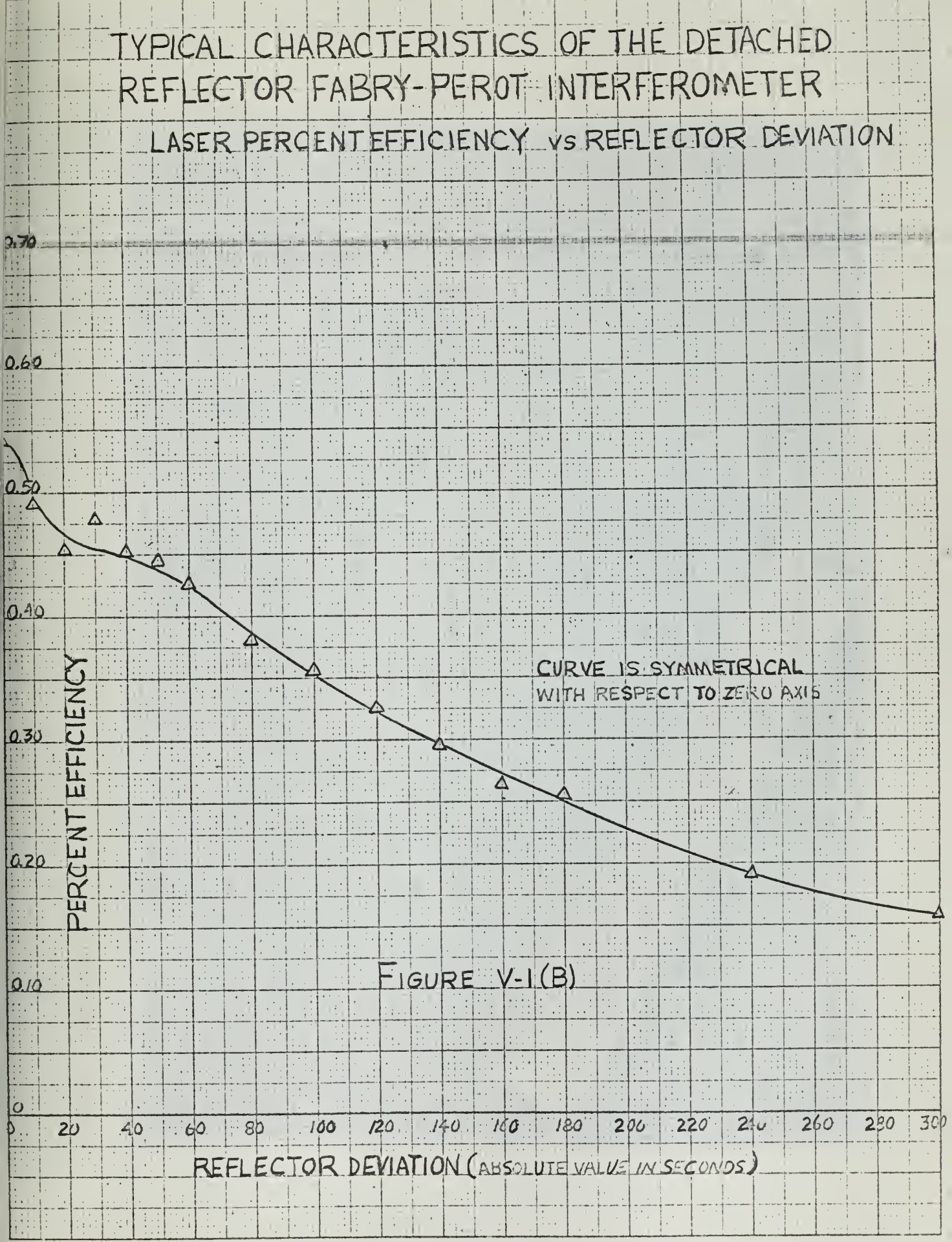

FIGURE V-1(B)

Figure V-1(c) Ruby and Flashtube

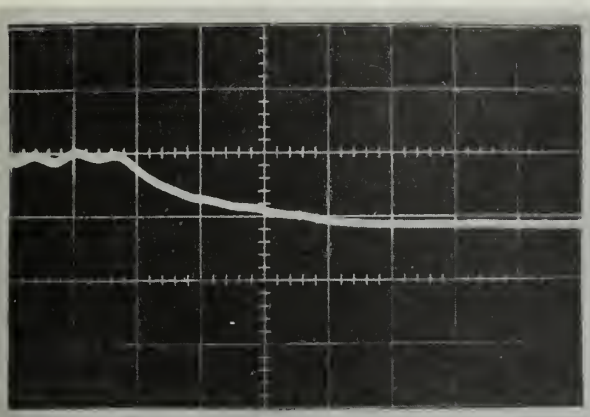

(d) Energy output for 0° angle of deviation; time base is 100 μs/cm for 5 mv/cm sensitivity.

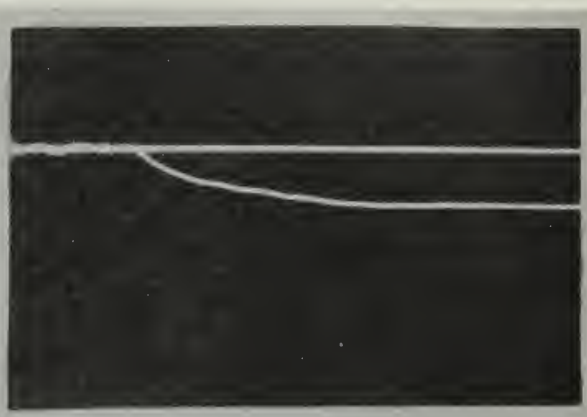

(e) Energy output for 60° angle of deviation; time base is 100 μs/cm for 5 mv/cm sensitivity.

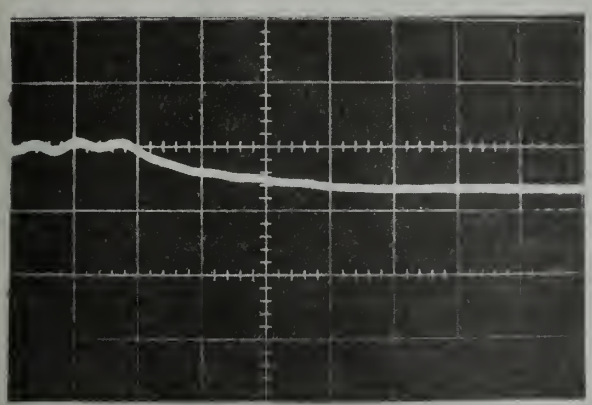

(f) Energy output for 120° angle of deviation; time base is 100 μs/cm for 5 mv/cm sensitivity.

(g) Energy output for 180° angle of deviation; time base is 100 μs/cm for 5 mv/cm sensitivity.

Figure V-1 Degradation of energy output for increasing angle of deviation between the detached reflectors

It was pointed out in Section III and reiterated in Appendix A, that the relative position of the applied $\bar{E}$ field on the Kerr cell and the direction of polarization ($\mathcal{E}$-vector) of the output laser beam should be at a 45° angle with respect to each other, for optimum system operation.

Since the Kerr cell utilized could only be mounted on the optical bench in an upright attitude, so that the applied $\bar{E}$ field was vertical, it was essential that the ruby be rotated to a 45° relative position.

During the initial phase of experimentation a sheet of polaroid material was used to determine the angle of rotation of the ruby $\mathcal{E}$-vector axis with respect to a plane formed by the cylindrical axis of the rod and the horizontal.

A Glan-Thompson prism, as shown in Figure V-2(c), was utilized to determine the rotational position of the polaroid at which maximum transmission through the sheet would occur.

The polaroid material was placed in the path of propagation of the laser beam, between the semi-transparent reflector and the phototube arrangement, as shown in Figure V-2(d). The ruby and flashtube holder was rotated to an arbitrary angle. The polaroid was rotated through 90° with energy measurements being recorded every 5° of rotation. The initial experimental run yielded an angle of $\theta = 70^{\circ}$, as shown in Figure V-2(c), for the position of maximum energy output, and hence the angle between the ruby $\mathcal{E}$-vector and the horizontal. It was concluded that this method of deter-

mining the ruby orientation was not the most expeditious manner possible and consequently experimentation along this line was abandoned in favor of using the Wollaston prism to do the same job.

Before considering how the prism was employed to determine ruby orientation, a word here is in order concerning the physical characteristics of the ruby rod. If one holds a 90° c-axis ruby in an orientation such that incident rays from a source of white light normally strike the cylindrical surface, then, upon rotation of the ruby rod about its longitudinal axis, one observes that the color of reflections from the ruby change from "light" to "dark", corresponding to the rotational positions of the rod. For a 90° c-axis ruby, the "light" and "dark" positions observed were 90° apart. (For a 0° c-axis ruby there are no distinguishable light and dark positions as one rotates the rod.) At this point, the fact that the c-axis and "dark" axis of the ruby were coincident, was unknown; actually this determiniation was a secondary objective of the experimentation under discussion.

Returning to the primary experimental objective, that is determination of ruby orientation, the Wollaston prism was inserted in the path of propagation between the semi-transparent reflector and a screen.

The prism was mounted in its holder at a 45° angle to the horizontal. The principle of determining the orientation of the ruby is elementary. When the ruby is positioned so that its $\mathcal{E}$ -vector is at a 45° angle with the horizontal

then, during laser action, only the extraordinary ray will be in evidence on the screen after the beam passes through the prism. The reasoning to support this assertion follows. With reference to Figure IV-6 in the previous section, one may recall that an ordinary ray (direction of polarization is perpendicular to the c-axis) in prism I, becomes the extraordinary ray in the second prism half. If the ruby $\mathcal{E}$-vector is exactly at 45° there will be no component of this vector which lies along the c-axis of prism I, i.e., there will be no extraordinary ray in prism I and consequently no ordinary ray in evidence on the screen. One may observe that both ordinary and extraordinary rays are represented on the screen by two distinctly separated spots when the ruby is inaccurately oriented with respect to the prism. By their relative position on the screen the spots may be associated with the ordinary and extraordinary ray from the prism. Orientation of the ruby so as to extinguish the ordinary ray on the screen was the process employed to achieve an angle of 45° between the ruby $\mathcal{E}$-vector and the horizontal.

To investigate the association between the observed "light" and "dark" axis of the ruby rod and the corresponding $\mathcal{E}$-vector and ruby c-axis directions, it was assumed that the "light" axis corresponded to the $\mathcal{E}$-vector direction, and the ruby was oriented accordingly in its holder.

By passing a collimated beam of light through the ruby rod, detached reflectors, and Wollaston prism onto a screen, it was observed that the spots on the screen associated with

the ordinary and extraordinary rays were yellow and red respectively. Considering the inversion effect of the Wollaston prism, these two colors would be associated with the extraordinary and ordinary ray directions respectively in the ruby.

The laser beam is red in color; theoretically then, the polarization of the extraordinary ray visible on the screen as a red spot, should be identical to the $\mathcal{E}$-vector direction in the ruby, which is the ordinary ray direction. Using a Glan-Thompson prism, the red spot was extinguished. The orientation of the Glan-Thompson prism was noted. It was crossed at an angle of 90° to the assumed direction of the $\mathcal{E}$-vector hence offering conclusive proof that the "light" axis of the rod, and the direction of polarization of the stimulated optical emission from the ruby are coincident. The results of this investigation are depicted in Figure V-2(a).

3. Optical Alignment of the "Pulsed-Reflector Mode" Laser

Optical alignment was achieved in a manner similar to that already described in Section IV for the normal mode system. The basic difference in alignment of the "Pulsed-Reflector Mode" system is that the presence of the Wollaston prism contributes several additional reflections observable in the eyepiece of the autocollimator. Consequently the autocollimator must be offset to isolate the blue and green field reflections associated with the extraordinary ray from the prism. A pictorial representation of the experimental setup is included in this section as Figure V-3. The impor-

tant points to be noted here are that the Kerr cell had no visible effect on the alignment, and no attempt was made to line up the ruby with the rest of the system. The alignment performed must be considered to be rough at best and there is extensive room for improvement.[2]

4. Effects of the Optical Switch on System Characteristics

After final alignment had been achieved to within the limitations imposed by the physical setup and the instruments utilized, attempts were made to determine the effect that the presence of a optical switch had upon laser threshold energy.

From the initial phases of experimentation, it was evident that repeated firing of the helical flashtube surrounding the ruby gave rise to temperature increases within the cavity. Threshold energy gradually increases with the increase in temperature of the ruby's environment. Consequently, cooling of the cavity was required. Compressed nitrogen gas was piped into the cavity at a low rate of flow. Data was then obtained on the variation of threshold energy versus Kerr cell voltage as shown in Figure V-4.

A decrease in output energy of 40% was observed due simply to the presence of the Kerr cell in the path of propagation of the laser output beam.[3] These measurements

2. An alternative method of optical alignment as suggested by Dr. E. J. Woodbury is noted in Section VI.

3. This effect was unexplainable at the time of experimentation. Subsequently it was suggested by Dr. Woodbury that the Kerr cell was acting as a lens defocusing the laser beam within the cavity.

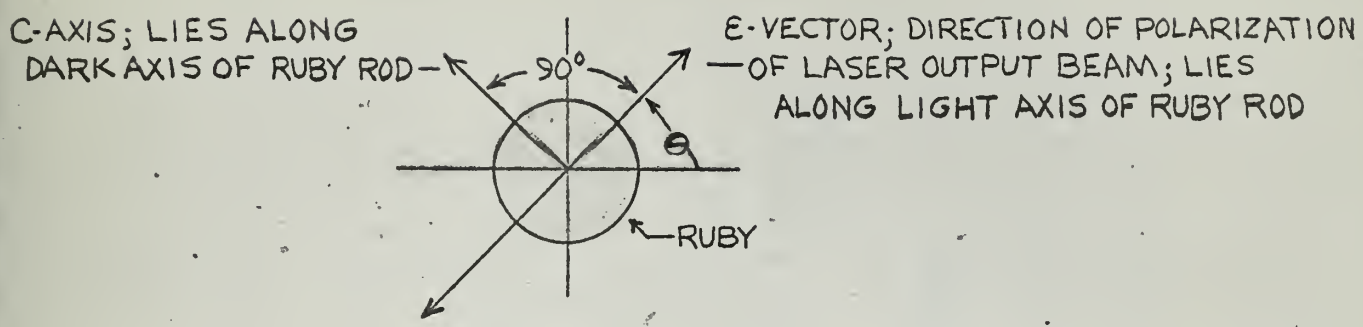

FIGURE V-2(A) ORIENTATION OF ε-VECTOR AND C-AXIS LOOKING AT THE END OF A 90° C-AXIS RUBY; DIRECTION OF PROPAGATION OF LASER BEAM IS OUT OF THE PAPER.

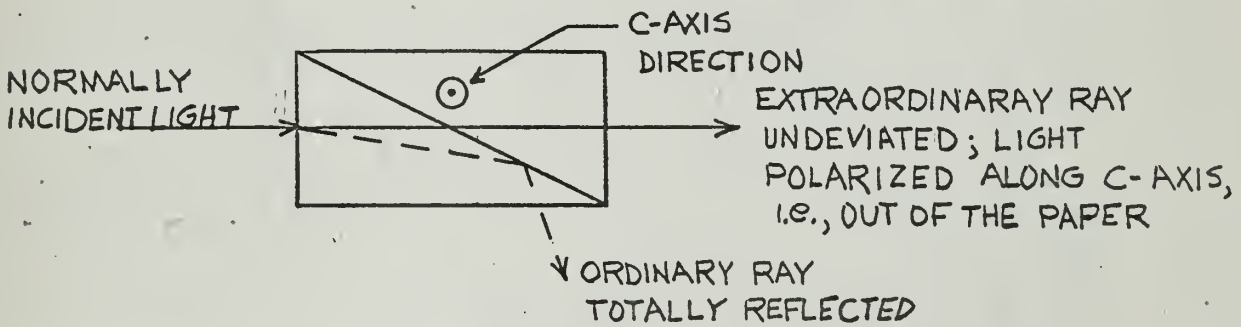

FIGURE V-2(B) GLAN-THOMPSON PRISM

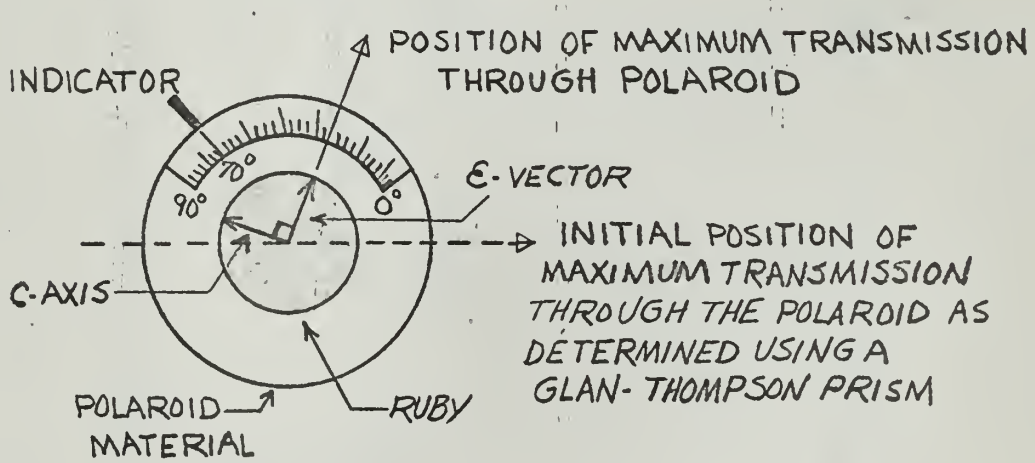

FIGURE V-2(C) END VIEW OF 90° C-AXIS RUBY THROUGH POLAROID MATERIAL; EXPERIMENTAL VALUE OF θ SHOWN AS ~ 70°. DIRECTION OF PROPAGATION OF LASER BEAM IS OUT OF THE PAPER.

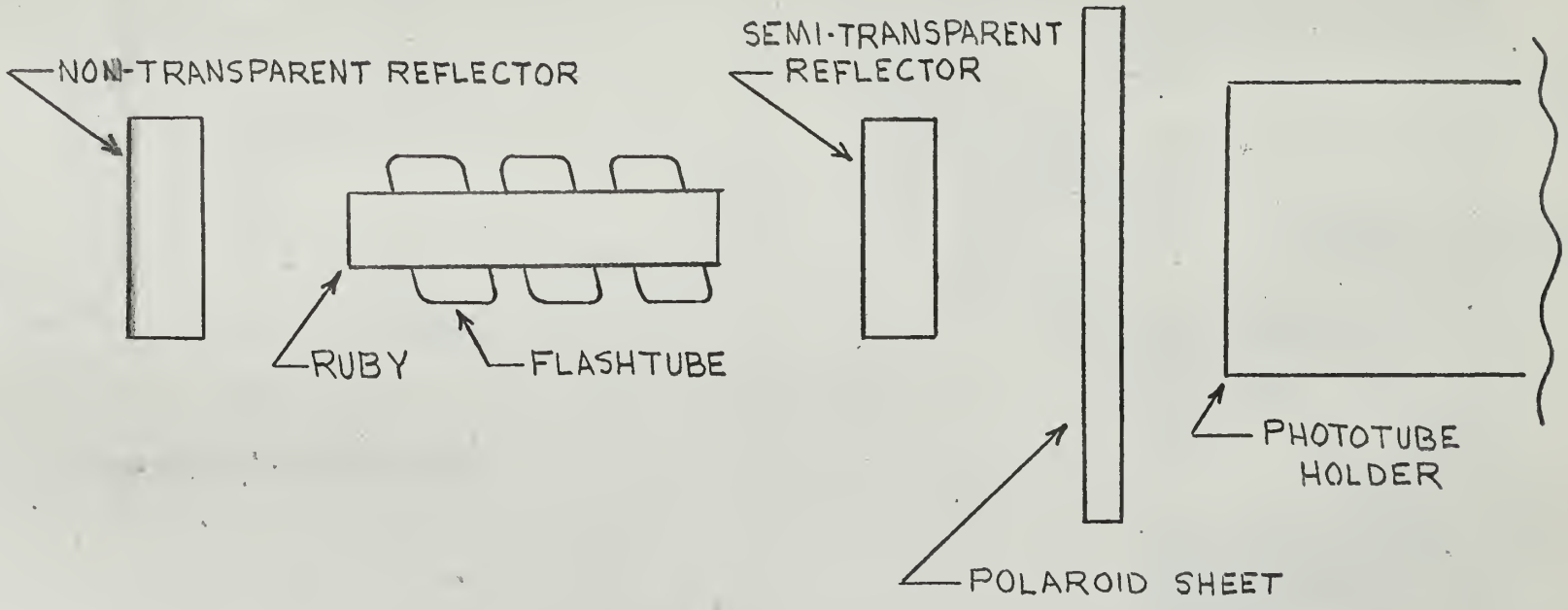

FIGURE V-2(D) LABORATORY SETUP FOR DETERMINATION OF LASER BEAM POLARIZTION

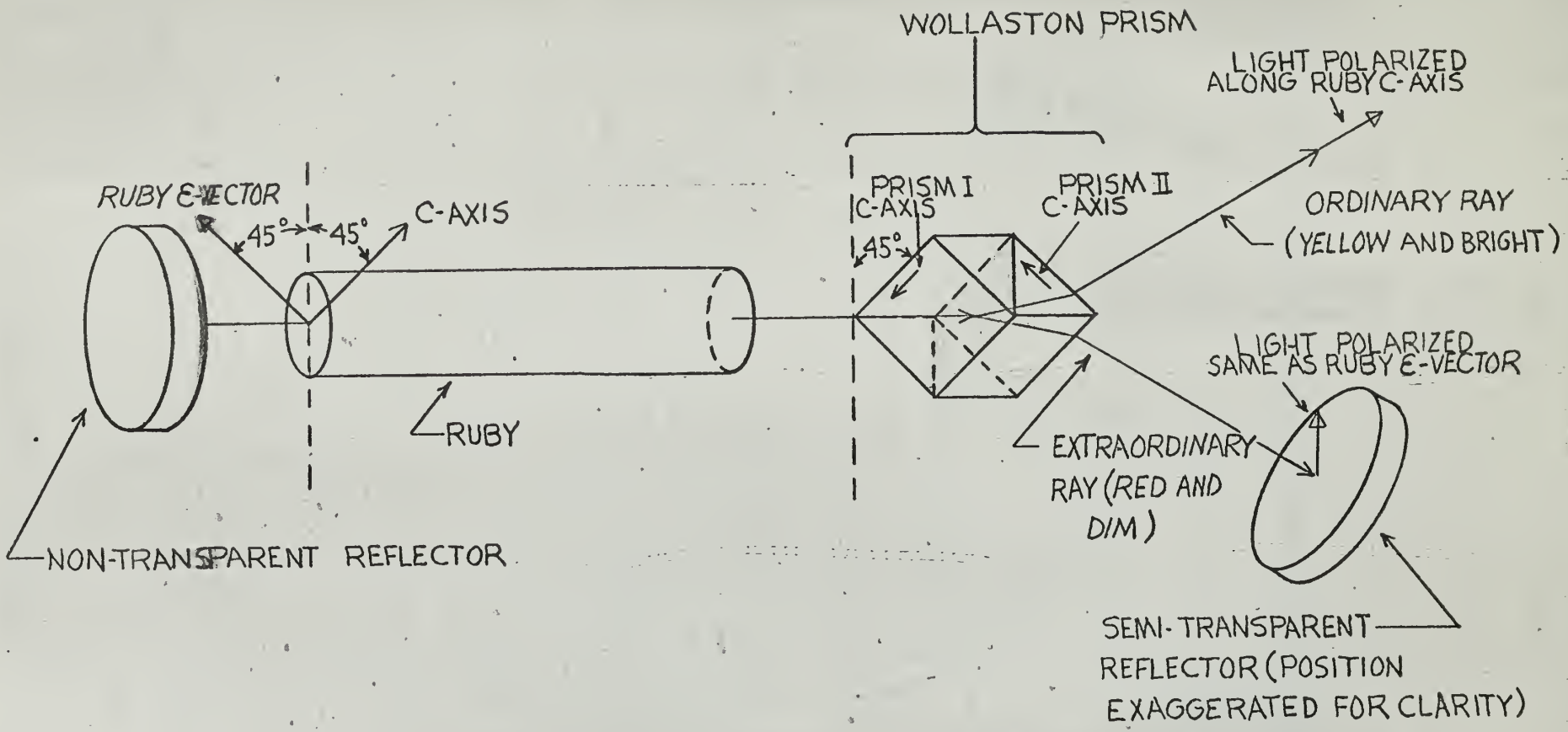

FIGURE V-3 SCHEMATIC DIAGRAM FOR OPTICAL ALIGNMENT OF THE PULSED REFLECTOR LASER SYSTEM

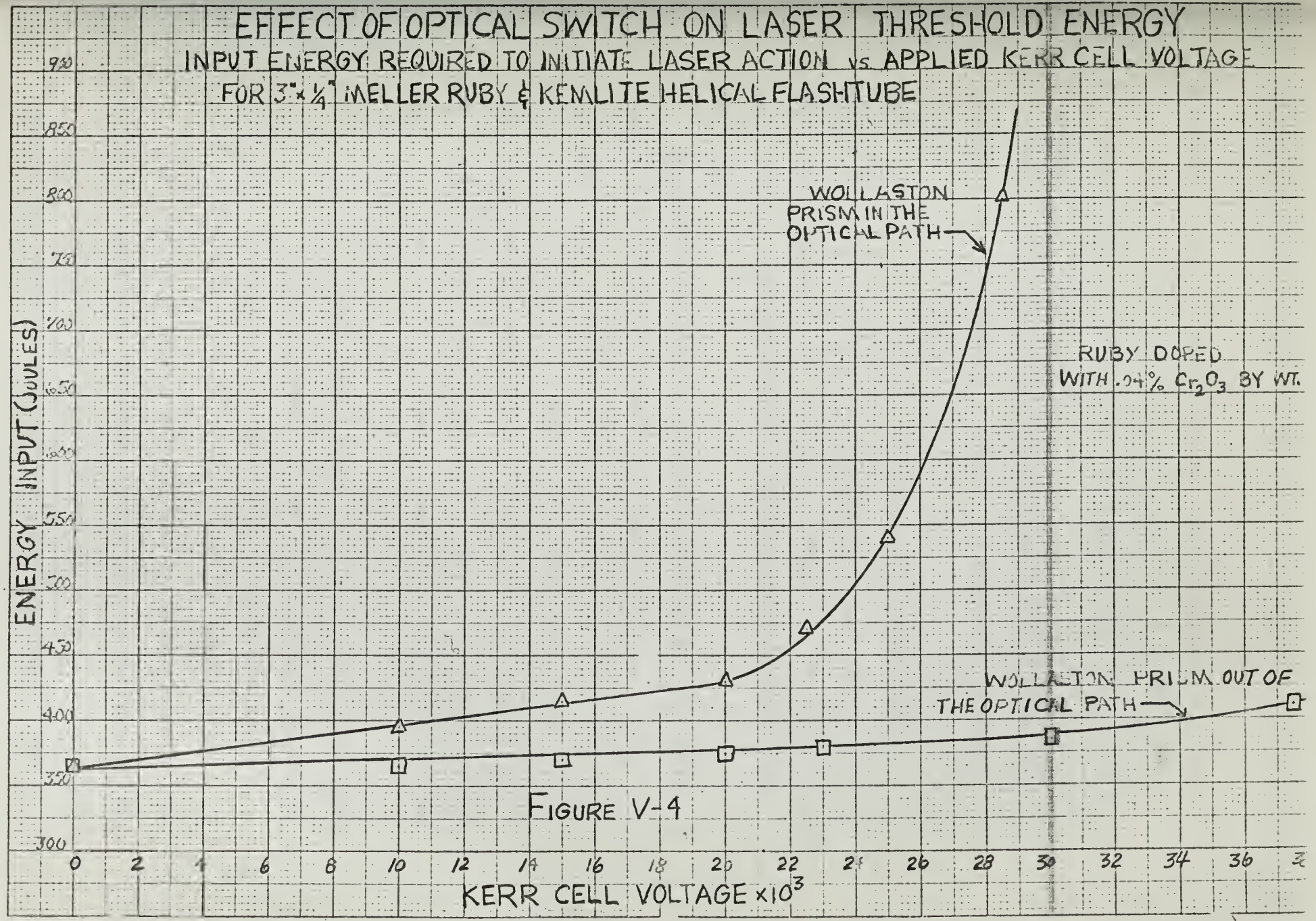
EFFECT OF OPTICAL SWITCH ON LASER THRESHOLD ENERGY
INPUT ENERGY REQUIRED TO INITIATE LASER ACTION vs APPLIED KERR CELL VOLTAGE
FOR 3" × ¼" MELLER RUBY & KEMLITE HELICAL FLASHTUBE
WOLLASTON PRISM IN THE OPTICAL PATH
RUBY DOPED WITH .04% Cr_2O_3 BY WT.
WOLLASTON PRISM OUT OF THE OPTICAL PATH
ENERGY INPUT (JOULES)
900
850
800
750
700
650
600
550
500
450
400
350
300
0
2
4
6
8
10
12
14
16
18
20
22
24
26
28
30
32
34
36
KERR CELL VOLTAGE ×10³

FIGURE V-4

were made with the experimental setup as shown in Figure V-5 (a). At the time measurements were made, the Wollaston prism was not in the path of propagation and there was no voltage on the Kerr cell.

For both experimental runs shown in Figure V-4, the flashtube was repeatedly fired until laser action was observed. The voltage on the Kerr cell was recorded as the "hold-off" voltage, or voltage at which energy input to the system would produce marginal laser action. For the case where the Kerr cell was the only element in the optical path, laser action was achieved with $\lambda/4$ retardation voltage on the cell.

Upon insertion of the Wollaston prism as the second element of the optical switch, laser action was observed for an energy input of 800 joules at 28.5 KV on the Kerr cell. Rather than exceed the energy input specifications of the flashtube, experimentation was halted at this point, and the energy input corresponding to $\lambda/4$ retardation voltage on the cell was not obtained. The data recorded indicated the following:

(1) The sharp increase in γ due to the insertion of the Wollaston prism would allow a higher percent of the total ion population to be inverted before the onset of laser action.

(2) With a mean reflectivity of approximately .70, and high internal losses due to surface reflections from the ruby and Kerr cell, nothing would be gained by ultimately applying more than

28.5 KV to the Kerr cell during power output measurements, as long as the Wollaston prism was in the optical path during the recordings.

The dual reasoning supporting the above statements is as follows. First of all, theoretically, for $\lambda/4$ retardation voltage on the Kerr cell, the threshold at which laser action will occur is infinitely large with the prism in the optical path. Above about 80% population inversion though, the percentage increase one obtains by resorting to even higher input energy at the exciter is such as to not warrant the resulting decrease in the lifetime of the flashtube. From Figure E-1 of Appendix E, for an increase in excess Cr^{+++} ions above threshold of 10%, that is, for instance from 80% population inversion to 90%, one must approximately double the rate $W_{13}\tau_2$, at which ions are pumped into the excited state E_2. Since $W_{13}\tau_2$ is proportional to pump energy the end result is that the one must double the input energy at the flashtube exciter. (Percent inversion here refers to the ratio $(N_2-N_1)/N_o$ where N_o is the total Cr^{+++} ion population density of the ruby)

The second reason for limiting the intensity of the pump flashtube, and the voltage on the Kerr cell, to values at which the Wollaston prism and Kerr cell are effective in quenching the laser action, stems from a practical consideration. The system is only roughly aligned, internal reflection losses are high, and a low reflectivity of the semi-transparent reflector implies that approximately 50% of the laser energy available will be coupled out of the cavity.

Under these conditions, the end results are:

(a) One is faced with a low Q cavity primarly because of the low mean reflectivity of the detached reflectors. This is undesireable;

(b) as a result of low reflectivity though, laser action is achieveable, because even if the losses amounted to 48% the system would still be operational, with 2% of the energy being coupled out of the cavity.

Obviously there is an optimum condition of operation and this will be presented in Section VI. For the system at hand, low reflectivity was desireable because this was the only way laser action could have been achieved. The point is, applying more than 28.5 KV to the Kerr cell and pumping the flashtube unnecessarily hard, would result in no real significant improvement in the peak power output until the controllable parameters of the system, e.g., the mean reflectivity, reflection losses, Kerr cell operating voltage, alignment etc., are improved.

Referring to equation (19) of Section II, one observes that the Q of the cavity is inversely proportional to (1-R). The system under consideration was obviously limited by a low Q due to the low mean value of the reflectivity. With no voltage on the Kerr cell, ideally, one desires a high mean value of reflectivity for the purpose of high regeneration and high Q. With $\lambda/4$ retarding voltage on the Kerr cell, and Wollaston prism in the optical path, the high reflectivity is now switched to a low value, and low regener-

ation occurs. The higher the Q of the cavity, the shorter the rise, decay, and delay times of the resulting giant output pulse of stimulated optical emission and hence, the higher the energy and power output one can obtain operating in the pulsed-reflector configuration.

5. Measurements

A schematic diagram of the laboratory setup used to record peak power and energy output from the pulsed reflector laser system, is shown in Figure V-5(a). The timing sequence was adjusted so that the voltage on the Kerr cell would be switched off 650 microseconds after the flashtube was fired. It was known beforehand that this timing was not critical to the successful operation of the system.[4]

Two serious problems arose during this phase of the experimentation. Measurements were hampered initially by transients due to the firing of the Kerr cell switching. Thyratron and photodiode saturation was immediately obvious once the Wollaston prism was inserted in the optical path, as shall be pointed out latter.

Peak power output was calculated from the measured value of voltage across a 1000 ohm resistor in the photodiode output circuit. In order to combat the transients in the system, which were of sufficient magnitude to completely overshadow the pulse (millivolt range) output of the photodiode, the following major steps were taken:

(1) A copper ground plane was placed on the labora-

4. See reference (36)

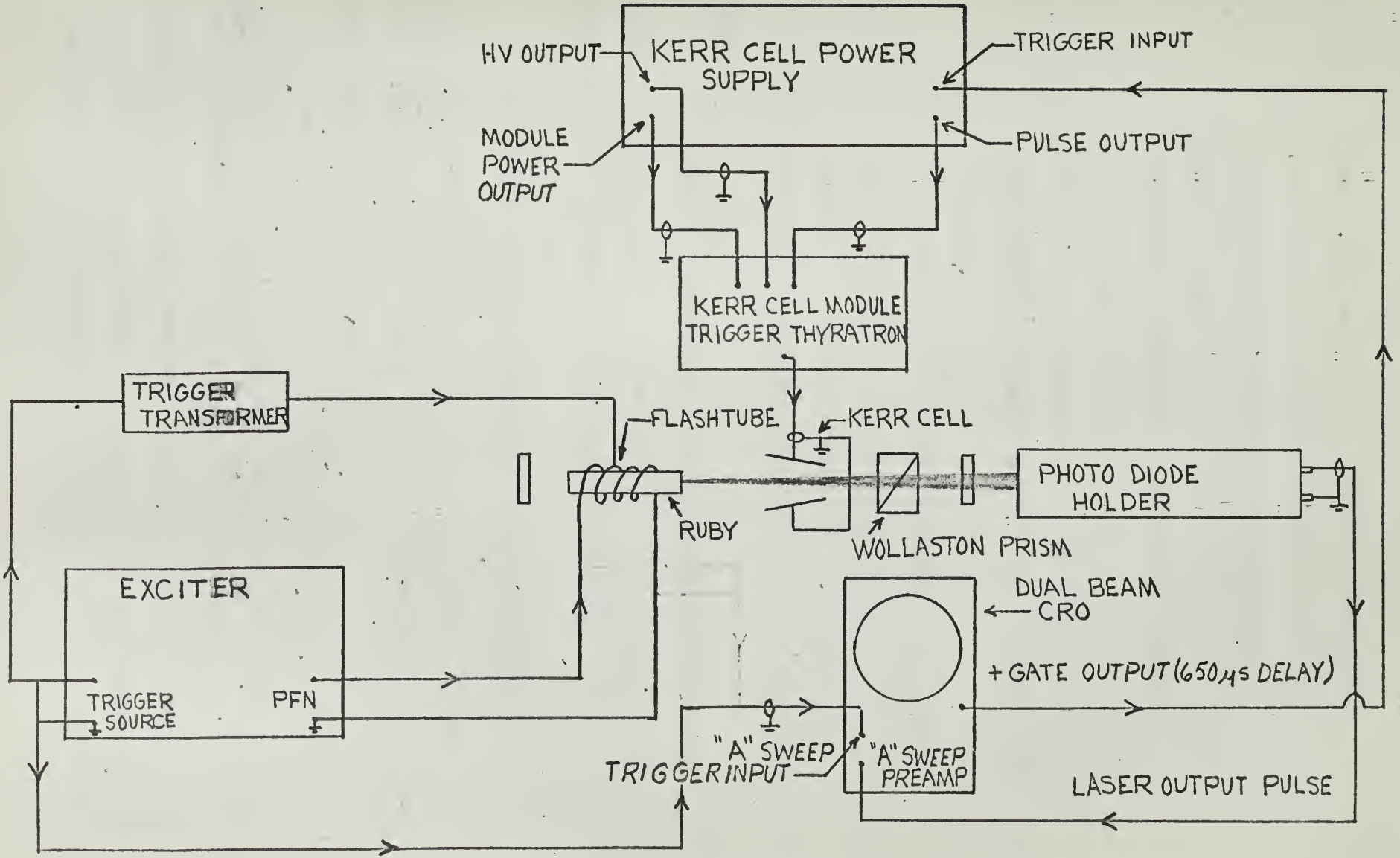

FIGURE V-5(A) SCHEMATIC DIAGRAM OF PULSED-REFLECTOR LASER EXPERIMENTAL SETUP

tory bench which held the laser system;

(2) The coaxial lead from the Kerr cell electrodes to the trigger thyratron was shortened to less than 2 inches long with a 1,000 ohm resistor inserted in series to suppress parasitic oscillations ;

(3) The Kerr cell was shielded by a copper housing which enclosed the cell and the attached low inductance bifilar ground loop;

(4) A 100 ohm resistor was inserted in series with the trigger input lead to the Kerr cell power supply to suppress parasitic oscillations.

The shielding and copper ground plane are visible in Figure V-6.

The waveform of stimulated optical emission from the normal configuration ruby laser was recorded and is shown in Figure V-5(c). Using the following equation

$$\text{Peak Power} = \frac{V}{R} \times \frac{1}{\rho} \times \frac{1}{\text{filter attenuation factor}} \qquad (3)$$

where V is measured from the oscilloscope trace in millivolts, the peak power output from the normal mode laser was calculated to be 1.5 kilowatts.

To produce giant output pulses characteristic of the "Pulsed-Reflector Mode", the Kerr cell was activated and then the pump flashtube was fired. About 650 μs after pumping was initiated the Kerr cell was suddenly turned off in a time of approximately .02 μ sec. The adjustment of the laser population excess to some new lower value caused the

change in stored energy associated with the change in maser populations to appear in the form of the giant pulse output shown in Figure V-5(d).

The peak power as calculated from equation (3) for a filter factor of $10^{-6.4}$ and $\rho = 1.85 \times 10^{-3}$ $\mu a/\mu w$, was 51.5 kilowatts. The resulting pulse shape had the following characteristics:

(1) There was a delay time of about 0.2 μs before the body of the pulse;

(2) The rise time constant was about 0.05 μs;

(3) The total duration of the pulse was about 0.5 μs.

The stray capacitance in the system was estimated to be 170 $\mu\mu f$, i.e., 20 $\mu\mu f$ for the input capacitance of the oscilloscope plus 30 $\mu\mu f$ per foot of signal lead coaxial cable, of which there was five feet from the scope to the photodiode. In effect then, one observes that a poor integration was being performed rather than a power measurement in Figure V-5(d). This would make the pulse duration higher than the actual value and the peak power calculated somewhat lower than the actual value. (Pulse durations of 0.12 μs have been obtained as reported in reference (36).) The resumption of spontaneous pulsations after the giant pulse occurred were not observed due to the short time base used in Figure V-5(c). One should expect a resumption of normal laser output pulsations approximately 10 μs after the giant pulse, with this value depending upon the time it takes for the excess population to decay to the 50-50 inver-

sion level.

Figure V-5(b) is a pictorial representation of the ideal giant pulse output and the corresponding build-up in excess population for the pulsed-reflector mode.

From equation (4) of Appendix B, where η for ruby is approximately 1.75 and for the Kerr cell surfaces $\eta = 1.50$, one may calculate the losses due to reflection from the ruby and Kerr cell surfaces to be 15% and 16% respectively, or $L_r = 7.5\%$, $L_k = 8.0\%$.

From equation (11) of Section III, one may arrive at an approximate value of γ of .68, for R = 0.70, $(1-L_r)^2 = 0.856$ and $(1-L_k)^2 = 0.846$. This implies from equation (10) of Section III, that the initial gain α_i built up during the quenched phase is approximately 0.34 cm^{-1} where l was taken to be $3\sqrt{1.75}$, the optical length of the ruby, and S_k was assumed to be 1.0. This value of α_i is somewhat high, as compared to results recorded in reference (36). One reason of course is that a 90° c-axis ruby was utilized for this experiment and also that the calculated reflection losses may be somewhat high.

An approximate equation for the rise time t_r shown in Figure V-5(b) is

$$t_r = \frac{t}{(\alpha_i l - \gamma/l)} \qquad (4)$$

where t is the transit time for light between the detached reflectors. The optical path length for light between the reflectors can be calculated knowing the physical separation to be 22 cm, and the physical length of the ruby and Kerr

cell to be 3 cm and 4 cm respectively. For an optical path length of 24 cm, the transit time is approximately 0.8×10^{-9} seconds. Therefore the observed value of $t_r = 0.05\ \mu s$ implies that α_i was approximately 0.175 cm^{-1}. The discrepancy between these two independent estimates of α_i can be partially attributed to the following:

(1) The value of $\alpha_i = 0.34\ cm^{-1}$ is high for reasons already stated.

(2) The value of $\alpha_i = 0.175$ should be a little low because by the time t_r was measured α must have dropped somewhat because of induced emission.

Choosing the average of these two values, one may estimate the initial fractional population excess, $f = \alpha_i/\alpha_0$ where α_0 for the R_1 line in ruby is 0.4 cm^{-1} from reference (23), for $T_K = 300^\circ$. Hence, f was 0.26/0.40, or 65 percent of total inversion.

If the switching of the Kerr cell takes place rapidly compared with the time it takes the populations to react appreciable, then the time t_Δ that it takes for the laser gain to fall from its initial value α_i to a value $\Delta\alpha$ lower is very nearly given by

$$t_\Delta = t_r \ln\left[1 + \frac{f\Delta\alpha}{\alpha_i W_{13} t_r (1+f)}\right] \qquad (5)$$

provided $\Delta\alpha/\alpha_i \ll 1$. To compare equation (5) with the experimentally observed value of pulse delay time t_d, one must estimate the pump rate W_{13}, and the depletion $\Delta\alpha$ that has occurred by the time the pulse becomes apparent on

the scope. No significant error should result if one takes $\Delta\alpha \cong 0.1\alpha_i$ and from Figure E-1 of Appendix E for $f = 0.65$, $W_{13} = 4/\tau_2$. This assumed value of W_{13} corresponds to a pump rate of 4×10^3 ions per second for an inverse spontaneous decay time of 1×10^3. The observed delay time is estimated from equation (5) then, to be $6.6\ t_r = 0.33\ \mu s$. This is not within satisfactory agreement with the observed value of $t_r = 0.2\ \mu s$. The experimental uncertainty in both α_i and t_r should be considered to justify the discrepancies between calculated and observed values, but one must not rule out the possibility that the theoretical framework which the foregoing discussion has relied upon may be inexact. Certainly one is proceeding in the right direction by utilizing the theory of Section III, but obviously calculations of γ become increasingly more difficult as additional objects are inserted in the laser path of propagation. This leads one to believe that the original theoretical framework is inadequate to define laser action in more involved pulsed-reflector systems.[5]

The measurement of peak power output is identical in approach and procedure to that just described when one inserts a Wollaston prism into the system along with the Kerr cell. The problem of photodiode saturation is now raised. It was immediately apparent that besides being the integral of the power, the waveform of voltage across the 1000 ohm load as shown in Figure V-5(e) was decreased severely by

5. See Section VI for additional reasons to support the discrepancies between theoretical and observed values.

photodiode saturation. The scope sensitivity limits one from inserting additional neutral density filters in the path of the laser beam.

One is unable to place a value upon peak power output from Figure V-5(e), but from the corresponding waveform of energy output the average power is calculated to be approximately 1.08 megawatts for a peak energy of 54 millijoules and a rise time of 50×10^{-9} seconds. If one assumes an output pulse with a triangular shape, which is a reasonable assumption, then the peak power output would be 2.16 megawatts or an increase in excess of 100 to 1 over the peak power output calculated for the stimulated emission shown in Figure V-5(c).

A theoretical calculation of the pulse length or duration is more difficult than the foregoing and requires a machine computation. Also, it is extremely difficult to estimate the total and peak power output for a given ruby, because various crystals are observed to operate in varying and difficult to measure fractions of their total volumes, owing to strains and imperfections in the crystals.

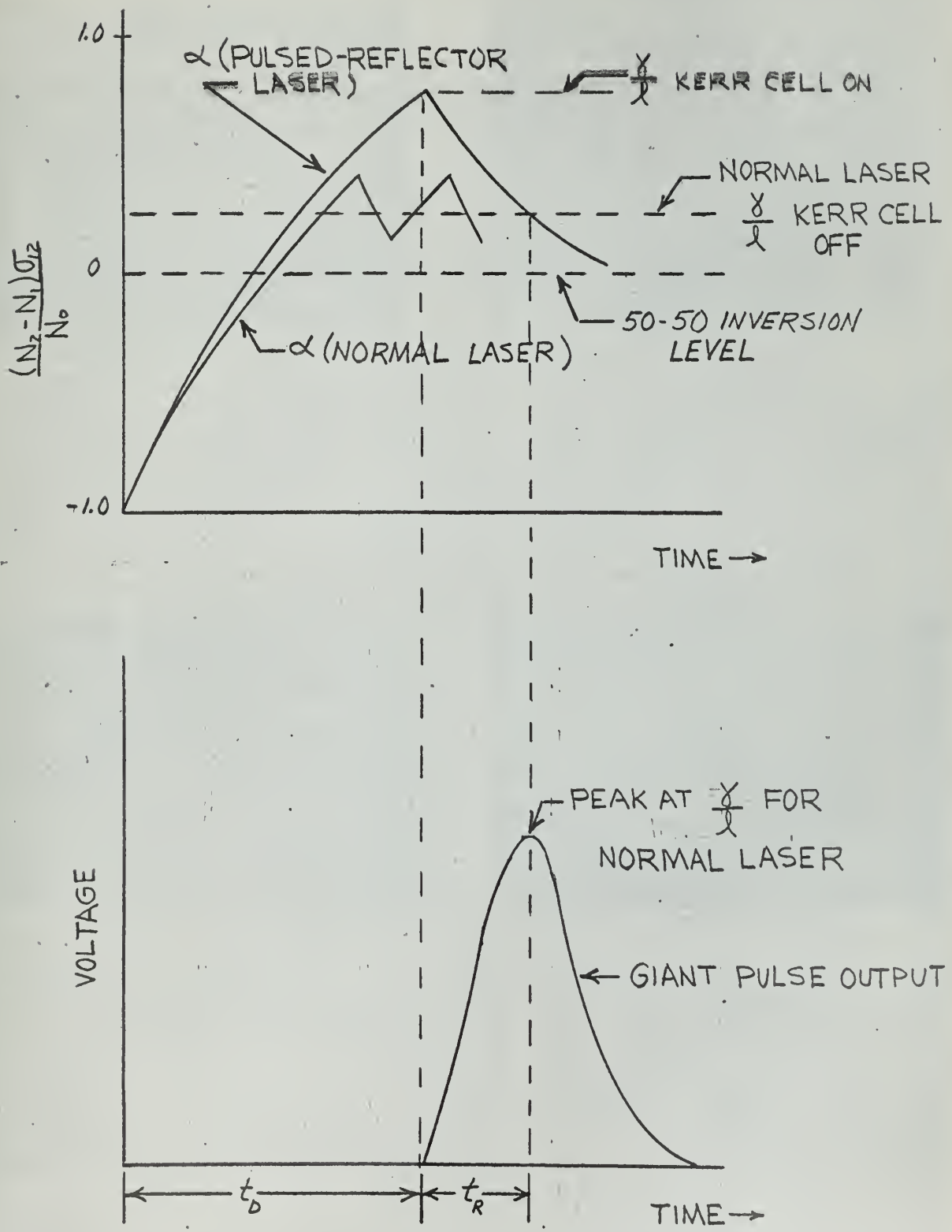

FIGURE V-5(B) BUILD-UP IN EXCESS POPULATION AND CORRESPONDING GIANT PULSE OUTPUT FOR PULSED-REFLECTOR MODE

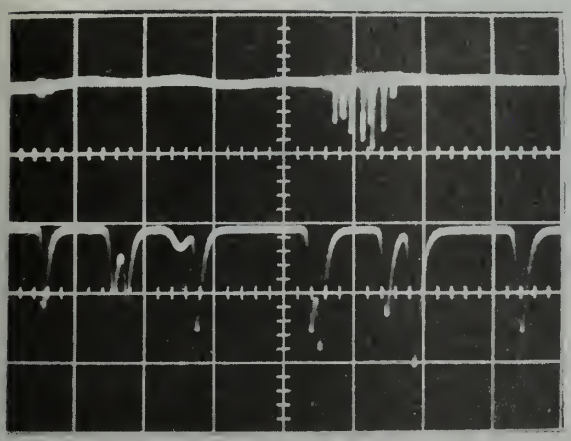

(c) Stimulated optical emission from conventional ruby laser. Time base of upper sweep is 50 μs/cm for 10 mv/cm sensitivity; time base of lower sweep is 5 μs/cm for 5 mv/cm sensitivity

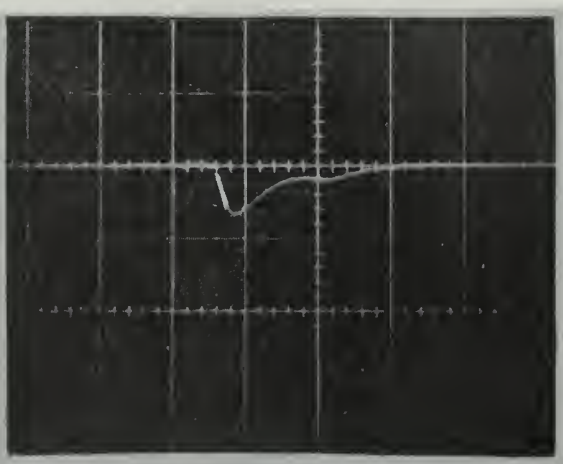

(d) Stimulated optical emission from the "Pulsed-Reflector Mode" laser; optical switching accomplished by a Kerr cell shutter. Time base is 0.5 μs/cm for 50 mv/cm sensitivity. Vertical diflection is proportional to peak power output

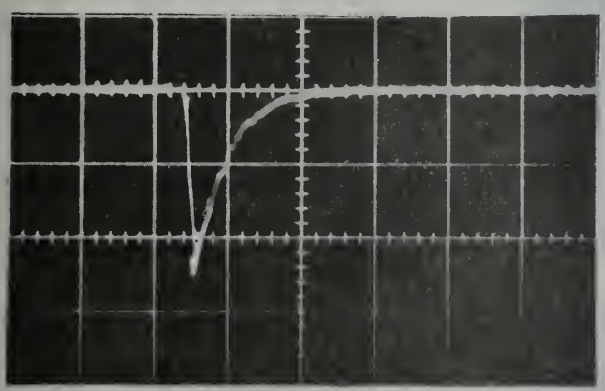

(e) Stimulated optical emission from the "Pulsed-Reflector Mode" laser; optical switching accomplished by a Kerr cell and Wollaston prism. Time base is 0.5 μs/cm for 5 mv/cm sensitivity. Vertical deflection is proportional to peak power output

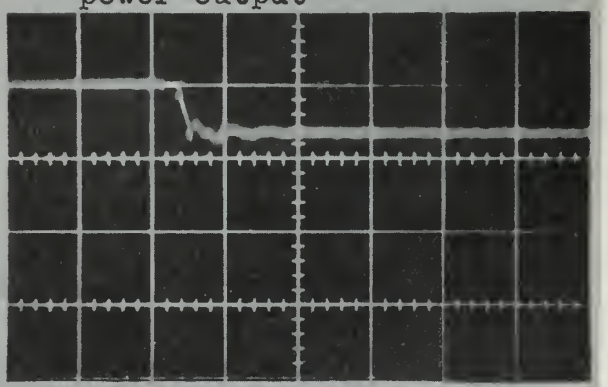

(f) Measurement of energy output from "Pulsed-Reflector Mode" laser system. Time base is 0.5 μs/cm for 5 mv/cm sensitivity. Vertical deflection is proportional to energy output

Figure V-5 Stimulated optical emission from both conventional, "Pulsed-Reflector Mode" ruby laser

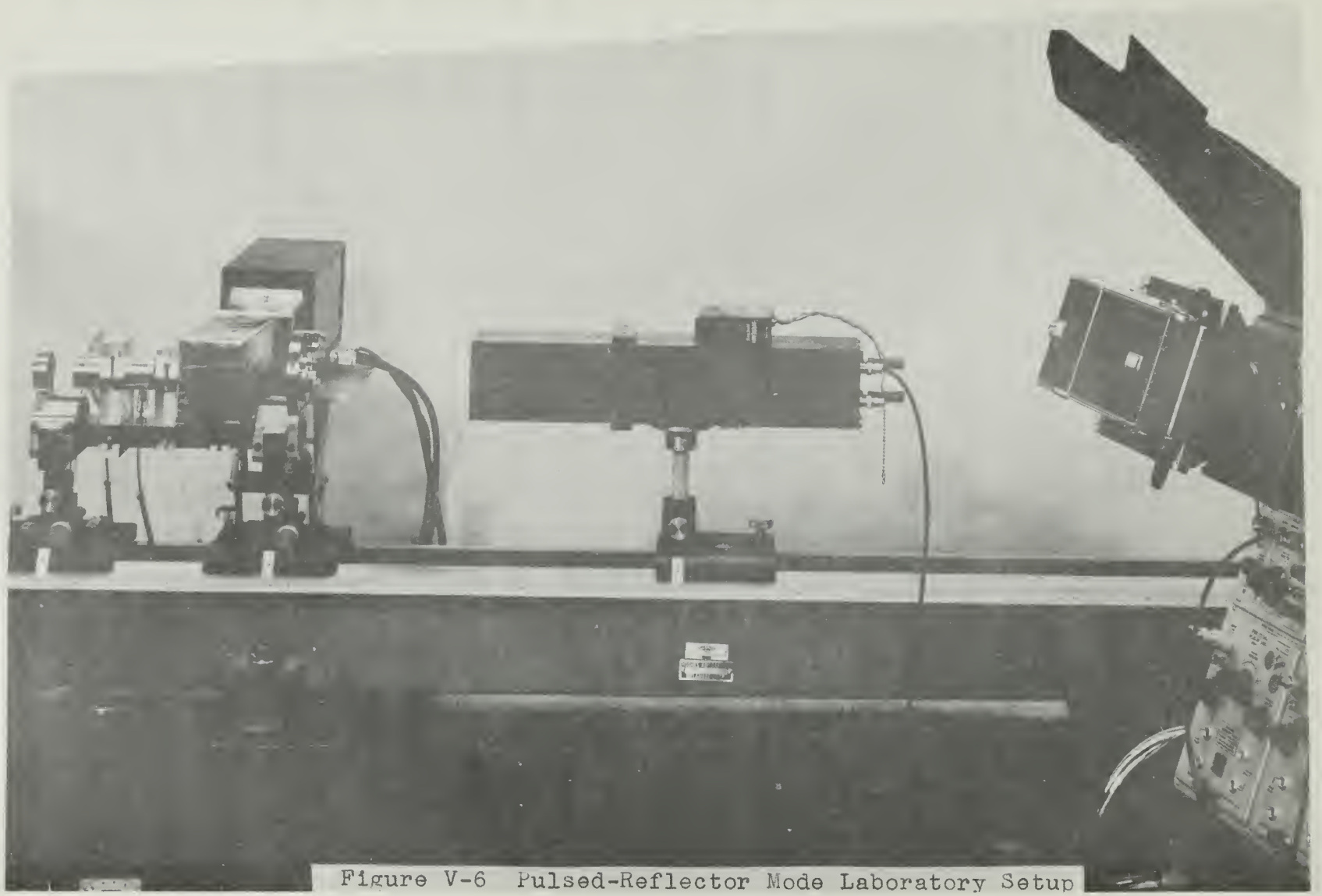

Figure V-6 Pulsed-Reflector Mode Laboratory Setup

SECTION VI

CONCLUSIONS

1. General

The outline of a mathematical framework to encompass the optical stimulated emission observed in the "Pulsed-Reflector Mode" laser was deemed necessary simply to serve as a basis of discussion. Any attempt to rigorously account for experimental results in the light of a theoretical discipline, with the objective being agreement to within experimental error, would be quite meaningless, when one stops to consider the number of variables involved in the system under investigation. For instance, power and energy output characteristics as well as laser threshold energy vary from ruby to ruby. The degree to which one is able to optically align the system plus the optical qualities of the Kerr cell, Wollaston prism and detached reflector surfaces, all bear significantly on the optimum data one may obtain. It must also be kept in mind that a severe limitation is imposed on measurements due to the inherent difficulties encountered in accurately calibrating and utilizing the phototube which forms the critical link in the instrumentation chain.

2. Instrumentation Considerations

With the foregoing statements in mind one may wish to consider the following conclusions concerning the instrumentation, which have been drawn from the experimental work performed.

(a) Substitution of a Tektronix type 519 oscilloscope for the type 555 used in the experimental

work, and shortening the signal lead from the scope to the phototube are essential, if one is to overcome the integrating effect obtained during power measurements.

(b) The phototube should be utilized in the photomultiplier rather than photodiode mode, since it is not possible to keep the photodiode linear over the measurement range required to investigate the high power and fast output pulses from the laser.

(c) Anti-reflection coatings on the Kerr cell and ruby surfaces as well as on the Wollaston prism should greatly enhance the system performance by decreasing the losses due to internal reflections.

A breakthrough in pumping source configuration and cavity design are essential, if the efficiency of the laser is to be increased beyond 0.7% which is the current state of the art value. This area is more noteworthy than just the few lines above, but it is beyond the scope of this paper. In the same sense, uniformity in ruby crystal fabrication is also a necessity before reproducibility of experimental results can be achieved.

3. Optimization of System Characteristics

As stated in the body of the paper, optical alignment of the pulsed-reflector system is the critical starting point if one intends to optimize the laser power output.

A method of alignment which exceeds in accuracy the optical alignment procedure used in the experiment is as

follows:

(a) Light from a high intensity arc is masked to appear as a point source and passed through a collimator so as to be normally incident on one of the detached reflectors.

(b) On the other side of the laser system, a high resolving power telescope is set up such that the collimated light passing through the system and out the second detached reflector will be intercepted by the lens of the telescope.

(c) In the eyepiece of the telescope, one should see a bright central spot associated with the central path of light propagation through the laser system. Surrounding the central spot should be a varied pattern of spots of lesser brilliance. These will be due to the internal reflecting surfaces of the system and will be of different colors depending on the originating surface.

(d) Presuming that the ruby and flashtube holder, Kerr cell and Wollaston prism have at least two degrees of freedom of movement, as each is adjusted one should notice that a set of spots in the eyepiece will move corresponding to the particular element which is being adjusted.

(e) It is possible to achieve extremely accurate alignment of all elements interposed between the detached reflectors by adjusting each element

until its associated spots in the eyepiece line up with the central one.

(f) This procedure should be carried out after basic alignment of the system as outlined in Section IV and Section V has been performed.

With regard to the effect of the optical switch on system performance, it is imperative that the loss in energy which is apparent upon insertion of the Kerr cell between the reflectors, be investigated more thoroughly. It is desireable to work with a physically smaller Kerr cell shutter so as to decrease the capacitance and hence the switching time, plus decreasing the voltages one must work at to obtain retardation through the cell. The degree of non-parallelism of the Kerr cell surfaces and the difficulty involved in placing anti-reflection coatings on these surfaces, could ultimately limit the applicability of the pulsed-reflector mode configuration.

With repeated laser action, it was soon noticed that the reflective coatings on the detached reflectors were becoming damaged due to the high intensity of the laser beam. Only a small area was damaged indicating that all of the observed output is coming from a very small volume of the ruby. It is highly probable that due to the damaged reflectors, the power output observed was less than its optimum value. An increase in pulse delay time t_d, and also pulse width, could be caused by damaged reflectors. This is another supporting argument to substantiate the observed discrepancy between experimental and theoretical values as

presented in Section V. The use of pyrex reflectors with low absorption loss reflective coatings should help to overcome this problem.

With the implementation of the foregoing improvements one should be able to achieve even higher peak power output and higher cavity Q by going to a higher mean reflectivity system. A hundred fold improvement in power output over that obtainable with a normal configuration is just an indication of what future developments may bring. Peak power output in the range of tens of megawatts is feasible and foreseeable for the near future.

BIBLIOGRAPHY

1. A. L. Schawlow and C. H. Townes, "Infrared and Optical Masers", Phys. Rev. 112, No. 6, pg. 1940, 15 December 1958.

2. J. Weber, Rev. of Modern Physics, 31, No. 3, pg. 681, July 1959.

3. J. Weber, Trans. IRE Prof. Group on Electron Devices, 3, June 1953.

4. J. P. Gordon, H. J. Zeiger and C. H. Townes, "The Maser-New Type of Microwave Amplifier, Frequency Standard and Spectrometer", Phys. Rev. 99, 4, pg. 1264, August 1955.

5. N. Bloembergen, Phys. Rev. 104, pg. 324, 1956.

6. T. H. Maiman, "Optical Maser Action in Ruby", Nature, 187, 6, pg. 493, August 1960.

7. A. Javan, W. R. Bennet and D. R. Herriott, "Population Inversion and Continuous Optical Maser Oscillation in a Gas Discharge Containing a He-Ne Mixture", Phys. Rev. Letters, 1 February 1961, pg. 106.

8. P. P. Sorokin and M. J. Stevenson, "Stimulated Infrared Emission from Trivalent Uranium", Phys. Rev. Letters, 5, No. 6, pg. 557, 15 December 1960.

9. P. P. Kisliuk and W. S. Boyle, "Pulsed Ruby Maser as a Light Amplifier", WESCON, San Francisco, Calif., 22 August 1961, Trans. IRE.

10. T. H. Maiman, "Optical and Microwave-Optical Experiments in Ruby", Phys. Rev. Letters 4, No. 11, pg. 564, 1 June 1960.

11. A. L. Schawlow, "Quantum Electronics", C. H. Townes, Editor Columbia University Press, 1960.

12. R. J. Collins, D. F. Nelson, A. L. Schawlow, W. Bond, C. G. B. Garrett and W. Kaiser, "Coherence, Narrowing, Directionality and Relaxation Oscillations in the Light Emission from Ruby", Phys. Rev. Letters, 5, No. 7, pg. 303, 1 October 1960.

13. R. W. Hellwarth, "Theory of the Pulsation of Fluorescent Light from Ruby", Phys. Rev. Letters, 6, No. 1, pg. 9, 1 January 1961.

14. A. L. Schawlow, "Optical Masers", Scientific American, 204, No. 6, pg. 52, June 1961.

15. E. Snitzer, "Proposed Fiber Cavities for Optical

Masers", Journal of Applied Physics, pg. 36, January 1961.

16. D. G. Nelson and R. J. Collins, "Spatial Coherence in the Output of an Optical Maser", Journal of Applied Physics, pg. 739, April 1961.

17. M. L. Stitch, "Power Output Characteristics of a Ruby Laser", Journal of Applied Physics, 32, No. 10, pg. 1994, October 1961.

18. A. M. Zarem, F. R. Marshall, and F. L. Poole, "An Electro-Optical Shutter for Photographic Purposes", Trans AIEE, 68, April 1949.

20. R. W. Hellwarth, "Advances in Quantum Electronics", J. R. Singer, Editor, Columbia University Press, 1961.

21. Condon and Odishaw, "Handbook of Physics", McGraw Hill.

22. T. H. Maiman, "Stimulated Optical Emission in Fluorescent Solids, Part 1 Theoretical Considerations", Phys. Review, 123, No. 4, pg. 1145, 15 August 1961.

23. T. H. Maiman, R. H. Hoskins, I. J. D'Haenens, C. K. Asawa, and V. Evtuhov, "Stimulated Optical Emission in Fluorescent Solids, Part 2, Spectroscopy and Stimulated Emission", Phys. Review, 123, No 4, pg. 1151, 15 August 1961.

24. A. G. Fox and T. Li, "Resonant Modes in an Optical Maser", Proc. IRE, 48, pg. 1904, November 1960.

25. W. G. Wagner and G. Birnbaum, "Cavity Modes in an Optical Maser", Proc. IRE, 49, pg. 625, March 1961.

26. M. L. Stitch, E. J. Woodbury and J. H. Morse, "Repetetive Hair Trigger Mode of Optical Maser Operation", IRE WESCON, San Francisco, August 22, 1961.

27. B. M. Oliver, "Some Potentialities of Optical Masers", IRE WESCON, San Francisco, August 22, 1961.

28. A. L. Schawlow, "Infrared and Optical Masers", The Solid State Journal, 2, No. 6, June 1961, pg. 21.

29. E. J. Woodbury, R. S. Congleton, J. H. Morse, and M. L. Stitch, "Design and Operation of an Experimental Colidar", IRE WESCON, San Francisco, August 22, 1961.

30. C. Kikuchi, J. Lambe, G. Makhov, and W. Terhune, "Ruby as a Maser Material", Journal of Applied Physics, 30, No. 7, pg. 1061, July 1959.

31. J. Kotik and M. C. Newstein, "Theory of Laser Oscilla-

tions in Fabry-Perot Resonators", Journal of Applied Physics, 32, No. 2, February 1961.

32. L. Bulberger and S. Vogel, "Lasers: Devices and Systems", Part I, Electronics, October 27, 1961, Part II, Electronics, November 3, 1961, Part III, Electronics, November 10, 1961 and Part IV, Electronics, November 24, 1961.

33. J. R. Singer and S. Wang, "General Analysis of Optical, Infrared, and Microwave Maser Oscillator Emission", Phys. Rev. Letters, 6, No. 7, 1 April 1961.

34. A. L. Schawlow and G. E. Devlin, "Simultaneous Optical Maser Action in Two Ruby Satellite Lines", 6, No. 3, pg. 96, 1 February 1961.

35. "Research on Coherent Generation of Optical Radiation", Interim Scientific Report No. 1, Hughes Research Laboratories, Atomic Physics Department, Contract No. AF33(616)-8233, 1 May 1961 through 31 July 1961.

36. "Research on Coherent Generation of Optical Radiation", Interim Scientific Report No. 2, Hughes Research Laboratories, Quantum Physics Department, Contract No. AF33(616)-8233, 1 August 1961 through 31 October 1961.

37. L. W. Taylor, "College Manual of Optics", Ginn and Company.

38. F. A. Jenkins and H. E. White, "Fundamentals of Optics", McGraw Hill Company, 2nd Edition.

39. G. W. Sears and M. W. Zemansky, "University Physics", Addison-Wesley Publishing Company, 2nd Edition.

40. J. R. Singer, "Masers", John Wiley and Sons Inc.

APPENDIX A

THE KERR EFFECT[1]

1. Physical Characteristics of a Kerr Cell Shutter.

Isotropic transparent substances become doubly refracting when placed in an electric field. This property, is known as the "Kerr effect". (Consider Figure A-1)

A beam of light, linearly polarized (synonomous to plane polarized) at an angle $\Phi = 45^{\circ}$ with respect to the applied electric field, enters the Kerr cell. Note that the cell is oriented so that the optic axis makes an angle of 45° with the $\mathcal{E}$ - vector of the incident light. The $\bar{E}$ vibration or extraordinary ray (sometimes called the P- component of the emerging light) is, in this case parallel to the optic axis, that is the applied $\bar{E}$ field on the cell, the O-vibration or ordinary ray (sometimes called the S- component of the emerging light) is perpendicular to the applied $\bar{E}$ field. It follows that the amplitude of the E and O rays is identical.

The electric vector $\mathcal{E}$, of the incident linearly polarized light, may be resolved into two components, one parallel to the applied $\bar{E}$ field and one perpendicular to the applied $\bar{E}$ field, i.e., the extraordinary ray and ordinary ray respectively.

These components traverse the cell with different velocities, and as a result, possess different wavelengths. Consequently, if the applied $\bar{E}$ field is kept fixed, the two

1. The material in this Appendix is presented in a more complete fashion in references (18) and (39).

components will differ more and more in space phase as they traverse the cell. That is to say, there will be a continuously increasing difference in time phase between the two components of light as they traverse the cell.

Since the state of polarization of the light at any point is dependent upon the difference in time phase between the two components, the light emerging from the cell will in general no longer be plane polarized.

If the angle φ of the plane of polarization upon entering the cell is 45°, and the angular time phase difference between the components, δ, is an odd multiple of $\pi/2$, the light emerging from the cell will be circularly polarized. If δ is an odd multiple of π, the emergent beam of light will be plane polarized at 90° to the plane of polarization of the incident light.

Figure A-2 illustrates the states of polarization for $\delta = 0, \pi/4, \pi/2, 3\pi/4, \pi$ etc. The value $\delta = \pi$ represents the condition for "full open" operation of the Kerr cell. For the orientation of Figure A-1 of polarizer and analyzer, if the voltage applied to the cell is such as to equal the voltage corresponding to the "full open" condition of the cell, then maximum intensity of the emergent beam would be in evidence. At "full open" voltage, the transmission is actually 50%, because half of the light is initially rejected by the polarizer. The following analysis will help to clarify the foregoing statements.

The Kerr constant B is defined by the equation,

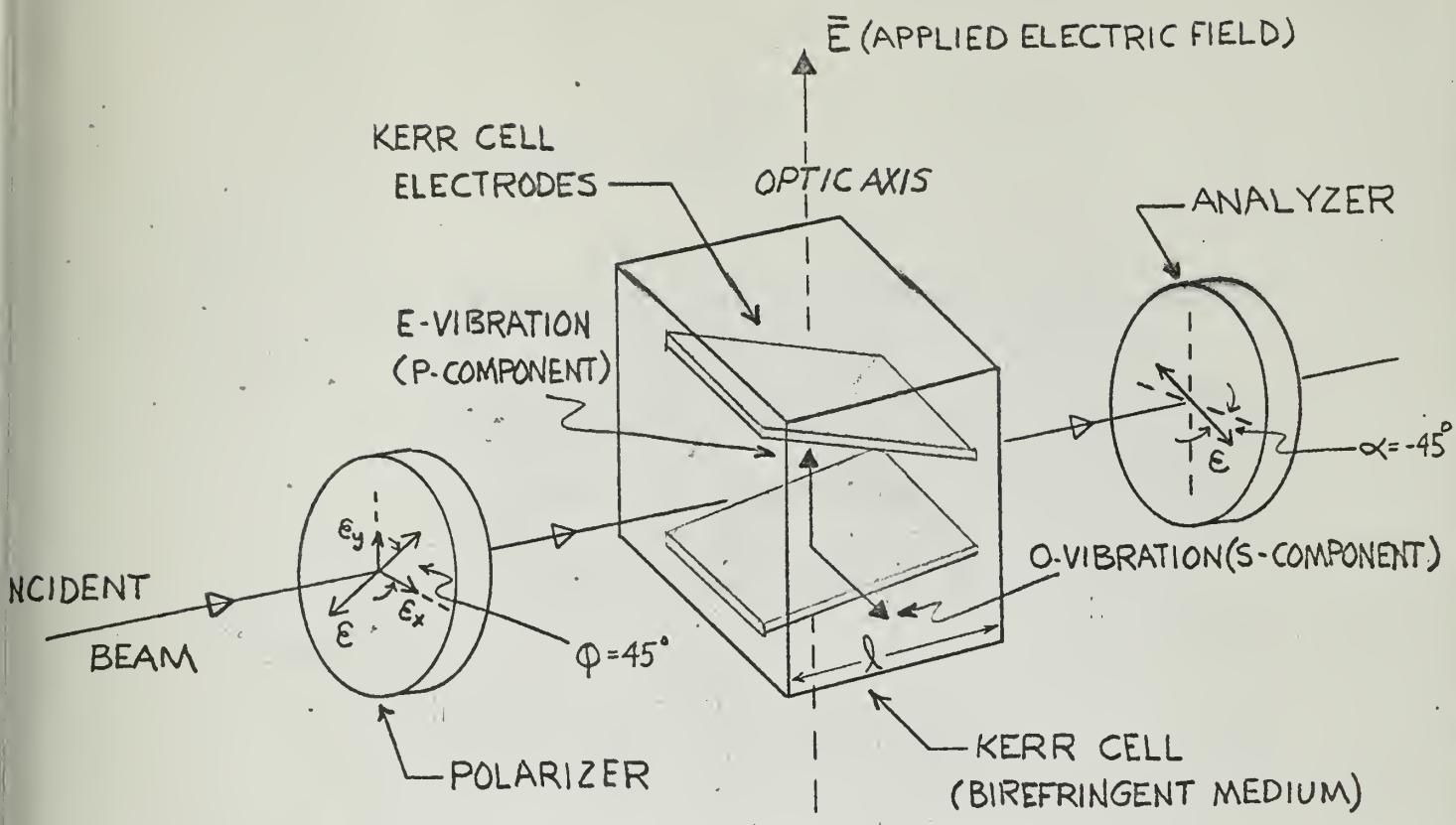

FIGURE A-1 KERR CELL AND CROSSED POLAROIDS

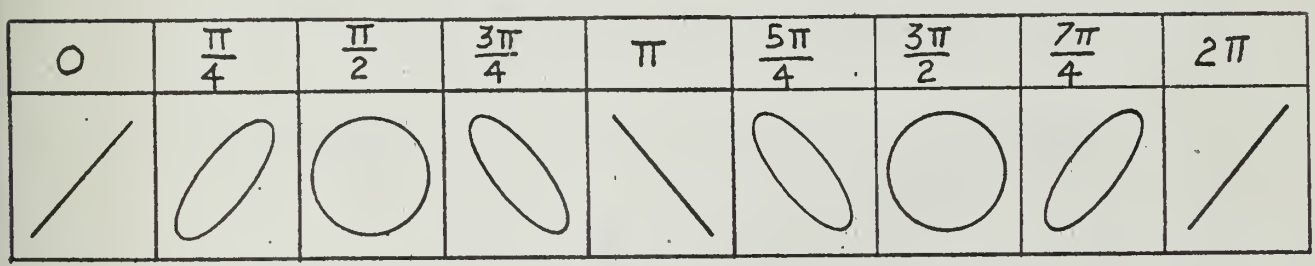

FIGURE A-2 VIBRATIONS RESULTING FROM THE COMBINATION OF VERTICAL AND HORIZONTAL SIMPLE HARMONIC MOTION OF THE SAME FREQUENCY AND AMPLITUDE FOR VARIOUS VALUES OF PHASE DIFFERENCE BETWEEN THE TWO MOTIONS

$$n_p - n_s = B\lambda\bar{E}^2 \qquad (1)$$

Where,

n_p = refractive index in a direction parallel to the applied electric field.

n_s = refractive index in a direction perpendicular to the applied electric field.

λ = wavelength of the incident light in vacuum (cm).

$\bar{E}$ = applied electric field in esu.

Now,

$$n_p = \frac{c}{v_p} \quad ; \quad n_s = \frac{c}{v_s} \qquad (2)$$

Where,

c = velocity of light in free space.

v_p, v_s = velocity of the components parallel and perpendicular to the applied electric field in the Kerr cell

Substituting equation (2) into (1), we obtain,

$$\frac{c}{\lambda}\left(\frac{1}{v_p} - \frac{1}{v_s}\right) = B\bar{E}^2 \qquad (3)$$

Since,

$$\nu = \frac{c}{\lambda} = \frac{\omega}{2\pi} \qquad (4)$$

then upon substitution, equation (3) becomes

$$\omega\left(\frac{1}{v_p} - \frac{1}{v_s}\right) = 2\pi B\bar{E}^2 \qquad (5)$$

multiplying both sides of equation (5) by the length of the Kerr cell electrodes, l,

$$\omega\left(\frac{\ell}{v_p} - \frac{\ell}{v_s}\right) = 2\pi \ell B \bar{E}^2 \qquad (6)$$

Now let

$t_p = \ell/v_p$ = time required for the p component of light to traverse the Kerr cell (extraordinary ray)

$t_s = \ell/v_s$ = time required for the s component of light to traverse the Kerr cell (ordinary ray)

The difference in transit times may be expressed as an angular phase displacement between the two components of light.

$$\delta = \omega t_p - \omega t_s = \delta_p - \delta_s \qquad (7)$$

and from equation (6), we obtain the relationship

$$\delta = 2\pi \ell B \bar{E}^2 \qquad (8)$$

Where,

ℓ = length of the light path under influence of the electric field in centimeters

B = Kerr constant for the substance in cm-gm-seconds esu.

It should be noted that the Kerr constant for nitrobenzene depends upon temperature as well as upon the wavelength of the incident light. (See Figure IV-5(b))

2. Electro-optical characteristics of the Kerr cell.

In Figure A-1, let $\mathcal{E}$ be the plane polarized light vector as it leaves the polarizer. Then

$$\mathcal{E} = i\mathcal{E}_x + j\mathcal{E}_y \qquad \text{for any t and } \ell \qquad (9)$$

and

$$\mathcal{E}_x = \left[e_o e^{-j\omega\left(\frac{\ell}{v} - t\right)} \right] \cos\varphi \qquad \text{real part} \qquad (10)$$

where

e_o = magnitude of the electric vector in the incident light

v = velocity of propagation of light in ℓ direction.

Due to the birefringent nature of the Kerr cell under the application of an electric field $\bar{E}$, $\mathcal{E}_x$ and $\mathcal{E}_y$ traverse the Kerr cell with velocities v_p and v_s respectively in the direction parallel and perpendicular to the applied $\bar{E}$ field vector.

Hence, the real part is

$$\mathcal{E} = i e_o e^{-j\omega\left(\frac{\ell}{v_p} - t\right)} \cos\varphi + j e_o e^{-j\omega\left(\frac{\ell}{v_s} - t\right)} \sin\varphi \qquad (11)$$

Using equations (4) and (7),

$$\frac{\omega\ell}{v_p} = \frac{2\pi\ell}{v_p} = \delta_p \; ; \; \frac{\omega\ell}{v_s} = \frac{2\pi\ell}{v_s} = \delta_s \qquad (12)$$

and upon substituting (12) into (11) one obtains the following,

$$\mathcal{E} = i e_o e^{-j(\delta_p - \omega t)} \cos\varphi + j e_o e^{-j(\delta_s - \omega t)} \sin\varphi \qquad (13)$$

which is a vector expression for the electric field in the light at the analyzer, at any time t.

The light which passes through the analyzer, is the component of $\mathcal{E}$ in the α direction, where

$$\mathcal{E}_\alpha = \mathcal{E}(i\cos\alpha + j\sin\alpha) \tag{14}$$

The intensity of the light emerging from the analyzer is proportional to the square of the maximum amplitude of the light vector. Hence,

$$|\mathcal{E}_\alpha|^2 = \mathcal{E}_\alpha \mathcal{E}_\alpha^* \tag{15}$$

and $\mathcal{E}_\alpha^*$, the complex conjugate of $\mathcal{E}_\alpha$ is given by,

$$\mathcal{E}_\alpha^* = e_0\cos\varphi\cos\alpha\left(e^{+j(\delta_p-\omega t)}\right) + e_0\sin\varphi\sin\alpha\left(e^{+j(\delta_s-\omega t)}\right) \tag{16}$$

Consequently, since the magnitude of light which passes through the analyzer will be given by the real part of (15), we have,

$$|\mathcal{E}_\alpha|^2 = e_0^2\left[\cos^2\varphi\cos^2\alpha + \sin^2\varphi\sin^2\alpha + 2(\sin\varphi\sin\alpha)(\cos\varphi\cos\alpha)(\cos\{\delta_p-\delta_s\})\right] \tag{17}$$

Using equation (7) and also $\cos\delta = 1-2\sin^2(\delta/2)$, equation (17) becomes

$$|\mathcal{E}_\alpha|^2 = e_0^2\left[\cos^2(\varphi-\alpha) - \sin 2\varphi\sin 2\alpha\sin^2\left(\frac{\delta}{2}\right)\right] \tag{18}$$

The transmission is defined as the ratio of intensities of emergent and incident light. Thus the percentage transmission is given by,

$$T = 100\,\frac{|\mathcal{E}_\alpha|^2}{e_0^2} \text{ per cent} \tag{19}$$

therefore,

$$_{\varphi}T_{\alpha} = 100\left[\cos^2(\varphi-\alpha) - \sin 2\varphi \sin 2\alpha \sin^2\left(\frac{\Gamma}{2}\right)\right] \text{ per cent} \qquad (20)$$

Where,

φ = angle between the plane of polarization of the entering light and the applied electric field.

α = angle at which the analyzer is set relative to the applied electric field

$\Gamma = 2\pi l B\bar{E}^2$ as in equation (8)

For optimum operation as a shutter $\varphi = 45^\circ$ and $\alpha = -45^\circ$ and the transmission therefore becomes,

$$_{\frac{\pi}{4}}T_{-\frac{\pi}{4}} = 50\left[\sin^2\frac{\pi}{2}\left(\frac{V}{V_0}\right)^2\right] \text{ per cent} \qquad (21)$$

upon substitution of equation (8) where V_0 = applied potential for the corresponding full-open electric field, $\bar{E}_0$.

Note that for linearly polarized (plane polarized) light output from an optical maser, the transmission without the polarizer in the light path becomes,

$$_{\frac{\pi}{4}}T_{-\frac{\pi}{4}} = 100\left[\sin^2\frac{\pi}{2}\left(\frac{V}{V_0}\right)^2\right] \text{ per cent} \qquad (22)$$

(See Figure A-3 for a plot of percent transmission versus voltage applied to the Kerr cell as percent of full open voltage.)

In order to maintain $\varphi = 45^\circ$ in the absence of a polarizer, the ruby and Kerr cell must be off set physically from each other by 45°. Consequently, either the ruby or Kerr cell must be rotated by 45° while the other is held fixed.

ELECTRO-OPTICAL CHARACTERISTICS OF A KERR CELL SHUTTER AS UTILIZED IN THE PULSE REFLECTOR MODE

PERCENT TRANSMISSION VERSUS VOLTAGE APPLIED TO SHUTTER AS PERCENT OF "FULL OPEN" VOLTAGE

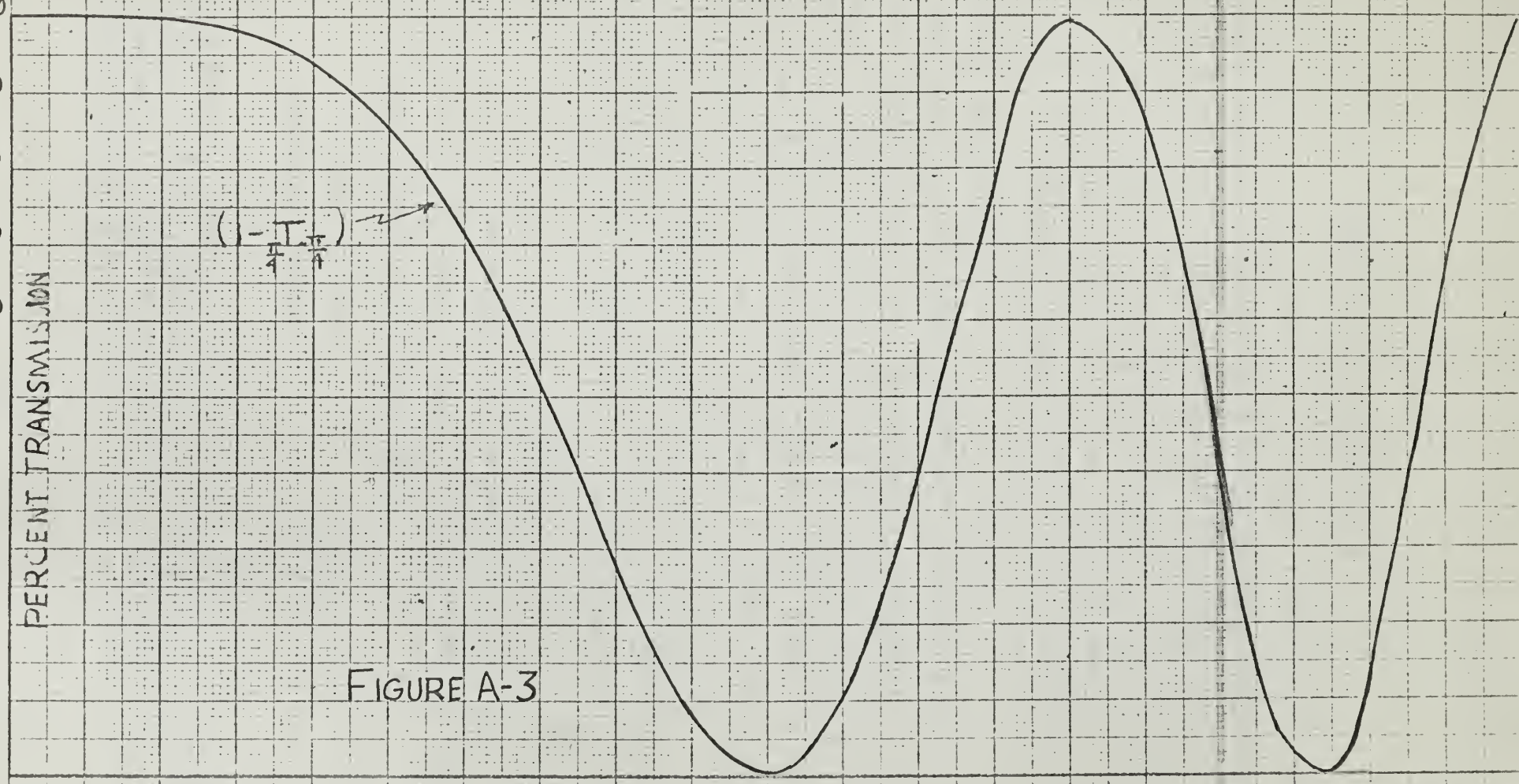

FIGURE A-3

APPENDIX B

A SHORT SUMMARY OF THE PHYSICAL PROPERTIES OF SYNTHETIC SAPPHIRE[1]

The physical properties of synthetic sapphire make it valuable for special applications where conventional materials are inadequate. Sapphire has high transmission in the ultraviolet, visible and infrared spectrum. It has a low dispersion and low susceptibility to abrasion, making it an ideal material for optical systems where the possibility of mechanical abuse exists.

The addition of a small amount of chromium to pure sapphire produces ruby. The paramagnetic resonance of the Cr^{+++} ion in the crystal lattice is used for both microwave and optical maser applications. In a "pink" ruby the chromium impurity is less than 0.1 percent, while in a "standard" ruby it is between 0.1 percent and 0.5 percent. The classification of "dark" ruby is reserved for sapphire with a chromium impurity concentrate of greater than 0.5 percent.

The following list of characteristics and equations applicable to synthetic sapphire, as well as ruby, are considered to be of useful value to the engineer involved in laser systems research and development.

Chemical Formula	Al_2O_3
Molecular Weight	101.94

1. The material presented in this Appendix is based on a report by R. A. McFarlane of the Adolf Meller Company entitled "A Summary of Available Data on the Physical Properties of Synthetic Sapphire". This report is available for those who desire a more comprehensive coverage than appears here.

Specific Gravity	3.98 gm/cm^3
Water Absorption	nil
Melting Temperature	2,040±10°C
Specific Heat	0.0249 at 91°K 0.1813 at 291°K
Bulk Modulus	300,000 psi
Modulus of Rupture and Rigidity	function of crystal orientation

The refractive index for the ordinary ray can be calculated from the following equation,

$$\eta_s = 1.74453 + \frac{101.0}{\lambda - 1598} \qquad (1)$$

where λ is the wavelength in angstroms. The refractive index for the extraordinary ray, η_p, is approximately .008 less than η_s.

If no internal absorption occurs, the transmittance of a plane-parallel plate can be expressed as a function of the refractive index as follows,

$$T = \frac{2\eta}{\eta^2 + 1} \qquad (2)$$

where internal reflections are considered. At wavelengths shorter than 0.3 μ internal absorption results in a sharp decrease of transmission. In the infrared portion of the spectrum, transmission is maintained out to approximately 4 microns. Internal absorption again causes a sharp decrease in T at longer wavelengths.

Overall transmittance must include Fresnel reflection losses. Consequently,

$$T = \frac{(1-L_r)^2 e^{-\alpha x}}{1-L_r^2 e^{-2\alpha x}} \qquad (3)$$

where T is the ratio of transmitted to incident light intensity, α is the coefficient of absorption, x is the thickness of the material in the direction of propagation, and L_r is the surface reflection coefficient given by

$$L_r = \frac{(\eta-1)^2}{(\eta+1)^2} \qquad (4)$$

To calculate the number of chromium ions in ruby per unit volume the following equation may be used.

$$N_o = 3.16 \times 10^{22} f \qquad (5)$$

where N_o is the number of Cr^{+++} ions per cm^3, and f is the fraction by weight of Cr_2O_3 in Al_2O_3.

The absorption coefficient is obtainable from

$$\alpha = \sigma N_o \qquad (6)$$

where σ is the atomic absorption crossection.

APPENDIX C

APPLICABLE TERMINOLOGY AND GENERAL INFORMATION FROM THE FIELD OF OPTICS[1]

1. Glossary of Commonly used Optical Terms

(a) Absorption is the transference of some or all of the energy contained in electromagnetic waves to the substance they transverse or are incident upon. Absorbed energy from incident or transmitted light waves is converted into energy of other forms, usually heat, within the medium with a resultant weakening of the light beam.

(b) Anisotropic refers to having different characteristics in different directions. Two identical light beams propagating through an anisotropic material in different directions will be affected in different manners.

(c) Angle of Deviation is the angular change in direction of a light ray after crossing the interface between two different media.

(d) A beam is a parallel, diverging or converging flow of electromagnetic radiation. In light, it refers to a directed bundle of light rays.

(e) Birefringence is the splitting of a light beam into two divergent components upon passage through a doubly refracting medium. The two components travel at

1. This section follows a more detailed treatment entitled "Optical Techniques for Electronic Engineers" contained in the October 20, 1961 issue of Electronics Magazine.

different velocities in the medium.

(f) A "Black Body" is an ideal body that would absorb all radiation incident on it.

(g) Coated optics are optical refracting and reflecting surfaces that have been coated with one or more layers of dielectric or metallic material for reducing or increasing reflection from the surfaces, either totally or for selected wavelengths and for protecting the surfaces from abrasion and corrosion.

(h) Coherence is aptly defined in Section II.

(i) A collimator is an optical system that transforms convergent or divergent light rays into beams of parallel rays.

(j) Doubly Refracting refers to the velocity of propagation of a wave through a crystal which depends on the relation of the plane of polarization to the axis of the crystal. If a beam of light is transmitted into a doubly refracting crystal, it will be separated into two parts having different directions of travel associated with the different states of polarization of the incident beam.

(k) A Fabry-Perot Interferometer is a high-resolution multiple-beam interferometer consisting of two optically flat and parallel glass or quartz plates held a short fixed and known distance apart. The adjacent surfaces of the plates or interferometer flats are made almost totally reflecting by a thin silver film or multilayer dielectric coating.

(l) Interference is the systematic reinforcement and attenuation of two or more light waves when they are superimposed.

(m) Laser is Light Amplification by Stimulated Emission of Radiation. (See Optical Maser)

(n) A monochromator is an instrument for isolating narrow portions of the spectrum, by means of dispersion of light into its component colors.

(o) Multilayer Dielectric Coating is described in the following sub-heading.

(p) Optical axis is the axis of symmetry, or the line joining the centers of curvatures of the surfaces of an optical system.

(q) An optical filter is a component or group of components placed in an optical system to reduce or eliminate certain selected wavelengths while leaving others relatively unchanged, or to modify the intensity of polarization of light.

(r) An Optical Maser is a source of nearly monocromatic and coherent radiation produced by the synchronous and cooperative emission of optically pumped ions introduced into a crystal host lattice or gas atoms excited in a discharge tube. The radiation has a sharply defined frequency and propagates in an intense highly directional beam.

(s) A polarizer is an optical device capable of transforming unpolarized or natural light into polarized light, or altering the polarization of polarized light.

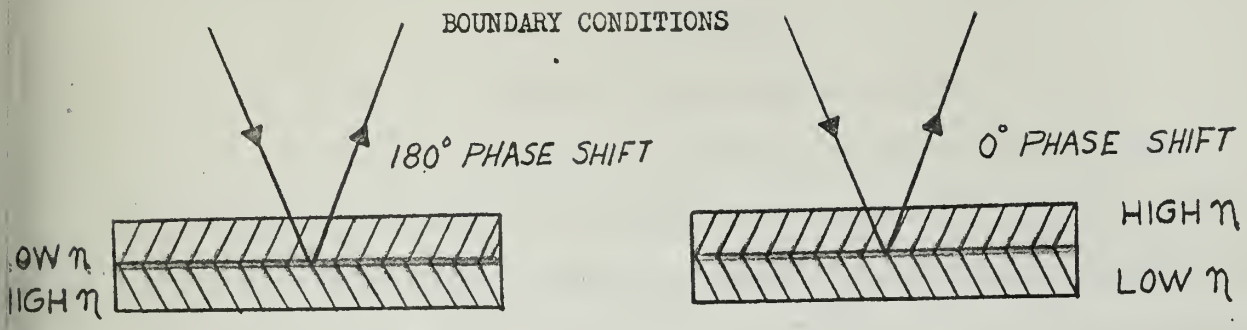

FIGURE C-1 Upon reflection at interface between two media, incident light undergoes phase shift of 180° if first medium is less dense than second; 0° if first is denser than second.

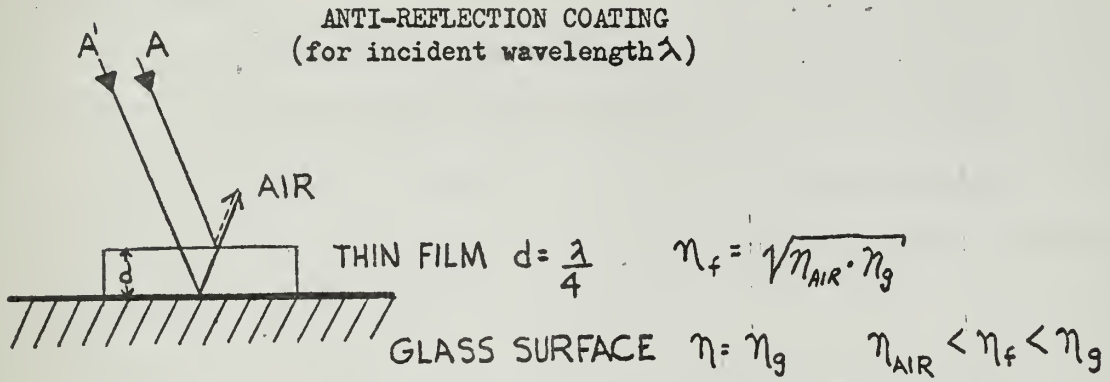

FIGURE C-2 At air-film interface, wave A' reflected from glass surface is exactly ½ wavelength out of phase with wave A reflected from film surface and destructive interference occurs eliminating reflected beam.

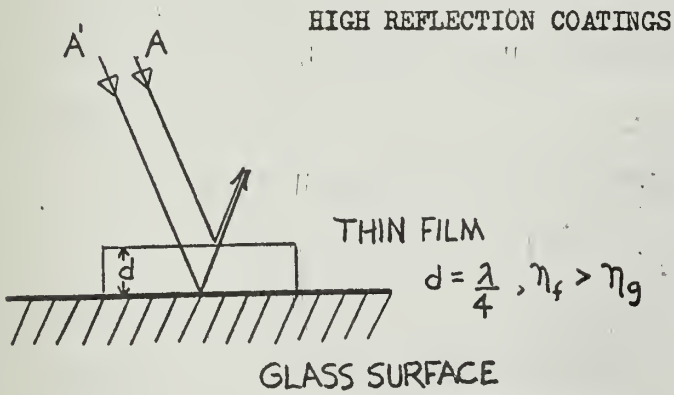

FIGURE C-3 For incident wavelength λ or multiples of λ, A and A' interfere constructively, producing high reflectance.

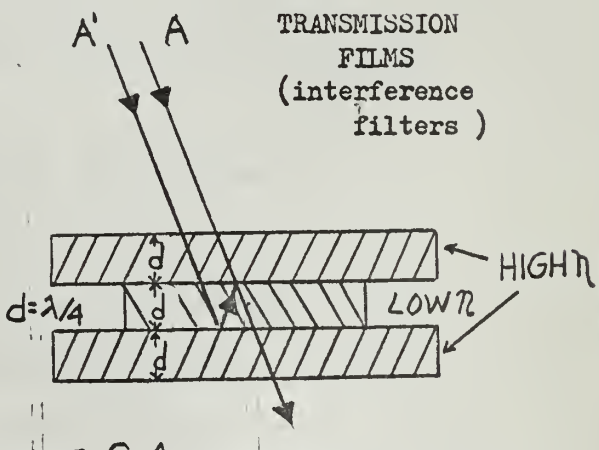

FIGURE C-4 For incident wavelengths of λ or multiples of λ A and A' interfere constructively producing transmission. Other wavelengths interfere destructively.

APPENDIX D

NOTES ON SPECTROPHOTOMETRY

Absorption spectrophotometry is based on the observation and comparison of absorption spectra of two materials, one a standard, the other a sample under investigation. The absorption spectrum is a curve showing the amount of radiant energy absorbed at each wavelength while the transmission spectrum depicts the per cent energy transmitted at each wavelength.

By definition, transmittance (T) is the ratio of the radiant energy transmitted by a sample (P), to the energy incident upon the sample (P_o). Both radiant energies must be obtained at the same wavelength with the same spectrophotometer slit width adjustment.

$$T = P/P_o \quad \text{per cent} \qquad (1)$$

Usually in a spectrophotometer, the transmittance of the standard is 100% or is defined as being 100%. Consequently, when the transmittance of a sample is given, it is necessary to specify the standard with which the sample was compared.

The absorbance (A), of a sample is defined as

$$A = -\log_{10} T = \log_{10} 1/T \qquad (2)$$

Where T is expressed as a decimal fraction, and not in per cent. As with the transmittance measurements, the standard with which the sample was compared should always be included with the absorbance data. The absorbance of the standard is usually defined to be zero. Absorbance units are usually given in decimal numbers i.e., T = 10%, 1%, 0.1% etc.,

corresponds to absorbance units of 1, 2, 3, etc., respectively.

Figure D-1 is a representation of radiation intensity plotted versus wavelength. Defined on the diagram are the following:

(1) Half intensity bandwidth - the span of wavelengths leaving the monochromator, each of which contributes at least half as much energy as does the wavelength with the greatest energy.

(2) Spectral bandwidth - is twice the half intensity bandwidth.

It should be made clear that in Figure D-1, the ordinate of the curve could just as well be per cent transmission, instead of the quantity P in equation (1).

Figure D-2 is a diagram of the classical spectrophotometer used to measure reflectance of a sample. Since transmittance is one minus the reflectance, the principles involved in the operation of the instrument shown are applicable to the problem of direct measurement of per cent transmission.

With reference to the diagram shown, light from a source A is dispersed by a prism B, and a narrow range of wavelengths is isolated by the adjustment of a slit width C. The beam passing through the slit is divided at D into two beams of equal intensity by a half silvered mirror or its equivalent. The transmitted beam strikes the standard material while the reflected beam from mirror E, strikes the surface of the sample. The quantity of light striking the standard may be reduced by a device shown schematically at

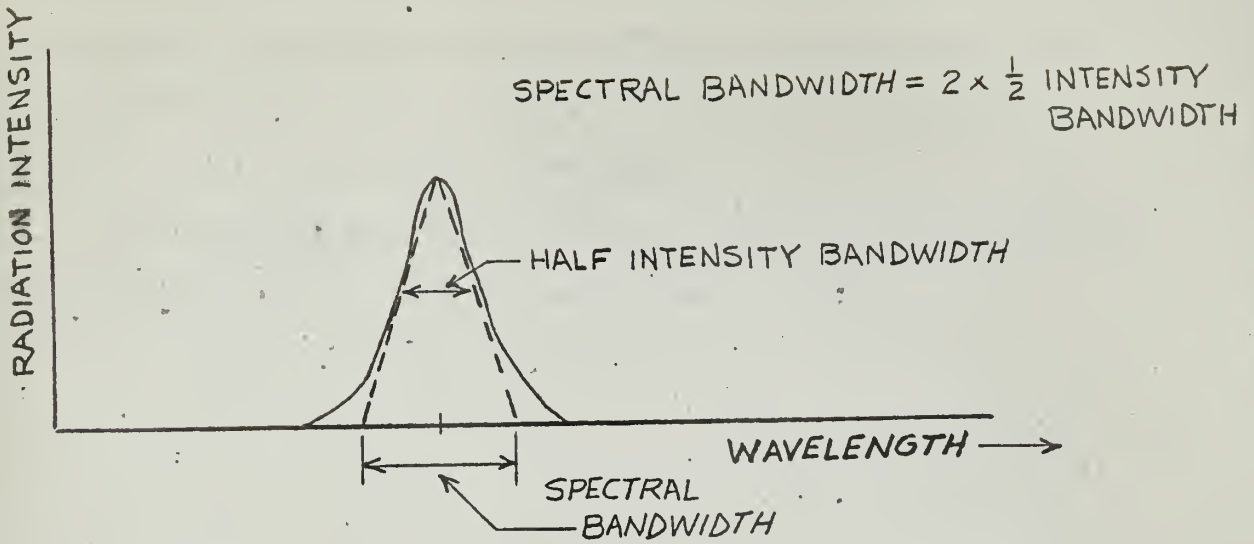

FIGURE D-1 BANDWIDTH MEASUREMENTS FROM SAMPLE TRANSMISSION CHARACTERISTICS.

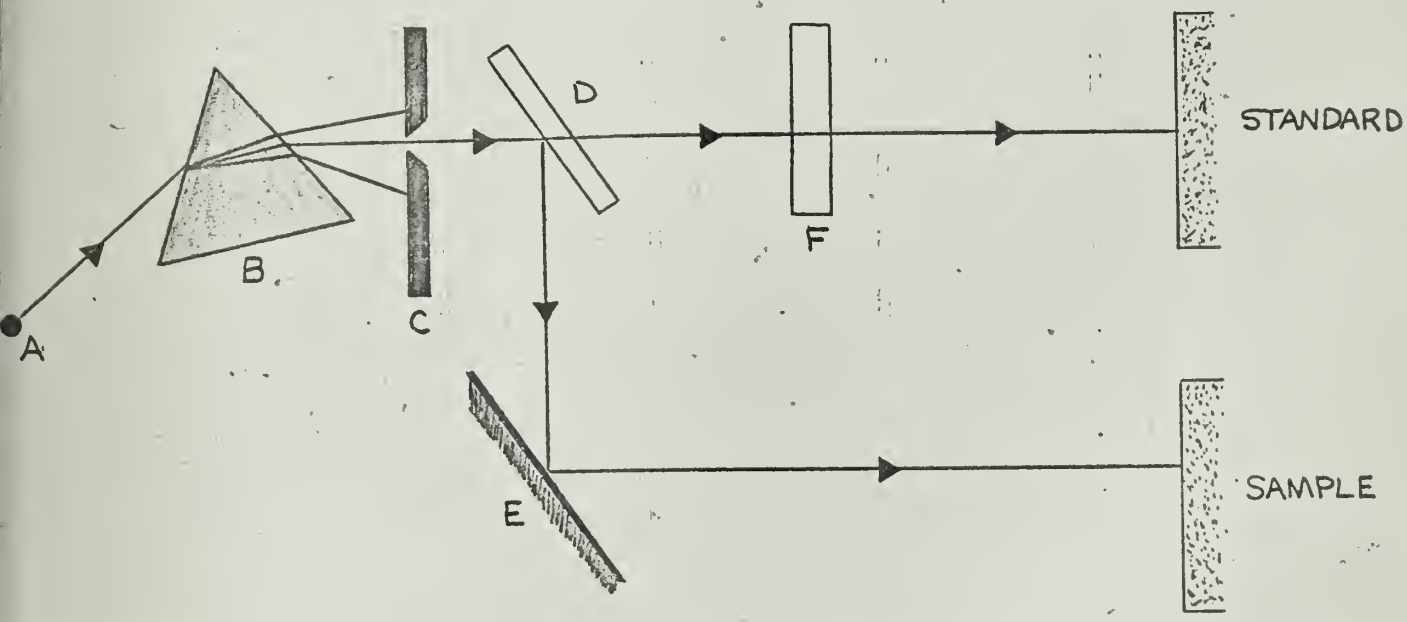

FIGURE D-2 DIAGRAM OF THE BASIC SPECTROPHOTOMETER; INSRUMENT DEPICTED MEASURES THE SPECTRAL REFLECTANCE OF A SAMPLE RATHER THAN ITS TRANSMISSIVITY.

F, until the sample and the standard appear equally bright. A measure of the decrease in brightness required to obtain a brightness match is a measure of the reflectance of the sample at the wavelength in question.

By adjusting the slit width one may vary the wavelength and hence obtain a complete reflectance curve.

APPENDIX E

FIRST ORDER APPROXIMATE ANALYSIS OF STIMULATED OPTICAL EMISSION FROM RUBY

1. Low Regenerative Environment[1]

In the absence of regenerative feedback, the population of the three states in the ruby optical maser are given by the following equations

$$\frac{dN_1}{dt} = -W_{31}(N_1 - N_3) + \frac{N_2}{T_2} \qquad (1)$$

$$\frac{dN_2}{dt} = W_{12}(N_1 - N_2) - \frac{N_2}{T_2} + \frac{N_3}{T_3} \qquad (2)$$

$$\frac{dN_3}{dt} = W_{13}(N_1 - N_3) - \frac{N_3}{T_3} \qquad (3)$$

but $W_{12} = 0$ in the absence of regeneration, so that (2) above becomes

$$\frac{dN_2}{dt} = -\frac{N_2}{T_2} + \frac{N_3}{T_3} \qquad (2a)$$

where the population N_3 decays to state 2 with lifetime T_3, N_2 decays to state 1 with characteristic lifetime T_2, and W_{ij}, the induced pumping transition probability per unit time is proportional to the pump power and the doping fraction.

Under steady state conditions, $dN_3/dt = dN_2/dt = dN_1/dt$

1. This section follows closely an analysis originated by Mr. W. A. Snyder of Hughes Aircraft Company. His tutorial assistance in the preparation of this material in the form in which it appears is gratefully acknowledged by the writer.

= 0 so, from equation (3)

$$\frac{N_2}{\tau_2} = W_{31}(N_1 - N_3) \tag{4}$$

or

$$N_2 = W_{31}\tau_2(N_1 - N_3) \tag{5}$$

and from equation (2a) above we have

$$N_2 = \frac{N_3\tau_2}{\tau_3} \tag{6}$$

So that substituting (6) into (5) it follows that

$$\frac{N_3\tau_2}{\tau_3} = W_{31}\tau_2(N_1 - N_3) \tag{7}$$

or

$$N_3 = \left[\frac{W_{31}\tau_3}{1 + W_{31}\tau_3}\right]N_1 \tag{8}$$

Equation (6) may also be written in the form

$$N_2 = \frac{\tau_2}{\tau_3}\left[\frac{W_{31}\tau_3 N_1}{1 + W_{31}\tau_3}\right] = \left[\frac{W_{31}\tau_2}{1 + W_{31}\tau_3}\right]N_1 \tag{9}$$

Since the total number of Cr^{+++} ions is fixed, then by conservation

$$N_1 + N_2 + N_3 = N_0, \text{ a constant.} \tag{10}$$

Hence, the steady state values for the fraction of the total population in each of the three states is as follows:

$$N_1 = N_0 - \left[\frac{W_{31}\tau_3}{1 + W_{31}\tau_3}\right]N_1 - \left[\frac{W_{31}\tau_2}{1 + W_{31}\tau_3}\right]N_1$$

and,

$$N_0 = N_1\left[1 + \frac{W_{31}\tau_2}{1+W_{31}\tau_3} + \frac{W_{31}\tau_3}{1+W_{31}\tau_3}\right]$$

or

$$\frac{N_1}{N_0} = \frac{1+W_{31}\tau_3}{1+2W_{31}\tau_3+W_{31}\tau_2} \qquad (11)$$

Also,

$$\frac{N_2}{N_0} = \frac{W_{31}\tau_2}{1+2W_{31}\tau_3+W_{31}\tau_2} \qquad (12)$$

In like manner it follows that,

$$\frac{N_3}{N_0} = \frac{W_{21}\tau_3}{1+2W_{31}\tau_3+W_{31}\tau_2} \qquad (13)$$

One may proceed to investigate the condition of population inversion as follows:

For values of $\tau_2 \cong 3 \times 10^{-3}$ sec (Maiman Brit. Comm. & Elex. Varsanyi, Wood, Schawlow Py. Rev, Let. 3, 544 1959)

and of $\tau_3 \cong 5 \times 10^{-8}$ sec (Maiman Phys. Rev. Let. 4, 564 1959)

$$\frac{N_2 - N_1}{N_0} = \frac{W_{31}(\tau_2 - \tau_3) - 1}{W_{31}(\tau_2 + 2\tau_3) + 1} \qquad (14)$$

so for $(N_2 - N_1)/N_0 \geq 0$

$$W_{31}(\tau_2 - \tau_3) \geq 1 \tag{15}$$

From the values of τ_2 and τ_3 given above, $\tau_2/\tau_3 = 10^5$ sec, and the condition of population inversion is essentially,

$$W_{31} \geq \frac{1}{\tau_2} \tag{16}$$

and equation (14) reduces to

$$\frac{N_2 - N_1}{N_0} \cong \frac{W_{31}\tau_2 - 1}{W_{31}\tau_2 + 1} \tag{17}$$

A plot of $(N_2 - N_1)/N_0$ versus $W_{31}\tau_2$ on four cycle semi-log paper would appear as the following graph:

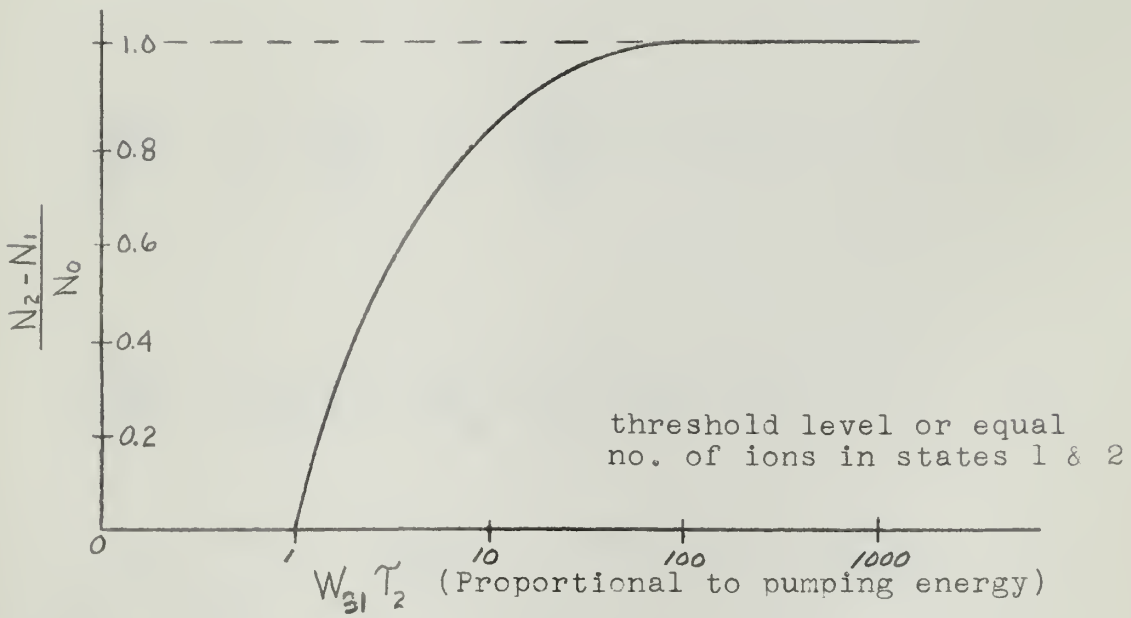

Figure E-1 The quantity $(N_2-N_1)/N_0 \triangleq$ as the fraction of the total population which is inverted. Typical value of $W_{31}\tau_2$ is $1 \leq W_{31}\tau_2 \leq 10$

It can be concluded, that for $\tau_3/\tau_2 \ll 1$ and $W_{31}\tau_3 \ll 1$,

that the Cr^{+++} ions are almost entirely located in states number 1 and number 2 since we can write equation (13) as

$$\frac{N_3}{N_0} \cong \frac{W_{31}\tau_3}{1 + W_{31}\tau_2} \cong 0 \text{ for } \frac{\tau_2}{\tau_3} \gg 1 \quad (18)$$

The transient behaviour of the state populations is found by solving simultaneously, the linear first order differential equations for the population of the three states. The solution can be obtained in the Laplace domain and the inverse Laplacian will provide the time domain solution. For no regenerative feedback and under steady state conditions, equations (1), (2a) and (3) can be rewritten as follows:

$$\frac{dN_1}{dt} + W_{31}N_1 - \frac{N_2}{\tau_2} - W_{13}N_3 = 0 \quad (19)$$

$$\frac{dN_2}{dt} + \frac{N_2}{\tau_2} - \frac{N_3}{\tau_3} = 0 \quad (20)$$

$$\frac{dN_3}{dt} - W_{31}N_1 + \left(W_{31} + \frac{1}{\tau_3}\right)N_3 = 0 \quad (21)$$

Let $T = W_{31}t$, $\alpha_2 = \frac{1}{W_{31}\tau_2}$, and $\alpha_3 = \frac{1}{W_{31}\tau_3}$, also n_{10}, n_{20}, and n_{30} = initial conditions of state population where $n_{10} = N_0$, $n_{20} = n_{30} = 0$ since all the ions are initially in the ground state. Thus, upon introducing the Laplace operator, equations (19), (20) and (21) become,

$$s n_1 + n_1 - \alpha_2 n_2 - n_3 = N_0 \qquad (19')$$

$$s n_2 + \alpha_2 n_2 - \alpha_3 n_3 = 0 \qquad (20')$$

$$s n_3 - n_1 + (1+\alpha_3) n_3 = 0 \qquad (21')$$

and the simultaneous solution of the above equation set yields the following:

$$n_1 = \frac{N_0 (s+\alpha_2)(s+1+\alpha_3)}{s\left[s^2 + (2+\alpha_2+\alpha_3)s + (2\alpha_2 + \alpha_2\alpha_3 + \alpha_3)\right]} \qquad (22)$$

$$n_2 = \frac{\alpha_3 N_0}{s\left[s^2 + (2+\alpha_2+\alpha_3)s + (2\alpha_2 + \alpha_2\alpha_3 + \alpha_3)\right]} \qquad (23)$$

$$n_3 = \frac{N_0 (s+\alpha_2)}{s\left[s^2 + (2+\alpha_2+\alpha_3)s + (2\alpha_2 + \alpha_2\alpha_3 + \alpha_3)\right]} \qquad (24)$$

One of the roots of the denominator polynomial in equations (22) through (24), is zero. In the general form, the denominator polynomial is $(s-p_1)(s-p_2)(s-p_3)$ with $p_1 = 0$. By the quandratic formula

$$p_{2,3} = -\left(1 + \frac{\alpha_2 + \alpha_3}{2}\right) \pm \sqrt{1 - \alpha_2 + \left(\frac{\alpha_3 - \alpha_2}{2}\right)^2}$$

Equations (22), (23) and (24) may now be written in the following general form

$$m_1 = \frac{N_0 (s + \alpha_3)(s + 1 + \alpha_3)}{s(s - p_2)(s - p_3)} \tag{22'}$$

$$m_2 = \frac{\alpha_3 N_0}{s(s - p_2)(s - p_3)} \tag{23'}$$

$$m_3 = \frac{N_0 (s + \alpha_2)}{s(s - p_2)(s - p_3)} \tag{24'}$$

By taking the sum of the residues, one may determine the following time domain transient response equations

$$\frac{N_1}{N_0} = \frac{\alpha_2 (1 + \alpha_3)}{p_2 p_3} + \frac{(p_2 + \alpha_2)(p_2 + 1 + \alpha_3) e^{p_2 T}}{p_2 (p_2 - p_3)} + \frac{(p_3 + \alpha_2)(p_3 + 1 + \alpha_3) e^{p_3 T}}{p_3 (p_3 - p_2)} \tag{25}$$

Similarly,

$$\frac{N_2}{N_0} = \alpha_3 \left[\frac{1}{p_2 p_3} + \frac{e^{p_2 T}}{p_2(p_2 - p_3)} + \frac{e^{p_3 T}}{p_3(p_3 - p_2)} \right] \tag{26}$$

and,

$$\frac{N_3}{N_0} = \frac{\alpha_2}{p_2 p_3} + \frac{(p_2 + \alpha_2) e^{p_2 T}}{p_2(p_2 - p_3)} + \frac{(p_3 + \alpha_2) e^{p_3 T}}{p_3(p_3 - p_2)} \tag{27}$$

For the existing condition $\tau_3 \ll \tau_2$ or $\alpha_3 \gg \alpha_2$,

$$p_{2,3} \cong -\left(1 + \frac{\alpha_3}{2}\right) \pm \sqrt{1 + \left(\frac{\alpha_3}{2}\right)^2} \tag{28}$$

For $\frac{\alpha_3}{2} \gg 1$, $\sqrt{1 + \left(\frac{\alpha_3}{2}\right)^2} \cong \frac{\alpha_3}{2}$ and therefore

$$p_2 \cong -1 - \frac{\alpha_3}{2} + \frac{\alpha_3}{2} = -1 \tag{29}$$

also unless the pump power is extremely great, $\alpha_3 \gg 1$, therefore

$$p_3 \cong -1 - \frac{\alpha_3}{2} - \frac{\alpha_3}{2} = -1 - \alpha_3 \cong -\alpha_3 \tag{29a}$$

For the following approximations, and upon resubstitution for α_2, α_3, we have

$$p_2 \cong -1$$

$$p_3 \cong -\alpha_3 = -\frac{1}{W_{31} \tau_3}$$

and also

$$p_2 p_3 = 2\alpha_2 + \alpha_3 + \alpha_2\alpha_3 = \frac{1 + W_{31}\tau_2 + 2W_{31}\tau_3}{W_{31}^2 \tau_2 \tau_3}$$

$$T = W_{31} t$$

and

$$p_2 - p_3 = -1 + \alpha_3 \cong \alpha_3 = \frac{1}{W_{31}\tau_3}$$

$$p_3 - p_2 = -\alpha_3 + 1 \cong -\alpha_3 = -\frac{1}{W_{31}\tau_3}$$

The following expressions for the state populations as a fraction of the total population are finally obtained.

$$\frac{N_1}{N_0} \cong \frac{1 + W_{31}\tau_3}{1 + W_{31}\tau_2 + 2W_{13}\tau_3} - \frac{(W_{31}\tau_2 - 1)e^{-W_{31}t}}{W_{31}\tau_2} - \left(\frac{\tau_3}{\tau_2}\right)\left[\frac{W_{31}(\tau_3 - \tau_2)e^{-t/\tau_3}}{W_{31}\tau_3 - 1}\right] \tag{30}$$

or since $\frac{\tau_3}{\tau_2} \ll 1$,

$$\frac{N_1}{N_0} \cong \frac{1 + W_{31}\tau_3}{1 + W_{31}\tau_2 + 2W_{13}\tau_3} + \frac{(W_{31}\tau_2 - 1)e^{-W_{31}t}}{W_{31}\tau_2} \tag{31}$$

$$\frac{N_2}{N_0} \cong \frac{W_{31}\tau_2}{1 + W_{31}\tau_2 + 2W_{13}\tau_3} + \frac{W_{31}\tau_3 e^{-W_{31}t}}{W_{31}\tau_3 - 1} - \frac{(W_{31}\tau_3)^2 e^{-t/\tau_3}}{W_{31}\tau_3 - 1} \tag{32}$$

$$\frac{N_3}{N_0} \cong \frac{W_{31}\tau_3}{1+W_{31}\tau_2+2W_{13}\tau_3} - \left(\frac{\tau_3}{\tau_2}\right)\left[\frac{(1-W_{31}\tau_2)e^{-W_{31}t}}{1-W_{31}\tau_3}\right] + \left(\frac{\tau_3}{\tau_2}\right)\left[\frac{W_{31}(\tau_3-\tau_2)e^{-\frac{t}{\tau_3}}}{1-W_{31}\tau_3}\right] \quad (33)$$

or

$$\frac{N_3}{N_0} \cong \frac{W_{31}\tau_3}{1+W_{31}\tau_2+2W_{13}\tau_3} - \left(\frac{\tau_3}{\tau_2}\right)\left[\frac{(1-W_{31}\tau_2)e^{-W_{31}t}}{1-W_{31}\tau_3}\right] \quad (34)$$

Since the term in equation 32 involving the transient decay term which varies as e^{-t/τ_3} is only important for times of the order of τ_3, it may also be dropped for further simplification of N_2/N_0. Note that for large values of time t, equations (31) through (34) correspond respectively to equations (11) through (13) which are the steady state evaluations of the state populations.

The value $W_{31} = W_{13}$, is given by the following relationship:

$$W_{13} = W_{31} = \frac{2n\sigma_{13}}{A} = 2\left(\frac{p}{A}\right)\frac{\sigma_{13}}{h\nu_{13}} \quad (35)$$

where E = nhv was utilized, so that p is the energy flow per unit time (i.e., the power) of the incident photon flux from

the pumping source,

A = surface area of the ruby

σ_{13} = absorption cross section

h = Planck's constant

n = incident flux in photons per second

p/A = flux density $\sim$ W/cm^2

W_{13} = induced transition probability per unit time between states one and three

In the design of a ruby laser, one may control, among others, the following parameters related to the ruby sample and the associated system components:

(a) Cr^{+++} ion concentration

(b) Ruby length

(c) Reflectivity of the detached end plates

(d) Losses due to surface reflections from the end of the ruby and any intervening surfaces in the path of propagation

(e) Ruby diameter

It is appropriate at this point, and of interest in the light of the foregoing analysis, to consider the effects of these controllable parameters on the threshold energy required to initiate stimulated emission.

In general, the effects to be considered are the following:

(a) As the Cr^{+++} ion concentration is lowered, the gain per passage through the ruby decreases and losses become more difficult to overcome, increasing the threshold.

(b) As the length of the ruby sample is decreased,

the gain decreases, again increasing the threshold.

(c) As the reflectivity of the detached end plates decreases which implies increased losses, and system components such as a Kerr cell. Wollaston prism etc. are added between the detached reflectors, increasing the losses even more, the threshold will increase progressively.

(d) As the diameter of the ruby increases and/or the Cr^{+++} concentration increases, the sample becomes optically thick and hence more difficult to pump.

Restricting our consideration to the first three effects, from equation (31) and the simplified form of (32), we have,

$$\frac{N_2 - N_1}{N_0} = \frac{W_{31}(\tau_2 - \tau_3) - 1}{1 + W_{31}(\tau_2 + 2\tau_3)} + \frac{\{W_{31}(\tau_2 + \tau_3) - 1\} e^{-W_{31}t}}{W_{31}(W_{31}\tau_2\tau_3 - \tau_2)} \quad (36)$$

But $\frac{\tau_3}{\tau_2} \ll 1$ therefore,

$$\frac{N_2 - N_1}{N_0} = \frac{W_{31} - \frac{1}{\tau_2}}{W_{31} + \frac{1}{\tau_2}} + \left[\frac{W_{31} - \frac{1}{\tau_2}}{W_{31}(W_{31}\tau_3 - 1)}\right] e^{-W_{31}t} \quad (37)$$

Letting $t = t_0$, the pump pulse duration, and recalling the oscillation condition for a sample in a Fabry-Perot interferometer as set forth in equation (5) of Section III, it follows that,

$$\frac{\gamma}{\sigma_{12}\ell N_o} = \frac{W_{31} - \frac{1}{T_2}}{W_{31} + \frac{1}{T_2}} + \left[\frac{W_{31} - \frac{1}{T_2}}{W_{31}(W_{31}T_3 - 1)}\right] e^{-W_{31}t_o} \quad (38)$$

where it must be remembered that

$$\frac{\alpha}{N_o} = \frac{(N_2 - N_1)\sigma_{12}}{N_o} = \frac{\gamma}{\ell N_o}$$

from Section II.[2]

Consider the case of short pulse operation, i.e., $t_o \longrightarrow 0$, in which case threshold can be expressed in terms of $W_{13}t_o$ which is proportional to the pumping energy.

Then,

$$\frac{\gamma}{\sigma_{12}\ell N_o} = 1 + \left[\frac{1}{W_{31}T_3 - 1}\right] e^{-W_{31}t_o} = 1 - e^{-W_{31}t_o} \quad (39)$$

since for t_o less than T_2 we have $W_{13} >> 1/T_2$ and $W_{31}T_3 << 1$. Hence,

$$e^{-W_{31}t_o} = 1 - \frac{\gamma}{\sigma_{12}\ell N_o}$$

and

$$W_{31}t_o = \ln\left[1 - \frac{\gamma}{\sigma_{12}\ell N_o}\right] \quad (40)$$

which relates the threshold energy to the three effects we

2. See reference (36) for a more detailed consideration.

initially started out to consider. In equation (40), γ would be defined by equation (12) of Section III.

2. High Regenerative Environment.[3]

In the energy level diagram of Figure II-1, the ground state is the terminal level for the spontaneous emission transition 2⟶1. Therefore, to produce a net stimulated emission component it is necessary to have an incident pump radiation intensity large enough to excite at least one-half of the total number of ground state ions into level 2.

A quantitative description of stimulated emission in ruby can be obtained from a solution of the more exact steady state rate equations given below: (Note that A_{31}, A_{21} and S_{32} were neglected in the previous sub-section)[4]

(1) $dN_2/dt = W_{12}N_1 - (A_{21} + W_{21})\, N_2 + S_{32}N_3 = 0$

(2) $dN_3/dt = W_{13}N_1 - (W_{31} + A_{31} + S_{32})\, N_3 = 0$

(3) $N_1 + N_2 + N_3 = N_o$

A_{21} and A_{31} are Einstein A coefficients to account for the spontaneous emission, and S_{32} is the transition probability for the nonradiative process (3⟶2). The remaining parameters have been previously defined.

A solution to the above equations is

3. The material contained under this sub-heading relies primarily upon Reference (22). For a more thorough coverage, the reader is advised to consider (17), (23) and (28) in conjunction with (22)

4. The actual lifetimes τ_2 and τ_3 were substituted in their place.

$$(4)\quad \frac{N_2}{N_1} = \left[W_{13}\left(\frac{S_{32}}{W_{31} + A_{31} + S_{32}} \right) + W_{12} \right] \Big/ (A_{21} + W_{21})$$

Assuming a quantum efficience of unity, that is, for every photon at frequency ν_{13} absorbed, one photon is emitted at frequency ν_{12} then, $A_{31} \ll S_{32}$. Also for very high pumping powers $W_{31} \ll S_{32}$. Consequently, equation (4) simplifies to

$$(5)\quad \frac{N_2}{N_1} \cong \frac{(W_{12} + W_{12})}{(A_{21} + W_{21})}$$

and

$$(6)\quad \frac{N_2 - N_1}{N_0} \cong \frac{(W_{13} - A_{21})}{(W_{13} + A_{21} + 2W_{12})}$$

Hence in the normal laser mode or high regenerative environment, in order to obtain stimulated emission at the frequency ν_{12}, it is necessary that $W_{13} > A_{21}$ from equation (6). This is the minimum condition. It is further required that the excess population $(N_2 - N_1)$ be sufficient to overcome system losses as we have already seen earlier in this paper.

As the pumping power is increased above the point where $W_{13} = A_{21}$ (equal populations), the crystal begins to emit stimulated as well as spontaneous radiation. The spontaneous emission power is $N_2 h \nu_{12} A_{21}$, and since N_2 normally increases by only a small amount over the equal population value, almost all additional power developed at the frequency ν_{12}

appears as stimulated emission. Since only this latter component constitutes useful output it would be desireable to pump at levels where $W_{13} > A_{21}$. Under normal mode operating conditions however, it is difficult in practice to reach the condition $W_{13} = A_{21}$. In the pulsed reflector mode system, the condition of $W_{13} > A_{21}$ is achieved by pumping the ruby towards a pseudo threshold quite higher than the normal threshold for stimulated emission. Laser action is held off by optical means as set forth in Section III, until N_2 has increased by a goodly amount over the equal population value. The pseudo threshold is suddenly removed, the ruby finds itself far above the threshold where stimulated emission would normally have transpired, and the sudden equalization of population values results in a giant pulse of stimulated optical emission.